FLIGHT DYNAMICS ANALYSIS OF GENERIC AIR-BREATHING HYPERSONIC VEHICLE USING BIFURCATION METHOD

A thesis submitted to the
UPES

For the Award of
Doctor of Philosophy
in
Aerospace Engineering

BY

Ritesh Singh

Mar 2024

SUPERVISOR (s)

Dr. Om Prakash
Dr. Sudhir Joshi
Dr. Yogananda Jeppu

UPES
UNIVERSITY OF TOMORROW

Department of Aerospace Engineering
School of Engineering
UPES
Dehradun - 248007: Uttarakhand

FLIGHT DYNAMICS ANALYSIS OF GENERIC AIR-BREATHING HYPERSONIC VEHICLE USING BIFURCATION METHOD

A thesis submitted to the
UPES

For the Award of
Doctor of Philosophy
in
Aerospace Engineering

BY
Ritesh Singh
(SAP ID 500048549)

Mar 2024

Internal Supervisor
Dr. Om Prakash
Professor
School of Engineering,
UPES

External Supervisor (s)
Dr. Sudhir Joshi
Professor
Department of Aerospace Engineering,
Graphic Era (Deemed to be University)

Dr. Yogananda Jeppu
Fellow
Aerospace Electronics Solutions,
Honeywell Technology Solutions, Hyderabad

Department of Aerospace Engineering
School of Engineering
UPES
Dehradun - 248007: Uttarakhand

2024 Mar

DECLARATION

I declare that the thesis entitled **Flight Dynamics Analysis of Generic Air-Breathing Hypersonic Vehicle using Bifurcation Method** has been prepared by me under the guidance of Dr. Om Prakash, Professor of Department of Aerospace Engineering, University of Petroleum & Energy Studies. No part of this thesis has formed the basis for the award of any degree or fellowship previously.

Ritesh Singh

Department of Electrical Engineering, Manipal University Jaipur, Dehmi Kalan, Off Jaipur-Ajmer Expressway, Jaipur-303 007, Rajasthan, India.

Date: 22 Mar 2024

CERTIFICATE

I certify that Ritesh Singh has prepared his thesis entitled **"Flight Dynamics Analysis of Generic Air-Breathing Hypersonic Vehicle using Bifurcation Method",** for the award of PhD degree of the University of Petroleum & Energy Studies, under my guidance. He has carried out the work at the Department of Aerospace Engineering, School of Engineering, University of Petroleum & Energy Studies.

Internal Supervisor

Dr. Om Prakash

Department of Aerospace Engineering, School of Engineering,

University of Petroleum & Energy Studies, Energy Acres, Bidholi, via, Prem Nagar, Dehradun-248007, Uttarakhand, India.

Date: 23 May 2023

CERTIFICATE

I certify that Ritesh Singh has prepared his thesis entitled **"Flight Dynamics Analysis of Generic Air-Breathing Hypersonic Vehicle using Bifurcation Method"**, for the award of PhD degree of the University of Petroleum & Energy Studies, under my guidance. He has carried out the work at the Department of Aerospace Engineering, School of Engineering, University of Petroleum & Energy Studies.

External Supervisor

Dr. Sudhir Joshi

Department of Aerospace Engineering, Graphic Era (Deemed to be University), Bell Road, Clement Town Dehradun, Dehradun-248002, Uttarakhand, India.

Date: 23 May 2023

CERTIFICATE

I certify that Ritesh Singh has prepared his thesis entitled **"Flight Dynamics Analysis of Generic Air-Breathing Hypersonic Vehicle using Bifurcation Method"**, for the award of PhD degree of the University of Petroleum & Energy Studies, under my guidance. He has carried out the work at the Department of Aerospace Engineering, School of Engineering, University of Petroleum & Energy Studies.

External Supervisor
Dr. Yogananda Jeppu
Date: 23 May 2023

ACKNOWLEDGEMENT

ABSTRACT

The technological necessity for Hypersonic Vehicles grows as Humanity expands its reach into Space and creates a demand for fast global transportation across large distances through the Earth's atmosphere. Access to Space with cargo on demand, fast travel to faraway locations on Earth, reliable, cost-effective, and routine access to Space: all of these are feasible with the help of Air-breathing Hypersonic Vehicles (AHVs). AHV's has long been recognized for its potential to enable both advanced military and efficient access to Space. Recognizing the potentially large benefits of this technology and the magnitude of the efforts to develop this technology, has attempted to lay out a high-speed Hypersonic Technology roadmap. Single-Stage-To-Orbit (SSTO) AHV under consideration, present significant challenges in many technological areas and especially in the area of flight control.

AHV vehicle's historical development of Hypersonic Vehicle model shows that the Winged Cone is established model and is considered for this research. AHV Winged Cone model is developed with 3DOF AHV longitudinal dynamic model with propulsion model of Turbojet, Ramjet, and Scramjet, and with Rocket propulsion system incorporated into the model. The AHV model presents the different operating flight regimes for 3DOF nonlinear model and 6DOF linear model development. The aerodynamic model is developed for the entire AHV flight regimes with Mach Number (M), 0 to 24. AHV longitudinal trim and stability assessment is performed using dynamic simulation considering different operating conditions and different sonic velocities. Stable simulations are achieved for different cases of trim simulation of AHV model for M=0.9, M=6 and M=10, and for M=4, M=15 and M=24 shows unstable behavior. Dynamic simulation with trim condition is considered for variable control surface deflection for δ_e and δ_r deflection. Flight dynamics and stability analysis for 3-DOF AHV dynamic simulation model is performed with Bifurcation Method using AUTO-07p platform. The Method shows that the parameters used for the different systems with

their dynamic model shows that elevator deflection δ_e is mostly considered as the BP (Bifurcation Parameter). CBA is implemented for the Longitudinal dynamics AHV model at M=0.9, for different choices of elevator deflection and with the aim to observe the control effects for different elevator deflection, $\delta_e = -12^0$ and 12^0. Bifurcation Diagram is obtained for data points with different forward and backward runs with the different iterations, shows the parameter values of α, θ and q. Linear AHV model is developed and is considered for steady and wing level flight condition operating at level and straight flight condition for velocity M=5 and altitude of 65000ft (19812m). The linear model obtained is decoupled from the longitudinal and lateral system interactions. This linear model is analyzed for open loop dynamic simulation for different inputs δ_a and δ_r deflection. The pole-zero plot of the model shows nonminimum phase for the poles and zeros, which results in system unstable. Hence, control design is implemented using state feedback architecture for the AHV dynamic model. The dynamic stability of the model is investigated, and state feedback control using pole placement is implemented to attain the stability of the model.

This research presents modelling, simulation, and aerodynamic model development of dynamic 3-DOF longitudinal AHV model. The nonlinear aero data model is developed for entire flight regime of hypersonic flight from $M = 0.9\ to\ 24$. The dynamic stability investigation with selected $M = 0.9, 4, 6$ and 24, is performed considering the Bifurcation Method. This study provides eigen values, based on which the stability analysis is considered. It is seen that at the Mach number, $M = 0.9\ and\ 6$ shows short period mode and $M = 4\ and\ 24$, shows the long period mode presence. Results presented here with Bifurcation Analysis shows a promising method for stability analysis for various trim points under consideration. This study presents the research for achieving Hypersonic Flight in near future. The coming decades will prove and outcast the research and development of AHVs with the involvement of high interest of the Nations to achieve the Hypersonic Technology, and hence could provide routine flight between Earth and Space.

TABLE OF CONTENTS

LIST OF FIGURES

LIST OF TABLES

NOMENCLATURE

u, v, w	Velocity along body axis
$\dot{u}, \dot{v}, \dot{w}$	Accelerations along body axis
p, q, r	Angular velocities
$\dot{p}, \dot{q}, \dot{r}$	Angular rates
F_{ax}, F_{ay}, F_{az}	Aerodynamic forces
L_a, N_a, M_a	Aerodynamic moment
ϕ, θ	Roll angle and Pitch angle
m, h	Mass and altitude
c_1 to c_9	Constants moments of inertia
V	Velocity
α, β	Angle-of-attack and side-slip angle
M	Mach number
C_L	Lift coefficient
C_D	Drag coefficient
C_m	Pitching moment coefficient
C_Y	Side force coefficient
C_l	Rolling moment coefficient
C_n	Yawing moment coefficient
L, D, Y	Lift, drag and side force
L_a, M_a, N_a	Rolling, pitching and yawing moment
$C_{L,\alpha}, C_{L,\delta e}$	Increment derivatives
δ_e	Elevator deflection
δ_a	Aileron deflection
δ_r	Rudder deflection
A_n	Normal acceleration
T	Thrust
AHV	Air-breathing Hypersonic Vehicle

GHV	Generic Hypersonic Vehicle
SSTO	Single Stage To Orbit
TSTO	Two Stage To Orbit
DOF	Degree-of-freedom
FCS	Flight Control Systems
LTI	Linear Time Invariant
BIBO	Bounded Input Bounded Output
RHS	Right hand-side s-plane
PI	Proportional Integral
PD	Proportional Derivative
PID	Proportional-Integral-Derivative
PLA	Pilot-lever-angle
EBA	Extended Bifurcation Analysis
SBA	Standard Bifurcation Analysis

CHAPTER 1
INTRODUCTION

One potential answer to the problem of how to make space travel more accessible and economical is Air-Breathing Hypersonic Vehicle (AHV). The possibility of SSTO (Single-Stage-To-Orbit) and TSTO space missions, as well as long-range cruise missions, will make use of AHV technology in the future increases. Recently, AHVs have gained widespread interest due to their ability to connect the fields of aviation and space exploration, and because of their speed, attitude, quick military response, lengthy duration, and powerful penetrating ability, they have bright prospects in both the military and the civilian sectors. Advantageous uses for AHVs include the facilitation of high-speed commercial aviation and the reduction in the cost and risk of LEO space missions. Accomplishment of NASA's Programme demonstrates how the demand for safe, affordable space travel for civilian and military uses has redirected attention to hypersonic technology. Both military and commercial communications interests in the area are actively monitoring its development.

1.1 MOTIVATION AND OVERVIEW

AHVs have *drawn international attention* and is seen as a possible solution in making *affordable and routine space flight, quick military response; and allowing for high-speed commercial air travel, reliable space missions to low Earth orbit, and low-cost cruise missions with great range.* Developing the need for rapid global transportation over long distances through the atmosphere of the Earth, this connects aeronautics and astronautics and has promising military and civilian applications. The SSTO and TSTO space missions, as well as long-range cruise missions, are only two examples of where AHV technology could be useful.

The developments of the airplane, rocketry science and other space application, exclusively afterward Second World War led to outgrowth of new era of

Hypersonic. All common public, engineers, scientists and space lovers, have a dream of flying to orbit and into space. As rockets have conquered the space launch for the last five to six decades, hypersonic air-breathing systems have potential to achieve this in near future. Hypersonic vehicles with high Mach can prove an appropriate platform for the second stage rocket and capable of SSTO over the coming decades. Investigation for the AHVs commenced during 1960's and was persistent over 1990's followed by US hypersonic programs. The development of an operational AHV will involve most important developments in propulsion technology, multidisciplinary modeling and simulation, and design benchmarks. On the development and research front of AHV, the focus is on the propulsion and engine technology so that hypersonic flight and wide-range speed in different sonic and hypersonic regimes can be achieved. Analysis provided by the US NASP (National AeroSpace Plane) and Hyper-X Programs reveals that the key technologies are needed for Hypersonic Transportation to be achievable in an efficient manner and are required to be addressed.

Fig. 1.1 The Hypersonic Confluence [1]

A significant concern is of the control methods and its design for the distinctive features of the AHVs must be prudently deliberated in association with the typical aircraft. Figure 1.1 exhibits blend of the Ballistic Missiles, Space Projects, Aeronautics Projects, and the Hypersonic Projects indicating the research programs development in [1] over the decades.

Over the last 40 years substantial developments in hypersonic technology have been carried out addressing the hypersonic engine, airframe and integrated system and many others. One of the critical technologies required for the AHVs flight success is propulsion technology. Vehicles having air breathing capabilities with the propulsion system have the range of flight at 30 km to 50 km altitude for the extended time frame during the flight. Thus, this propulsion system must maintain the low altitude flight to attain the high dynamic pressure for better engine performance and to maintain sufficient intake of the air for the air-breathing engines. All the vehicles developed undergo extreme thermal loads, which are required to have advanced Thermal Protection System (TPS). Unlike the conventional aircraft, AHVs require a propulsion system which can be highly integrated into the vehicle design. Figure 1.2 shows the operation range of the engine possibilities as stated in [2] of the system reliant on the fuel as a choice for the air-breathing propulsion. The termination of NASP in initial years of 1990's, but investigation in the scramjet technology continued. To achieve hypersonic flight, it is apparent that combined propulsion technology would be required. Combination of propulsion cycles can be accomplished with high speed and for Mach 5 and beyond, with combined cycle of turbojets, ramjets and scramjets can be used.
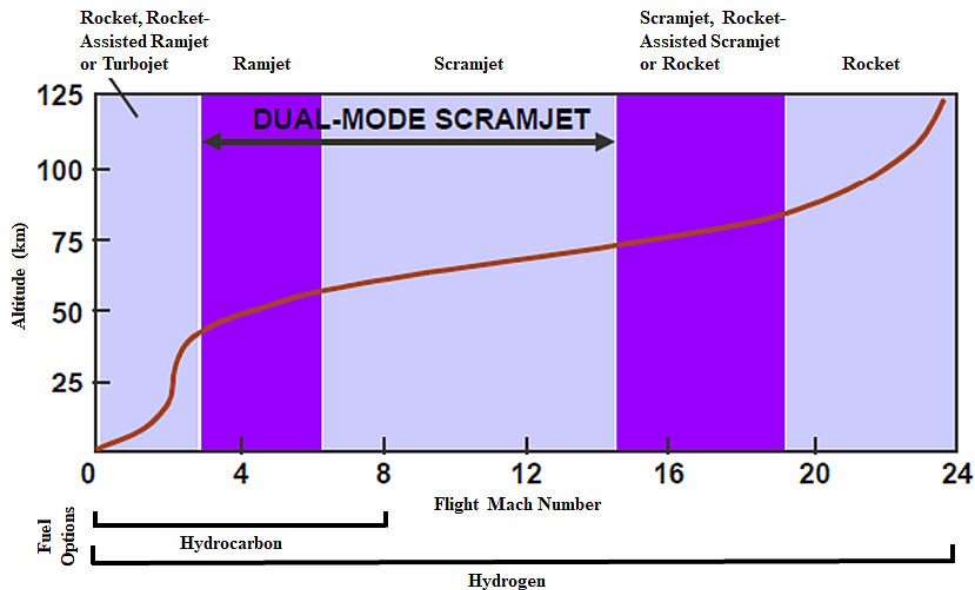
Fig. 1.2 Engine possibilities based on Mach number [2]

The NASA Hyper-X program emphases the paramount aerospace research encounters of the AHVs flight. The major assignment is to develop a vehicle which can achieve high-speed between Mach 7 to 10 without any rocket. The SR-71 called as Blackbird is designed with manned air-breathing capability that cruised to Mach 3.2 proving the world's fastest aircraft in 1960's as stated in [3], and NASA's X-15 accomplished Mach 6.7 speed in the year 1967.

The technologically advanced X-43A (Hyper-X initiative) is designed to aim, to conduct and establish strategic propulsion interrelated technologies for AHVs by NASA associated research centers. The US National Aerospace Initiative (NAI) have illustrated the history of the flight from the 1960 to the present flight speed of the vehicles and the hypersonic technology development and demonstrations as stated in [4]. The program's ultimate goal is to show a 1 Mach gain in annual persistent flight by 2012. The challenges and the difficulty with the aerodynamics of the hypersonic vehicles describe the different aerodynamics phenomena in [5] that take place at different altitude and flight speeds. It shows the aerothermodynamics design requirements for the major types of hypersonic space transport vehicles with minimal trajectories as winged Re-entry Vehicles (RV), Hypersonic Cruise Vehicles (CV), Ascent and Re-entry Vehicles (ARV) and Aero-assisted Orbit Transfer Vehicles (AOTV). In 1995 US AFRL started the HyTech (Hypersonic Technology) Program and with the cost-cutting and lack of support, USAF initiated HySTP (Hypersonic Systems Technology Program) as stated in [5]. The HyTech aimed for the development of the hydrocarbon led scramjet technology upto Mach 8. In 1998 ARRMD (Affordable Rapid Response Missile Demonstrator) program in [6] was DARPA (Defense Advanced Research Projects Agency) initiated which got terminated in 2000, and other initiatives of vehicle concepts like HyFly (Hypersonic Flight Demonstration) and SED (Scramjet Engine Demonstrator), as stated in [6] were promoted and initiated. NASA successfully conducted the flight demonstration of the investigational X-43A using Scramjet Technology in 2004 and 2005. With the advancements of the AHV over the years, the X-51 SED made its first flight in the year 2009. The Falcon HTV (Hypersonic Test Vehicle) performed the 'glide phase' maneuvers in 2011 to successfully test its

aerodynamics. The X-51A US Air Force's waverider design achieved the Mach 5.1 flight speed during the test.

1.2 Introduction to Hypersonic Vehicle

Vehicles travelling at Mach 5 or faster are known as AHVs. With that kind of velocity, a safer, cheaper, and more efficient method of space travel can be introduced. As a result, many advanced nations are investing heavily in risky research into hypersonic vehicles. When it comes to moving from theoretical foundations to practical engineering applications, the control system design of AHVs continues to be a pressing bottleneck. To make air-breathing hypersonic flying practical and efficient, controller design is a critical issue.

The lifting body of an AHV is long and slender, and its leading edge is sharp to reduce drag. Structural dynamics, the propulsion system, aerothermodynamics, and the control system are the four main functional subsystems that make up the AHV model. Each of these subsystems has two secondary coupling effects due to interactions with other subsystems. As a result of the interaction between the structure and the control system, servoelastic effects occur; as a result of the interaction between the structure and the propulsion system, aeropropulsive effects occur; as a result of the interaction between the aerothermodynamic flow field and the propulsion system, control actuation is reduced; and so on. Non-minimum phase behavior, aeroservoelasticity, aerothermoelasticity, and low-frequency oscillations in the vehicle's dynamics are all secondary effects that emerge as a result of the interplay between these main causes. The model characterizing an AHV's dynamics lies at the centre of these four tertiary effects.

The US National Aerospace Plane has been conducting study on AHV technology since the 1960s. Despite the extensive study, it is generally agreed that significant breakthroughs for propulsion engine technology and material technology, as well as refined transdisciplinary modelling and design techniques, are necessary for the creation of a fully functional vehicle. Hypersonic speeds, or the ability to switch between subsonic, supersonic, and hypersonic flight regimes, were once the primary focus of air-breathing

hypersonic research, which led to the creation of ramjet and scramjet engines, as shown in Table 1.1.

Table 1.1 General Plane Characteristics for Different Flight Regimes

Regime	Mach Number	Plane Characteristics for different Sonic Speeds	Engine Characteristics	Control Characteristics
Subsonic	< 0.8	Propeller-driven, commercial turbofan aircraft with high aspect-ratio (slender) wings, and rounded features like the nose and leading edges.	Turbofan, turbojet, and ducted fan.	Higher aspect ratio, gives a higher lift/drag ratio
Transonic	0.8 - 1.2	Swept wings that delay drag-divergence, and often feature designs adhering to the principles of the Whitcomb area rule.	Turbojet	Swept wings
Supersonic	1.2 - 5	Sharp edges, thin airfoil sections, and all-moving tailplane/canards are common. Modern combat aircraft, include the F-104 Starfighter and BAC/Aerospatiale Concorde.	Turbojets, boosted turbojets, by-pass turbojets, and boosted by-pass turbojets, ramjet airbreathing jet	Tailplane/canards, very long and slender fuselage, and large delta wings
Hypersonic	5 - 10	Highly integrated (due to domination of interference effects: non-linear behaviour), Small wings.	scramjet airbreathing jet, Shock-Ramjet Engine	Small wings
High-Hypersonic	10 - 25	Blunt configurations (because of the aerodynamic heating rising with a reduced radius of curvature).	Rocket boosters, Air-breathing engines, scramjet engines	Blunt design configurations
Re-entry Speeds	> 25	Ablative heat shield; small or no wings; blunt shape.	Rocket powered	small or no wings

Hypersonic transportation is a promising new mode of transportation, however research conducted by the National Aerospace Plane (NASP) and the Hyper-X Programmes have revealed that additional critical technologies are needed to realize its full potential. It's important to take into account the differences between AHVs and conventional planes while designing the controls. Hypersonic air-breathing vehicles differ significantly from ordinary aircraft in which propulsion technology must tightly be incorporated with the vehicle. Research on scramjet-powered flight continued, albeit on a much lesser scale, after the National Aerospace Plane was scrapped in the early 1990s. Some projects were designed to prove the viability of individual technologies crucial to achieving sustained hypersonic flight.

One of the most difficult problems in aeronautics research is the flight of AHVs, and NASA's newest multi-year research programme, Hyper-X, is

dedicated to this issue. Since the current record holder for fastest air-breathing aircraft, the SR-71, cruises just above Mach 3, and in 1967, the X-15, powered by rockets at NASA, reached a top speed of Mach 6.7, creating aircraft capable of Mach 7 and Mach 10 speeds is the major mission. NASA's Hyper-X Programme, run out of the Dryden and Langley Research Centre's, has as its primary objective the demonstration and flight validation of essential propulsion and related technologies for AHVs using the specialized prototype (X-43A) built for the job.

Recent examples include NASA's 2004 and 2005 flights of the X-43A, a technology demonstration powered by scramjets. The X-51 first flight using Scramjet Engine Demonstrator is arranged for the latter part of 2009. The X-43A, an experimental plane developed by NASA, has proven the viability for scramjet. During 2011, unmanned HTV (Falcon Hypersonic Test Vehicle's) 'glide phase' maneuvers were performed to examine the aerodynamics, and during test connection was lost. More than five times the speed of sound was reached on the final test flight of a hypersonic experimental aircraft on May 1, 2013. The Air Force X-51A Waverider reached a high speed of Mach 5.1 during the test flight, covering more than 230 nautical miles in less than six minutes before deliberately crashing into the Pacific Ocean off the coast of California.

1.3 Flight Dynamics Analysis

Flight dynamics analysis can be broken down into three distinct types of methods: analytical, computational, and experimental. The analytical tools are the same approaches of applied mathematics that are utilised in other areas of mechanics. Stability, autonomous control, stochastic processes, and optimisation are all parts of system theory, a growing topic of practical mathematics. In order to achieve controlled flight, vehicle stability is required but not sufficient. In various regions of their flight regime, even the best aeroplanes have experienced some degree of instability, while vehicles that are entirely stable may have poor handling. Stability boundary determination for nonlinear and time-varying systems requires extensive analytical and computational effort, which may not be justified by the importance of dynamic

performance criteria. When computing stability of small disturbances from a steady state, the linear eigenvalue problem that is typically a part of the system study can be very helpful and may provide enough information about stability from a practical standpoint. From a computational standpoint, the most salient truth is that, in the last several decades, the availability of machine computation has completely revolutionised the way this field is actually practised. System performance, system design, and optimisation issues that were once intractable are now routinely dealt with.

The experimental methods used in the study of flight dynamics are largely novel. The first category includes aerodynamic input finders. The world's leading aerodynamics labs now have access to wind tunnels and shock tubes that replicate realistic flying conditions. Aeroballistics ranges, rocket-boosted and gun-launched free-flight model techniques, and conventional laboratory apparatus are all available for dynamic experiments. The proliferation of these broad infrastructures has coincided with the proliferation of a wide variety of sensors and equipment, primarily electronic, for measuring forces, pressures, temperatures, acceleration, angular velocity, and so on. Aerodynamicists' reliance on experiment has been greatly diminished by advancement using CFD. In many cases, wind tunnel studies are no longer necessary because CFD calculations can provide the same information. Verification of the CFD codes themselves, through comparison to experiment, is, of course, essential.

Second, the flight dynamics study makes heavy use of a flight simulator, which is an experimental tool. The focus of his research is on how well the pilot complements the aircraft. For completely novel air travel scenarios, this is a mandatory first step. Long before the prototype stage, the pilot's control over the vehicle must be guaranteed. While research into mathematical models of human pilots has led to some promising findings, it is still impossible to do this without actual flight testing. In addition to being an effective instrument for educating new pilots on the latest and greatest aircraft models, the specialised simulators that have been developed for them have also proven useful as a research tool for investigating vehicle handling attributes and pilot dynamics. The time and money required to teach pilots to fly new types of aeroplanes has been drastically cut thanks to the advent of high-fidelity simulators.

1.4 Bifurcation Method Analysis to Aircraft Dynamics

Implementation of bifurcation techniques for study of flight dynamics dates back to late 1970s and beginning in early 1980s with the publishing of the first works in the open literature. The field of flight dynamics received a much-needed boost from bifurcation approaches, which bridged the gap between trivial change in linear approximation to nonlinear six degrees-of-freedom simulation. Numerous nonlinear occurrences are of great magnitude to battle dynamics have been studied systematically and effectively thanks to the advent of bifurcation methods as stated in [7]-[8]. However, after 30 years, clearly, other branches of aerospace engineering have not adopted bifurcation approaches or become standard practise when designing aircraft systems. Most aerospace engineers still think of bifurcation methods a nonlinear investigation technique of combat dynamics.

1.4.1 For Flight Dynamics Application

Analysis of flight dynamics pre-bifurcation approaches relies on, firstly, analysis of linear stability at a given trim state, and secondly, the transition between trim states and the overall transient response is identified via nonlinear simulation. Obviously, we require a trim procedure to identify the trimming conditions. By employing a continuation algorithm, bifurcation techniques standardised and mechanised the computation of trimming conditions with stable property across broad selection of inputs. In addition, the method approach gives us common dialectal to talk about a wide range of nonlinear phenomena in [9]: we can talk about jump occurrences with transitions as of saddle-node points, and we can talk about periodic-oscillations as limit cycles that start with Hopf points. Although time history simulations is required, so that it can perform selective and strategically using data gathered using method implementation. Advent of bifurcation techniques is watershed moment in the evolution of flight dynamics. It is accurate to state that the bifurcation marked the beginning of a new era in the study of battle dynamics. Nonlinear dynamical flight phenomenon prediction is where bifurcation approaches have proven to be most useful. Bifurcation analysis allowed for the early prediction, onset explanation, and dynamics understanding of spin, wing rock, and inertia-

coupled roll motions. Therefore, bifurcation methods became well-known as an effective instrument for analysing the stability of flight dynamics, particularly for high angles-of-attack. Considerably, it has become synonymous with this specific use case, and it is not uncommon for individuals who are not familiar with the topic to reject it as a "high-alpha tool."

1.4.2 For Control Study Application

Bifurcation techniques have also made strides in the design of flight controls and control systems as stated in [10]-[11]. Bifurcation approaches, from the perspective of the control designer, reveal details concerning, firstly, the existence and stability of fundamental equilibria and aims to deliberate the reassignment of stability of these equilibria, and secondly, other trimming states with steady conditions with respective branches. States which is undesirable, are attempted to prevent them from occurring; but, if the control system is saturated, they become possible. the degree to which they can be perturbed before the system loses its stability characteristics is indicative of the control design's robustness. This is the zone where the control designer can use his or her imagination to make use of bifurcation techniques during the design and evaluation of controls.

Considering control designed for linear dynamical systems using local consideration produces numerous operational sites are still widely used in designing FCS. Gain scheduling is used to knit together a network of local controllers that can exert influence over the full flight envelope. By doing so, the controller design is approximatively taken into consideration for nonlinearities in the flight dynamics of the aircraft and changes in system attributes for operating conditions. Numerical continuation with bifurcation analysis can be used to create a gain scheduled control law. Since most designs for control laws only ensure local properties, bifurcation method is implemented for test and control-law aimed at secondary steady states. As such, it can provide a groundwork representing enhancement of flight envelope limiters. Using aerodynamic derivatives as continuation parameters to assess susceptibility to parametric uncertainties and ensuring closed-loop stability in regions outside of those for which the control rule was created, are two examples of how

bifurcation analysis can be used to assess robustness. The zone of attraction can be roughly estimated by determining the next steady-state (equilibrium, limit-cycle) surface.

Control designer toolkit is still missing its implementation using bifurcation methods, despite their obvious use. This may be due to the fact that bifurcation approaches, is still considered a tool for time domain analysis of nonlinear systems, and do not mesh well with the frequency domain (primarily PID) methods that have traditionally been used for flight control design. PID control design often uses frequency domain parameters, however bifurcation analysis communicates with eigenvalue analysis, even if stability is a shared goal.

One probable explanation for bifurcation methods' lack of adoption in the field of combat control design is the common belief that they are only useful for problems with large initial conditions. However, as mentioned before, spin recovery, upset/loss-of-control recovery, and flying envelope limiters are all possible applications of bifurcation algorithms.

Integration of bifurcation approaches and control system design methodologies is urgently needed, especially in the frequency domain. In most control systems, robustness measurements in the frequency domain are readily available and easily verified, in contrast to the time domain. This is one of the key reasons why control system engineers prefer using frequency domain methods, as well as pointing out how important it is to have reliable strategies for converting frequency domain criteria into their time domain analogues in order to spread the bifurcation approach among control engineers. As algebraic equations, numerical continuation algorithms may easily handle these criteria. This method is analogous to that of computing manoeuvre cuts and applying continuation to solve optimisation difficulties.

1.5 Research Objectives

The study's primary aims are:
- Validation of Dynamic Model of Generic AHV.
- Bifurcation Analysis of Longitudinal Dynamics of Generic AHV for different Operating Flight conditions.

- Flight Dynamics Analysis of Generic AHV for different sonic velocity conditions.
- Flight Dynamics Analysis of Generic AHV for different Control Inputs.

1.6 Research Methodology

Creation of resources and methods to aid in conducting the research at each step, such as modeling & simulation, bifurcation analysis, control design, validation is carried out. Create control-relevant modes of varying complexity and dependability for use in optimizing, analyzing, and validating vehicle controllers. To provide vehicle simulation for support of advanced control methods design and analysis. Create a simulation environment where models can be incorporated in a consistent and modular manner for maximum benefit from the simulation. Inaccurate predictions of the hypersonic flight regime's aerodynamics, propulsion, and control coefficients are the primary cause of the type of uncertainty anticipated for the hypersonic vehicles' dynamics.

| Aero Data Generation of AHV from empericial relation as stated in [12]-[13] |
| Identification of Aerodynamically Static Stable/Unstable limitting Cases (regions) from the generated AHV Aero Data. |
| 3DOF Dynamic Simulation for Dynamic Trim & Stability Analysis of AHV |
| Trim Analysis of 3DOF for Mach number=0 to 24 for different δe deflection |
| Simulation for different Cases of Mach number=0 to 24 |
| Bifurcation Analysis of Longituidnal Dynamics of AHV for different Mach number of limiting stability* Cases for Qualitative Analysis |
| Quantitaive Stability Analysis using Linearized Eigen Values obtained from Bifurcation & Continuation results of different Cases |
| Control Design of AHV for the limiting Cases of Mach number |

*Bifurcation results of negative Angle-of-Attack of numerical computations which are not related to study.

Fig. 1.3 Methodology Flow Chart

Nevertheless, hypersonic vehicle controllers must ensure system stability and deliver satisfactory control performance. The non-linear AHV model is analyzed using the Bifurcation Method for the various continuation techniques to generate the Control Law for large envelop flying situations. The software packages like MATLAB, Simulink and AUTO-07p will be used to perform the Modeling, Simulation and Bifurcation Analysis using the Continuation Method. The software packages like MATLAB, Simulink are used to perform the Modeling and Simulation, and AUTO-07p for Bifurcation Analysis using Continuation Method, as stated in [14]. The methodology carried out for this research is represented using Fig. 1.3. The methodologies used for the different stages of the research can be categorized as -

- Mathematical Modeling & Simulation
- Bifurcation Analysis
- Flight Control Systems

1.6.1 Mathematical Modeling & Simulation

Choosing which physical variables and interactions are insignificant and crucial for the correctness of the model is the first step in arriving at a properly reduced model. It is common practice to begin with a basic model in order to get a feel for the answer, and then proceed to a more detailed mathematical model for a thorough investigation.
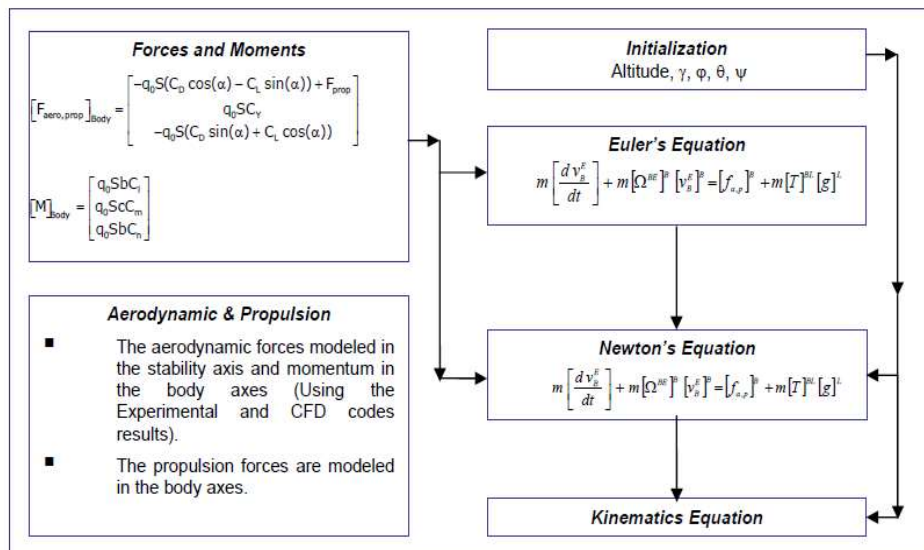
Fig. 1.4 Model Development and Simulation [15]

To simplify a model, however, one must prioritize which physical variables and connections are essential for the model's accuracy. The preliminary stages of creating something devoted to the development of a modelling environment useful to control engineers in understanding multifaceted relations amongst aerothermodynamics, propulsion, control, and structural dynamics designed for specific arrangement.

To establish feasible equations of motion and to combine the complete flight dynamics, elastic property, and propulsion dynamics for the modeling to obtain the non-linear model. Winged-cone Configuration of the AHV is used for this analysis and nonlinear system approach used for mathematical modeling using the procedure shown using Fig. 1.4 with Fig. 1.5.
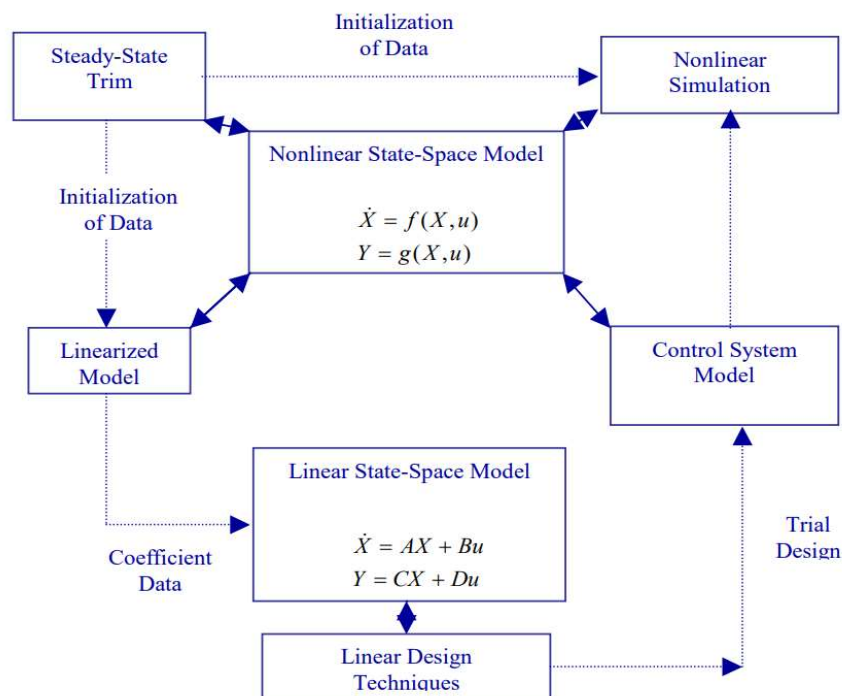
Fig. 1.5 Modeling and Simulation Flow [16]

1.6.2 Bifurcation Method

There are several nonlinear phenomena that factor heavily into the workings of dynamics of flying that may be studied effectively using bifurcation analysis, and flight control is one of these domains. There is great potential for bifurcation methods to enter the aviation design process and dramatically improve it. The

non-linear AHV model's performance in its many flight regimes is analyzed using the Bifurcation Method. Non-linear behavior will be analyzed using Bifurcation of the dynamical system, which shows all critical points where equilibrium results in change in the stability.

Types of Bifurcation can basically be classified as two kinds of bifurcations: static and dynamic. Crossing the imaginary axis by a system's real eigenvalue, a static bifurcation occurs between a set of trim points. For instance, a) a saddle-node bifurcation' (Fig. 1.6 b) wherein the increase in trimming state undergoes a transition. i.e., 2 trim positions, 1 stable with 1 unstable, appear or depart with change in control parameter, b) a 'pitchfork bifurcation' (Fig. 1.6 c) is combined in variation with trimming point changes, that is, stable (unstable), trim loses (gains), stability with 2 new stable (unstable) trim are created, with symmetric and near to original trimming point, and c) a 'transcritical bifurcation' (Fig. 1.6 d), between a trimming point convergence (divergence) oscillation occurs with stable (unstable) limit-cycle is a dynamic occurrence. For instance, a single stable trim point associated with a Hopf Bifurcation (HB) point (Fig. 1.6 f) transitioned with un-stable trimming occurrence exhibiting stable periodic-oscillation. Periodic oscillations, also known as limit cycles, begin at HB.

Bifurcation Methodology needs first-order ordinary differential equations to represent a dynamical system as, $\dot{x} = f(x, U)$, where x, U, f are vectors of n, m state variables, control parameters and as nonlinear mathematics functions respectively. Typically, the bifurcation method, in implementation 1 parameter is changed in time considering others remain constant. Take u to a constant control-parameter that needs change, and P is set to (m-1) static control-parameter. Therefore, keeping tabs on all the possible trim states x^* is essential for the bifurcation method such that $f(x^*, u, P) = 0$ is fulfilled. The continuation approach is used to allow the free control parameter u to be adjusted within bounds while holding the fixed control parameter P constant.

Continuation Algorithms: depends on proposition called implicit function, demonstrating that a nonsingular occurring at (x_0, u_0, P) for the systems state variables with reference to the Jacobian matrix, the system can be solved by a sequence of linear equations, then there exists a neighborhood around

(x_0, u_0, P), so that there is an u nearby for every other u that is $u_0 + \Delta u$, $f(x, u, P) = 0$ with unique result.
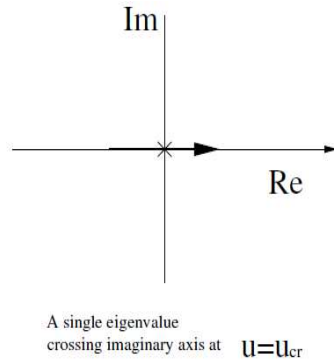
(a)
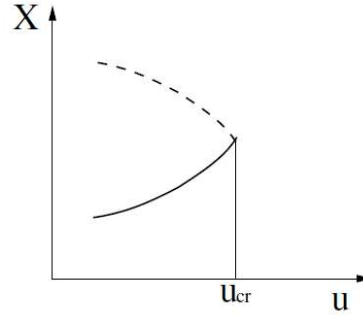
(b) Fold or Saddle-node bifurcation
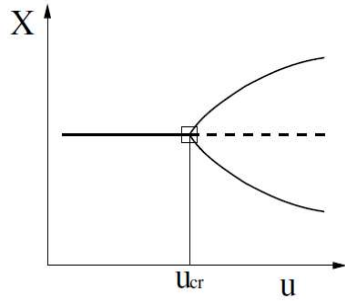
(c) Pitchfork bifurcation (Super critical)
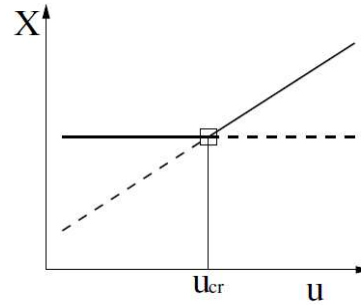
(d) Transcritical bifurcation
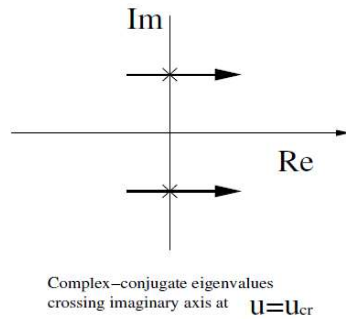
(e)
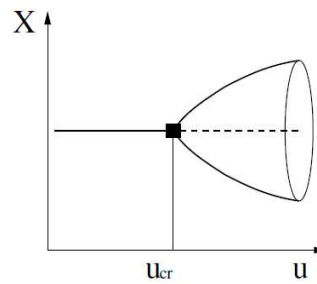
(f) Hopf bifurcation (Super critical)

Fig. 1.6 Types of bifurcation (trim occurrence) (line - stable, dashed-line - unstable, empty-square - static point, solid-square - Hopf point) [17]

An algorithm that keeps going to perform an SBA, the public can use the free software package AUTO2000. To determine all potential trim results for system considering one free control parameter remains adjusted though the others are held constant, the SBA technique employs a continuation algorithm. The local-stability details indicated using each trim point is likewise computed by the continuation algorithm.

Bifurcation Diagram: Global performance of a system can be represented by its bifurcation diagram, which is a two-dimensional projection for calculated trim-solutions with the relation with variable control-parameter. The 'Bifurcation Points' for branch with trim results occur with the nodes at which the branch loses stability. Unstable dynamical behavior can occur at bifurcation points, which are associated with the transition across the complex plane's left-to-right axis for system eigenvalues.

Analysis Procedure involved in the Bifurcation Method can be summarized as follows:

- Represent the dynamical system as a set of first-order ODE's.
- Fix all parameters but one (continuation parameter)
- Determine equilibrium states and their stability with a changing continuation parameter using a continuation algorithm.
- Repeat the steps for the various values of the fixed parameters.
- Use bifurcation diagram to infer global dynamical behavior.

Advantages: The benefits of using a bifurcation analysis method are:

1. It is equally straightforward to investigate any high-order dynamical system $\dot{x} = f(x, U)$ for a variety of nonlinear functions f. For example, to do a bifurcation assessment for aircraft equipped through CAS, heavily envhanced aircraft models are investigated.

2. With the help of bifurcation analysis, we can determine that there are several coexisting trims states x^* for a given value of u and P.

3. Bifurcation analysis is greatly aided by the continuation algorithm's capacity to calculate data on the trim and periodic solution's local stability at each iteration.

4. Diverse bifurcation corresponds to the initiation of distinct state dynamics; therefore one can use bifurcation study to foresee how the system will act; for example, one can use the Hopf bifurcation to predict wing rock or an unstable phugoid, and one can use the pitchfork bifurcation to predict a departure in flight dynamics.

1.6.3 Flight Control Systems

For many reasons, flight control problems for Hypersonic Vehicles goes far beyond the difficulties encountered with the previous aircraft and spacecraft designs. The control obstacles such as with the other high-performance aircraft like, hypersonic vehicles dynamics exhibit a nonlinear, multivariable, time-varying, non-minimum phase type of behavior. Most of the analysis will have to be best approximated such that FCS of the AHV will possibly have to operate using a simplified model of the system which includes some uncertainty in the parameters. Approaches and control methods which can be used for this advanced control, should recognize the change in dynamics and adapt to these changes in real time application. Advanced control design techniques can be used to design and handle the non-linear complexity of the problem. An adaptive method can be used for designing the controller for the nonlinear flight dynamics. Intelligent control techniques can be designed to provide robust flight control using optimization techniques, and guaranteed stability of the system. AHVs dynamics and control presents a major concern with the FCS design due to the dynamic behaviour and extremely coupled nonlinear nature. AHVs control design should provide stability to the FCS and, consistent performance and robustness, as AHVs are enormously subtle to atmospheric conditions and aerodynamic parameters. Control design performance is difficult to achieve with the best performance with all the flight regimes and flight conditions, and so the control design schemes need to be adaptive. In the open literature, mostly longitudinal dynamics of AHV is used for the hypersonic flight analysis for control design, as it is unstable, has non-minimum phase and has model uncertainty. For the control system design, models like longitudinal dynamics model, control-oriented model and 6DOF rigid-body model, and other different models discussed in the previous section are used for the stability and controller

design. The different controllers designed for the AHVs can be broadly characterized and represented using Fig. 1.7.
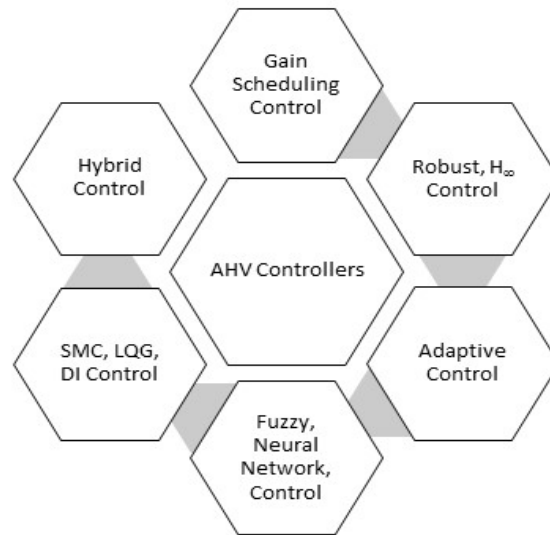
Fig. 1.7 AHV different control techniques

1.7 Thesis Organization

Thesis outline of this research is categorized with seven chapters. This chapter presents the overview and introduction to the Hypersonic Vehicles. It shows how Bifurcation Method can be used to implemented, and analysis for flight dynamics and control analysis as a tool. It also highlights the research objectives of the work with research methodology carried out.

Chapter 1 presents introduction to the research and background of Air-breathing Hypersonic Vehicle with flight dynamics analysis overview. It also presents Bifurcation Method Analysis to flight dynamics and control analysis applications and introduction. It outlines the methodology used for the research objectives as mathematical modelling and simulation, bifurcation investigation with controller design.

Chapter 2 features literature review for different Air-breathing Hypersonic Vehicle models used over the decades, its flight control system design with different classical and advanced control techniques, and Bifurcation Method implementation to different aircraft models.

Chapter 3 presents dynamic AHV model introduction, description, and model development. It also outlines the development of 3DOF nonlinear model and

6DOF linear model with the aerodynamic model. It discusses the AHV propulsion model development and different operating flight conditions consideration and, with the validation of the model.

Chapter 4 presents Flight dynamic analysis for different sonic velocity conditions using high-altitude with Mach number. It also presents the nonlinear simulation of the generic AHV, model trim analysis and flight dynamic stability of the model using trim analysis.

Chapter 5 presents the bifurcation analysis of generic AHV for longitudinal dynamics and its implementation using AUTO-07p software platform. Flight dynamic analysis for different operating conditions using bifurcation method is carried out.

Chapter 6 presents the closed loop simulation of the AHV model and flight dynamic analysis for different control inputs. It also presents the open loop simulation with stability analysis followed by control design using state feedback method.

Chapter 7 provides conclusion and summary of the research findings, as well as its significance to the Hypersonic Technology. It also outlines the limitation and future research in context to society benefit and developments to achieve SSTO flights in achieving LEO and other Space missions.

CHAPTER 2
LITERATURE REVIEW

The development phase for an AHV has restarted multiple times, with each project addressing a different difficulty. This has spawned some truly excellent writing on the subject, but it has also left some glaring gaps between the decades in which the topic has been revived. In the 1960s, researchers sought to perfect a rocket-powered launch vehicle resembling a wave rider. Although rocket propulsion was set to be replaced by the advent of scramjet engines in the 1970s. It took another two decades to perfect the scramjet program, which was already an extremely ambitious endeavor. The many obstacles presented by scramjets had to be overcome once they were accepted as a practical choice. The aero-propulsive effects challenge was tackled first in the 1990s. However, the aerodynamics could only be modelled using Newtonian impact theory, and the structural modelling was limited to a free-free Euler-Bernoulli beam. Propulsion system modelling shifted from adding heat to a dual-mode scramjet through a constant-area, frictionless duct, and aerodynamics modelling progressed from Newtonian impact concept to oblique shock theory with viscous effects.

Design stages for AHV has undergone multiple iterations, with each phase tackling different challenges. This has generated a lot of writing on the subject, but the topic has been rebooted so many times over the years that there are still some information gaps. The development of a rocket-powered wave-rider launch vehicle was a top priority in the 1960s. Emphasis shifted to scramjet based propulsion in 1970s as a replacement for rockets, but it took another 20 years to perfect them. Once scramjets became a viable option, the next challenge was to address their various issues. The aero-propulsive effects were studied in the 1990s, however only a simple Euler-Bernoulli beam was modelled for the structure, and Newtonian impact theory was used for the aerodynamics. There has been a lot of development during the previous two

decades for AHV modeling. Aerodynamics modeling has evolved to include viscous effects and oblique shock theory, and with heat added to a frictionless conduit of constant area, the modelled propulsion system has developed into a dual-mode scramjet engine.

2.1 Historical Developments - Hypersonic to AHVs

This section describes advancement to hypersonic technology and models from inception. Conception of hypersonic flight appeared in late 1930s, and Eugene Sanger with his wife Irene Bredt realized the first conceptual hypersonic design with rocket powered using enhanced glide design called as Silbervogel (Silver Bird) as stated in [18] in 1938, is shown in Fig. 2.1 (a). It was developed as space transporter and worldwide attack aircraft and was first comprehensive investigation and requisite of SSTO hypersonic vehicle. The Sanger-Bredth perceptive methodology of global hypersonic flight worked as a benchmark for the upcoming hypersonic research, and it led the way-forward for many future aerospace vehicle designs.

Vehicle X-15 design shown in Fig. 2.1 (b) in [19], gave the hypersonic study an incremental rise ahead in its time. It features fuselage (long), wings (short) and small rocket engines for steering, achieved Mach 6.7 hypersonic speed and reached at the edge of the outer space, as stated in [20]. This proved useful for the X-15 with a high-altitude hypersonic platform for future research. The modified version of X-15 are X-15-1, X-15-2 (later X-15A-2) and X-15-3 were used to achieve different research goals in [21]. The program was carried out from 1955 to 1968 by the joint effort of the NASA, USAF and US Navy in [22]. During its development period the developed hypersonic models of X-15 was used to design missiles and spacecraft in the later years, such as Space Shuttle. X-15 is a mid-wing monoplane, with a slender cylindrical fuselage, and with a wedge-shaped vertical stabilizer and was equipped with a unique landing gear in [23]. It was the first piloted entry vehicle, as stated in [24] and X-15 hypersonic flight research provided current research in rocket propulsion technology, like thrust modulation, reusability and rocket engines, and these technologies advanced in Apollo and Space Shuttle programs.

Vehicle X-20 shown in Fig. 2.1 (c) in [25] represents hypersonic flight with boost-glide technology and with delta wing configuration for reusable space access. It was developed as Space weapon system and was called Dyna-Soar for 'Dynamic Ascent' and 'Soaring Flight' in [26]. The X-20 concept initiated by Eugen Sanger in the year 1928 and improved in the coming years. The program was carried out from 1957 to 1963 by USAF. The program was terminated due to political, economic and administrative reasons in 1963. X-20 was the first boost-glide space-plane program designed for military application to space access and for future military piloted space capabilities, as stated in [26]. Its objective was to discover and establish maneuverable re-entry of piloted orbital space-vehicle resulting in controlled landing at selected landing site. The X-20 was equipped with dynamically flying capability, controlled equilibrium flight and aerothermodynamic technology with wide-ranging maneuverability at hypersonic speeds. It provided a platform for the different advanced technologies for the upcoming projects i.e., Space Shuttle and many of its subsystem designed into the X-15 research flight.

Vehicle X-30 was originally considered a feasible study for the SSTO vehicle using air-breathing technology with the capability of horizontal take-off and landing is shown in Fig. 2.1 (d), in [27]. The program was carried out from 1986 to 1994 by the joint effort by NASP and DARPA, and was called Copper Canyon. The initiative got terminated for the budget reduction and methodological anxieties in 1993. The engine configuration includes the combined cycle propulsion with the ramjet and scramjet, and tail part of the vehicle is attached with the rocket in [28]. X-30 is equipped with tail rocket which provides the orbital insertion propulsion and thrust augmentation for the atmospheric flight in [28]. X-30 has integrated air vehicle with propulsion systems, intricate integrated controls, waverider aerodynamic configuration in [29], and is designed to accelerate and achieve LEO with speed of 25 times of sound.

Vehicle SKYLON is SSTO aerospace plane with extremely advanced SABRE idea for transportation to LEO is shown in Fig. 2.1 (e) in [30]. The project is the new era towards the future advanced space transportation with SSTO capability developed by REL using the AHV propulsion technology and

SABRE. The program started in the early 1980s to the present date, leading to the innovatory pathway to space access and the hypersonic transportation a reality. SKYLON engine is incorporation of an air-breathing and with rocket engine with minimum replication of the equipment in [30]. SKYLON SABRE has increased thrust-to-weight proportion in comparison with the different AHV concepts with low specific impulse in [30]. SKYLON SABRE engine technology is capable of powering re-usable SSTO vehicles providing efficient way to the orbit in [31].

Vehicle Hyper-X initiative was started to overcome the dominant hypersonic study challenges prominent to AHV developments as shown in Fig. 2.1 (f) in [32]. The program started from 1995-1996 by NASA, with a major step in scramjet propulsion and in hypersonic research, leading to easy access to space, as stated in [33]. The X-43 program successfully achieved the cruising thrust at 9.68 Mach. The Hyper-X technology has the prospective to reduce cost with high safety and mission flexibility for future SSTO or TSTO access to space, as stated in [34]. The X-43A with its Pegasus booster was used to accelerate to the speed of Mach 7 and the project was terminated due to the lost control into the area of Pacific Ocean, as stated in [35]. The X-43B project was proposed to launch with a RBCC and TBCC, by combining both propulsion together to achieve Mach 0.7 to 7 hypersonic speed in [35]. The X-43C is a joint project with NASA and USAF with dual mode scramjet propulsion design using hydrocarbon fuel for hypersonic powered flight accelerating from Mach 5 to 7 and is premeditated for the future AHV for space.

Vehicle FALCON program has developed a series of HTV's, in which the HTV-3X shown in Fig. 2.1 (g) in [36] uses hydrocarbon fuel and the far term FALCON HCV shown in Fig. 2.1 (h) in [36] uses hydrogen fuel. The FALCON program started in 2003 by USAF and DARPA, to progress, promote and validate the hypersonic technologies which would lead to global reach missions. The HTV-3X provided the platform for the needed integrated technology for the air-breathing hypersonic aircraft. The FALCON HCV is an investigation vehicle with global reach and with reusable space entry application. The HTV-3X basic aerodynamic shape progressed from the waverider shape of the FALCON HCV. The HTV-3X objective is to create a

reusable hypersonic benchmark which employs an integrated AHV propulsion system and can accelerate up to the speed of Mach 6, as stated in [37].

Vehicle X-51 program shown in Fig. 2.1 (i) in [38] is a scramjet-powered vehicle called as SED was started as Hypersonic Technology initiative. The program laid its foundation in the mid 1990's and the X-51A SED started in 2005, by the joint effort of AFRL and DARPA with a major step in SED-Waverider vehicle concept, as stated in [39]. The objective of X-51 SED program is to achieve the vehicle accelerating speed from boost at 4.5+ Mach to 6+ Mach using endothermic hydrocarbon fuel. The X-51A SED is also called an AVD due to the inclusion of the cruiser, interstage and booster. The design of X-51A with waverider concept was technologically advancement for the ARRMD program, it uses JP-7 hydrocarbon fuel and achieved the speed of 6 Mach to 6.5 Mach, as stated in [39].

Vehicle HIFiRE initiative started for investigating the hypersonic flight using low-cost flight test approach utilizing sounding rockets, in progress and development with the upcoming new generation of hypersonic vehicles is shown in Fig. 2.1 (j) in [40]. The HIFiRE flights objective is to understand the environments in which the hypersonic flights must operate. The program HIFiRE carried out different successful flights in which HIFiRE-4 and HIFiRE-6 were fully dedicated for the hypersonic guidance and control of the vehicles, as stated in [41].
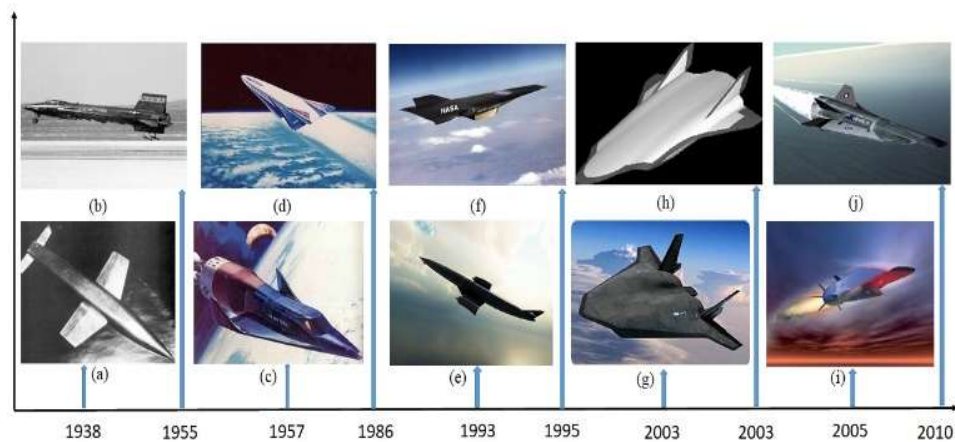
Fig. 2.1 (a) Sanger Silbervogel [18] (b) X-15 [19] (c) X-20 Dyna-Soar [25] (d) X-30 [27] (e) SKYLON C1 [30] (f) X-43 [32] (g) HTV-3X [36] (h) FALCON HCV [36] (i) X-51A [38] (j) HIFiRE-8 [40]

The HIFiRE-4 test primary focused on the flight data collection for aerodynamics, control and dynamic stability for hypersonic flight with an advanced waverider configuration. The initiative is joint collaboration of AFRL, US and with the DST of Australia in [42]. HIFiRE program comprised with widespread ground tests and HIFiRE-1 was successfully launched in March 2010 using ground launched sounding rocket.

This section shows the hypersonic development of the different vehicles from the 1930's to till date. Vehicles like X-15, X-20, X-30 have created a benchmark for the upcoming model design and developments. From the 1990s the pace of hypersonic vehicle development has increased, and it resulted in new research developments and different initiatives like Hyper-X, X-51, HTV-3X, SKYLON and HIFiRE to achieve the modern dreams of hypersonic flight.

2.2 Flight Dynamics & AHV Model Review

The research on flight dynamics for hypersonic vehicles in [43] presents the different models for winged-cone model like truth model, curve-fitted model, control-oriented model and re-entry model, and outlines potential challenges for the analysis of large flight envelop, aerodynamic effects, actuators dynamics, nonminimum phase and dynamics interaction. The mathematical models discussed in [44], shows that only dynamic characteristics are presented in open literature, and we need to include the integration and its issues with the other sub models. The propulsion model discussed in [45]-[46] with Scramjet propulsion shows that the studied configuration provides statically unstable in pitch and presents strong coupling in attitude dynamics with engine responses. During the past six decades the different flight dynamic models have been used for the modeling, simulation, control and stability analysis of hypersonic vehicles and are presented in the following section.

2.2.1 Longitudinal Dynamic Models

The Winged-cone Generic Hypersonic Vehicle (GHV) in [12] model is shown in Fig. 2.2 and development is carried by NASA, aimed to develop manned, horizontal takeoff and landing, approaches for SSTO configuration and conical accelerator. The GHV model is extensively used for the control approach and

its development for the AHVs. The longitudinal dynamics of the winged-cone GHV in [12] is represented by the dynamic model Eqn. (2.1-2.5) is extensively used for the hypersonic modeling and control. The non-linear longitudinal winged-cone GHV is discussed in [47] and model dynamics is given by,

$$\dot{V} = \frac{T\cos\alpha - D}{m} - \frac{\mu \sin\gamma}{r_E^2} \tag{2.1}$$

$$\dot{h} = V\sin\gamma \tag{2.2}$$

$$\dot{\gamma} = \frac{L + T \sin\alpha}{mV} - \frac{(\mu - V^2 r_E)\cos\gamma}{V r_E^2} \tag{2.3}$$

$$\dot{\alpha} = q - \dot{\gamma} \tag{2.4}$$

$$\dot{q} = \frac{M_{yy}}{I_{yy}} \tag{2.5}$$

The state variables are given by $x = [V\ h\ \alpha\ \gamma\ q]'$ and the controls as $u = [\delta_e\ \phi]'$. The aerodynamics force and moment coefficients C_L, C_D, C_M and M_{yy}, and L, D, T, r_E and $\overline{q}$ are referred from the winged-cone GHV model. And the control δ_e and ϕ input is given by, $C_T = 0.02576\ \phi$, for $\phi < 1$ and otherwise $C_T = 0.0224 + 0.00336\ \phi$, and $C_M(\delta e) = 0.0292(\delta e - \alpha)$ respectively.

The control-oriented modeling presented in [48] is achieved with the replacement of moment and complex forces with curve fitted approximation and by ignoring the weak coupling of the flexible AHV dynamics. The longitudinal model is enhanced with an actuator dynamics to improve the controlling of the AHV and ignoring, the elevator coupling zero due to weak occurrence, altitude and flexible states, and the dynamics of the model is presented using Eqn. (2.6-2.10).

$$\dot{V} = \frac{T\cos\alpha - D}{m} - g \sin\gamma \tag{2.6}$$

$$\dot{h} = V\sin\gamma \tag{2.7}$$

$$\dot{\gamma} = \frac{L + T \sin\alpha}{mV} - \frac{g \cos\gamma}{V} \qquad (2.8)$$

$$\dot{\alpha} = q - \dot{\gamma} \qquad (2.9)$$

$$\dot{q} = \frac{M_{yy}}{I_{yy}} \qquad (2.10)$$

A hypersonic cruise concept model in [49] shown in Fig. 2.2, with waverider design is proposed with the propulsion airframe integration methodology. It uses the concept of combined propulsion technique with turboramjets and scramjet. In [50] nonlinear physics based longitudinal model for the AHV is presented and complex interface between aerodynamics and propulsion is discussed. The AHV longitudinal vehicle nonlinear model equations are given by the dynamic model Eqn. (2.11-2.17),

$$\dot{V_t} = \frac{1}{m}(F_T \cos\alpha - F_D) - g \sin(\theta - \alpha) \qquad (2.11)$$

$$\dot{\alpha} = \frac{1}{mV_t}(-F_T \sin\alpha - F_L) + Q + \frac{g}{V_t}\cos(\theta - \alpha) \qquad (2.12)$$

$$I_{yy}\dot{Q} = M + \tilde{\psi}_1 \ddot{\eta}_1 + \tilde{\psi}_2 \ddot{\eta}_2 \qquad (2.13)$$

$$\dot{h} = V_t \sin(\theta - \alpha) \qquad (2.14)$$

$$\dot{\theta} = Q \qquad (2.15)$$

$$k_1 \ddot{\eta}_1 = -2\zeta_1 \omega_1 \dot{\eta}_1 - \omega_1^2 \eta_1 + N_1 - \tilde{\psi}_1 \frac{M}{I_{yy}} - \frac{\tilde{\psi}_2 \tilde{\psi}_1 \ddot{\eta}_1}{I_{yy}} \qquad (2.16)$$

$$k_2 \ddot{\eta}_2 = -2\zeta_2 \omega_2 \dot{\eta}_2 - \omega_2^2 \eta_2 + N_2 - \tilde{\psi}_2 \frac{M}{I_{yy}} - \frac{\tilde{\psi}_1 \tilde{\psi}_2 \ddot{\eta}_2}{I_{yy}} \qquad (2.17)$$

where $\eta_i, N_i, \zeta_i, \omega_i$ are the generalized elastic coordinates and forces respectively, damping coefficient and natural frequency of elastic modes respectively and detailing of dynamics can further be referred from [50]. The

conceptual project models of AHV analyzed over the decades are summarized in Fig. 2.2.

2.2.2 Lateral and Longitudinal Dynamic Models

A 3-Dimensional Vehicle Simulation Framework model in [51] is shown in Fig. 2.2 with parameterized vehicle geometry is designed to assess the GHV controllability traits, configuration tradeoffs and control designs. It presents the six degree of freedom GHV model developed using rigid-body motion equations based on Newtonian method and with one dimensional propulsion model. The dynamics of the GHV model is given by the dynamic model Eqn. (2.18-2.23).

$$\dot{u} = (rv - qw) + \frac{F_{B,x}}{m} \tag{2.18}$$

$$\dot{v} = (pw - ru) + \frac{F_{B,y}}{m} \tag{2.19}$$

$$\dot{w} = (qu - pv) + \frac{F_{B,z}}{m} \tag{2.20}$$

$$\dot{p} = \frac{(I_{yy} - I_{zz})qr + M_{B,x}}{I_{xx}} \tag{2.21}$$

$$\dot{q} = \frac{(I_{zz} - I_{xx})rp + M_{B,y}}{I_{yy}} \tag{2.22}$$

$$\dot{r} = \frac{(I_{xx} - I_{yy})pq + M_{B,z}}{I_{zz}} \tag{2.23}$$

The translation and angular velocity are given by $\vec{V}_B$ and $\vec{\omega}_B$ with their components as u, v, w and p, q, r respectively, and I_{xx}, I_{yy}, I_{zz} are the moment of inertial components, with all components represented in the body frame. GHV model attitude and position is given by Euler angles and Earth fixed inertial frame respectively. The frame transformation T_{EB} matrix is the Body to Earth frame conversion and the kinematics for both attitude and position are given by Eqn. (2.24-2.25),

$$\left\{\begin{array}{c} \dot{\phi} \\ \dot{\theta} \\ \dot{\psi} \end{array}\right\} = \begin{bmatrix} 1 & \sin\phi\,\tan\theta & \cos\phi\,\tan\theta \\ 0 & \cos\phi & -\sin\phi \\ 0 & \frac{\sin}{\cos\theta} & \frac{\cos\phi}{\cos\theta} \end{bmatrix} \left\{\begin{array}{c} p \\ q \\ r \end{array}\right\} \tag{2.24}$$

$$\left\{\begin{array}{c} \dot{x}_E \\ \dot{y}_E \\ \dot{z}_E \end{array}\right\} = T_{EB}(\phi,\theta,\psi) \left\{\begin{array}{c} u \\ v \\ w \end{array}\right\} \tag{2.25}$$

The modelling technique with Parameterized Configuration in [52] methodology shows the possibility of integrated design of the AHV aerodynamics, scramjet propulsion and control method, given by Fig. 2.2. Model shows scramjet engine modelling designed to integrate air frame and propulsion for the engine model using experimental approaches. The 6-DOF AHV rigid model dynamics is given by the dynamic model Eqn. (2.26-2.37).

$$\dot{V} = (1/m)(T\cos\alpha\,\cos\beta - D) - (1/R^2)(G_M\sin\mu) \tag{2.26}$$

$$\dot{\mu} = (1/mV)[T(\cos\alpha\,\sin\beta\,\sin\gamma + \sin\alpha\,\cos\gamma) + L\cos\gamma - Y\sin\gamma] -$$

$$(1/VR^2)\,[(G_M - V^2R)\cos\mu] \tag{2.27}$$

$$\dot{\varphi} = (1/mV\cos\mu)[T(\sin\alpha\,\sin\gamma - \cos\alpha\,\sin\beta\,\cos\gamma) + L\sin\gamma + Y\cos\gamma] +$$

$$(1/R)(V\cos\mu\,\tan\phi_{lat}\,\sin\varphi) \tag{2.28}$$

$$\dot{R} = V\sin\mu \tag{2.29}$$

$$\dot{\phi}_{long} = (1/R\cos\phi_{lat})(V\cos\mu\,\sin\varphi) \tag{2.30}$$

$$\dot{\phi}_{lat} = (1/R)(V\cos\mu\,\cos\varphi) \tag{2.31}$$

$$\dot{p} = (c_1 r + c_2 p)q + c_3\overline{L} + c_4 N \tag{2.32}$$

$$\dot{q} = c_5 pr - c_6(p^2 - r^2) + c_7 M \tag{2.33}$$

$$\dot{r} = (c_8 p - c_2 r)q + c_4 \overline{L} + c_9 N \tag{2.34}$$

$$\dot{\phi} = p + (r \cos\phi + q \sin\phi)\tan\theta \tag{2.35}$$

$$\dot{\theta} = q \cos\phi - r \sin\phi \tag{2.36}$$

$$\dot{\psi} = (1/\cos\theta)(r \cos\phi + q \sin\phi) \tag{2.37}$$

Here V, μ, φ and γ called as velocity, angle-of-track, yaw angle, roll angle track respectively. Aerodynamics force and moment coefficients C_L, C_D, C_M, L, D, Y, $C_l, C_m, C_n, \overline{L}, M$ and N; thrust coefficient T, constants c_1 to c_9 are the coefficients of inertial component and geometric interactions is discussed in [52].

The Road Runner Model in [53] of the generic AHV shown in Fig. 2.2 is developed as a benchmark for the control system design and analysis. It presents the adaptive design approach for tracking and stability using gain schedule method and LQR PI controller. The model is small, unmanned, blended wing body and has 4 control surfaces comprising of 2 elevons and rudder each. The lateral and longitudinal dynamics of the model using state space approach is represented as $\dot{x} = f(X, U)$ and the states and control input are given by the dynamic model Eqn. (2.38-2.39).

$$X = [V_T \ \alpha \ q \ \theta \ h \ \beta \ p \ r \ \phi \ \psi \ \lambda \ \tau]' \tag{2.38}$$

$$U = [\delta_{th} \ \delta_{elv} \ \delta_{ail} \ \delta_{rud}]'. \tag{2.39}$$

Here V_T, α and β, are vehicle velocity, angle-of-attack and sideslip; λ, τ, h are model latitude, longitude and altitude respectively. Control matrix M is transformation matrix between the control input U_5 and U given by $U = MU_5$, with U_5 is defined as throttle, deflection of right and left elevons $(\delta_{r,elv}, \delta_{l,elv})$ and rudders $(\delta_{r,rud}, \delta_{l,rud})$ expressed using Eqn. (2.40).

$$U_5 = \begin{bmatrix} \delta_{th} & \delta_{r,elv} & \delta_{l,elv} & \delta_{r,rud} & \delta_{l,rud} \end{bmatrix}' \qquad (2.40)$$

The Geometry Generated Model in [54] shown in Fig. 2.2 is inspired by the Road Runner Model and is used in the advancement and analysis of control systems for the AHV and uses geometry approach for AHV design. The 6 DOF nonlinear model equations are used assuming the model is rigid. The dynamics of the model is given by the Eqn. (2.41-2.42) with the state space representation as $\dot{X}_v = f(X_v, U_v)$, where the state vector $X_v \in \mathbb{R}^{13}$ and control vector $U_v \in \mathbb{R}^5$ are given by,

$$X_v = [u\ v\ w\ p\ q\ r\ q_1\ q_2\ q_3\ q_4\ \lambda\ \tau\ R]' \qquad (2.41)$$

$$U_v = \begin{bmatrix} \varphi & \delta_{e1,r} & \delta_{e1,l} & \delta_{rud,r} & \delta_{rud,l} \end{bmatrix}' \qquad (2.42)$$

where u, v, w and p, q, r are the AHV airspeed and angular velocity component, and λ, τ and R are AHV's latitude, longitude and Earth distance from center respectively, and q_1, q_2, q_3 and q_4 are the quaternion components. Here $\varphi, (\delta_{e1,r}\ \delta_{e1,l})$ and $(\delta_{rud,r}\ \delta_{rud,l})$ are the engine fuel air equivalence ratio, elevon deflection of right and left, and rudder defection of right and left respectively.

The MAX-1 model in [55] shown in Fig. 2.2 is known as Michigan/AFRL Experimental 1 (MAX-1) is used for the analysis of the ascent of the GHV using Surrogate optimization, which uses the dual mode ramjet-scramjet propulsion engine. It implements using the assumption of the ellipsoidal shape Earth and gravity model for the equation of motions. 6-DOF rigid-body dynamics for model is given with $\dot{x} = f(x, u)$, here x and u are states and controls, respectively is represented by the model Eqn. (2.43-2.44). Here the states with their control input variables are expressed below.

$$x = [L\ \lambda\ h\ V\ \gamma\ \sigma\ \phi\ \alpha\ \beta\ P\ Q\ R]' \qquad (2.43)$$

$$u = [ER\ \delta_e\ \delta_a\ \delta_r]' \qquad (2.44)$$

Here L, λ and σ are the geodetic latitude, longitude and velocity heading angle and, δ_e and δ_a are the average deflection angle of elevator of lift and right, and the difference angle of right minus the left elevator angle, respectively.
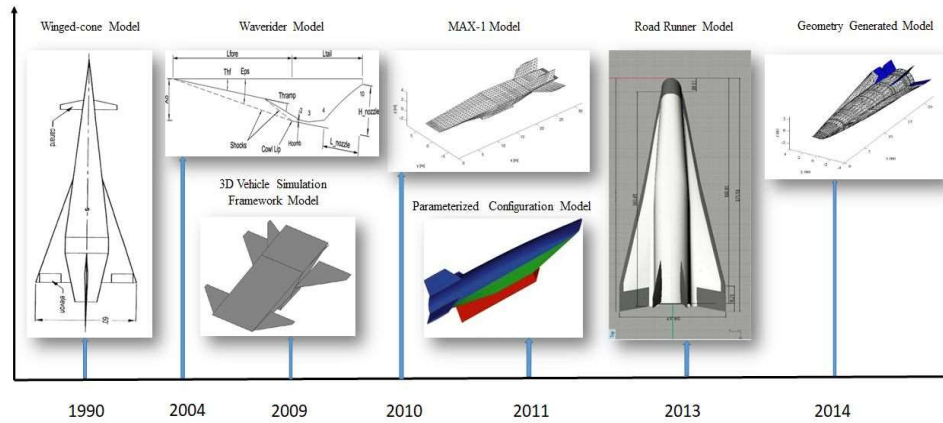
Fig. 2.2 Dynamic models design used over the decades for AHVs

We conclude that the dynamic model of the Winged cone is widely used for investigation of AHV, considering longitudinal model. Considering other models waverider model finds more usage. Hence, Winged cone, Road Runner and X-43A, are completely established models available to public for research and these models can be used in the study of flight dynamics and control systems.

2.3 Flight Control System Review

The dynamics and control of hypersonic vehicles that require propulsion technology is presented in numerous open literatures. The highly coupled and nonlinear character of the dynamic behavior of hypersonic vehicles presents a significant challenge for the design of flight control systems. To ensure flight control system stability and satisfactory control performance, however, controllers developed for hypersonic aircraft must travel at extremely high speeds. Maintaining good control performance under these circumstances is difficult, and adaptive control design approaches are required for optimal performance in any and all flight scenarios.

The limitations and open issues in current control-oriented models of AHVs are highlighted, and different associated control methods are presented.

Because of their complicated dynamic characteristics, uncharted flight situations, and stringent control requirements, AHVs require a control system that is highly maneuverable, durable, and adaptable. Many different control methods, such as small deviation linearization in [57], Gain Scheduling in [58], Linear Parameter Varying in [59], feedback linearization, Sliding Mode Variable Structure Control in [60], Backstepping in [61], Neural Network in [62], Fuzzy control in [63], Predictive control, artificial intelligence, and other hybrid methods are attempted due to the complexity of AHVs and the novel trends of modern control methods are magnificently presented, as stated in [56]-[63]. Despite years of study, the method for modelling the dynamics of AHVs is still evolving. Many researchers owe a debt of gratitude to NASA Langley Research Centre, which in 1990 created the first six-degrees-of-freedom model for AHVs and provided a plethora of supporting data. In 1994, Chavez and Schmidt developed a first-principles 3-DOF dynamic model for hypersonic vehicles that captures a variety of complex interactions. Both of the aforementioned models, however, were developed with a rigid body assumption that discounted the interplay between structural dynamics and aerodynamics. However, these models were not accurate representations of the true flying characteristics. Bolender and Doman [64]-[65], constructed a flexible nonlinear 3-DOF dynamic model from fundamental principles, taking into account the couplings between air, heat, elasticity, and the propulsion system in [66]-[67]. In [68], curve-fit approximations for complex force and moment functions and ignoring some weak couplings and slower portions of the system dynamics, a control-oriented model in closed form was developed, which is very helpful for the controller design. Despite the fact that scientists at home and abroad have put in a great deal of effort into modelling AHVs in recent years, the models in [68] continue to serve a pivotal part in the creation of controllers, as stated in [69]-[71].

Several academics have tackled the task of flight control design for such systems using various control design methodologies. Sliding mode control in [72], Linear Quadratic Gaussian control in [73], stochastic robust control in [74], and neural network adaptive control in [75] are just few of the recent feedback control strategies for the hypersonic vehicle that are grounded in

differential geometric nonlinear control theory. The problem with this approach is that the controller design requires precise understanding of the plant dynamics and repetitive analysis. In [72] multi input multi output (MIMO) adaptive sliding mode controller designs are developed, which is robust to parametric uncertainties and presents appropriate performance with relatively low-amplitude control inputs. Nonlinear control laws that are effective across the full range of flight are developed using nonlinear dynamic inversion (NDI) and Monte Carlo evaluation. In [75], we see an example of an adaptive MIMO controller for a hypersonic vehicle that employs neural network control techniques. In the event that the estimated plant loses controllability, the suggested neural adaptive controller ensures closed-loop stability and convergence of the tracking error. Combat air vehicles and missiles, both of which use flight control systems, can be converted to a strict-feedback form, and thus can benefit from the back-stepping design approach in [76], which gives an efficient solution to a large group of nonlinear systems with miss-matched conditions. However, "explosion of complexity" occurs with the back-stepping technique, wherein the controller's simplicity grows significantly as the order of the system increases. This is due to the recurrent differentiations of certain nonlinear functions.

The complexity introduced by back-stepping control technique is overcome by the use of Dynamic Surface Control (DSC) method in [77]-[78]. This technique uses a first order low pass filter at every step-in order to avoid the derivative of the nonlinear function. For the control of a hypersonic vehicle whose dynamics are unknown, a DSC-based system employing fuzzy logic and an adaptive technique is applied in [79]. Closed-loop designs for hypersonic vehicles benefit from methods like the neural network-based dynamical systems stability (DSS) technique for a class of nonlinear dynamic models. Robust variations of these techniques have also been developed for systems with modeling uncertainty. Nonlinear functions like parameter uncertainties and cross coupling effects are approximated using some of the techniques like radial basis function (RBF) neural network.

One effective solution to this issue is to implement an adaptive control law, as has been discovered through research. The nonlinear flight dynamics are

controlled by an adaptive technique using back-stepping and neural networks in [80], but back-stepping control techniques suffer from complexity of control laws, as stated in [77], [81]-[82]. Some control techniques like robust control and H∞ control have proven powerful design methods. In [66], advanced control technique of H∞ approach is used with μ synthesis. Intelligent control techniques can be designed to provide a robust flight control using optimization techniques, to guarantee stepwise stability of the system. Hence the control techniques are still in research phase and many more analysis are still in developing process for the hypersonic vehicles.

2.4 Bifurcation Method Review

The bifurcation method provides promising application for flight controls and its effective analysis of nonlinear phenomena occurring in the flight dynamics. Bifurcation technique can provide an improvement suggestion in the flight dynamics design procedure considerably. The significance of bifurcation method has a capability to present global stability and improvements of control design parameters for the aircraft. Bifurcation methods may be used to investigate the trim with stability for dynamical systems, involving nonlinear influences, computationally. With this method analysis, nonlinear behavior may be better understood since it keeps track of all trim points at which equilibriums are created or destroyed, or at which the stability of equilibriums varies.

Analysis of nonlinear AHV model using Bifurcation methods presents a new technique to understand the trim and stability of the dynamic system with the nonlinear properties. Nonlinear dynamics analysis of the aircraft in [83] shows the bifurcation and continuation method is used for the analysis of high alpha impact on aircraft stability and dynamic. The technique delivers quantitative data for global-stability and suggests ways for control of aircraft's nonlinear behavior. Application for bifurcation method is presented in [84] for the flight dynamics, outlines a beneficial method for analyzing and control of the dynamical systems. The method has remarkable prospective in the analysis of aircraft performance using wind tunnel data and excellent flight controls could be proposed for the system predicting dynamic behavior. Analysis of bifurcation method to nonlinear aircraft highlighting the problems of the flight dynamics

like roll coupling, stall, spin and others are deliberated in [85]. It discusses the stability of the aircraft equation of motions highlighting the equilibrium solutions, periodic solutions and regions of attraction. The method discussed, shows potential in closed loop analysis of nonlinear dynamics and, implementation and design of control technique is possible. Merits, demerits of the method with a development and implementation point of view for the aircraft is discussed and suggested in [86]. Review of computational methods and distinctive analytical approach for the method is presented, and aircraft control presents the promising area for the method analysis which can provide remarkable application using bifurcation technique with control methods. A computation technique for parameters of flight dynamics using continuation diagrams is presented in [87]. In [88], bifurcation with continuation method shows detailed theoretical 6 DOF nonlinear model of the aircraft for the analysis of dynamics and stability of the flight. Implementation of bifurcation method for flight controls is presented in [89] for 6 DOF nonlinear dynamics of F-16 for straight, level and coordinated turn. The bifurcation method using computational approach is discussed in [90] with nonlinear closed-loop analysis and for controller design. In [91] bifurcation method is used with SMC to analysis the nonlinear 6 DOF F-18 aircraft model with high alpha. Different flight maneuvers are analyzed with the level flight operating condition, and robustness of the controller with the closed loop analysis is described. Nonlinear Dynamic Inversion based control law validation, analysis and design using bifurcation method with global stability is discussed in [92]. Extended Bifurcation Theory (EBA) in [93] outlines the study of open loop dynamics of the landing arrangement of F-18/HARV and shows the importance of bifurcation method in development and design phases of fighter aircraft. Analysis of bifurcation method is presented in [94] for the parafoil payload system showing the effects of trim and stability of the flight dynamics parameters. Analysis of bifurcation method to the 4 DOF flight model is carried out on the longitudinal dynamics and effect of parameters on autonomous parafoil payload delivery system model in [95] is observed. The nonlinear hypersonic vehicle dynamics is analyzed with the bifurcation and continuation method in [96] using the scheme of multi model and design of controller.

2.5 Chapter Summary

The literature survey reveals that deep research has been conducted in investigating the hypersonic vehicle model, control system design and bifurcation method application through different aircraft models.

On comparing all the models in the open literature, the ***Winged-cone***, *Roadrunner, X-43A and X-51A* six-DOF models are entirely established models which can be used for the flight dynamics analysis using bifurcation method and control design. The different other models are merely hypotheses at this point, even though they could be used as six-DOF models for the future control design. The all AHV models are shown in the Table 2.1.

The review of bifurcation method shows that the parameters used for the different systems with their dynamic model shown in Table 2.2, shows that elevator deflection (δ_e) is mostly considered as the BP (Bifurcation Parameter) for Bifurcation Method.

For many reasons, flight control problem for hypersonic vehicles goes far beyond the difficulties encountered with the previous aircraft in [97] and spacecraft designs.

Table 2.1 Summarized 6-DOF AHV Model

Model	Year	Reference
Winged Cone Model	1990	[12]
Road Runner Model	2013	[53]
MAX-1 Model	2010	[55]
Geometry Generator Based Model	2014	[54]
Waverider Model	2005	[49]
Huifeng Model	2011	[52]
Frendreis Model	2009	[51]
NASA'S X-43A	2006	[33]
NASA'S X-51A	2014	[39]

Table 2.2 Bifurcation Parameters for different Systems

Sr. No.	System	Bifurcation Parameter	Dynamic Model
1	F-16 Aircraft	Velocity and δ_e	6 DOF
2	F-18/HARV Aircraft	δ_e	6 DOF
3	F-8 Crusader Aircraft	δ_e	3 DOF
4	High α flight Aircraft	δ_e	3 DOF
5	HHIRM	δ_e and δ_a, δ_r	5 DOF
6	Parafoil-Payload	δ, μ	4 DOF

The control obstacles such as with the other high-performance aircraft like, hypersonic vehicles dynamics exhibit a nonlinear, multivariable, time-varying, non-minimum phase type of behaviour. Most of the analysis will have to be best approximated so that AHVs FCS will possibly have to operate using a simplified model of the system which includes some uncertainty in the parameters in [98]. Design techniques and stability for control are in research phase and many more analysis are still in developing process for the AHVs. These challenges and issues in the design of controllers for the AHVs faced by the control law development can be highlighted by the Fig. 2.3. It discusses the control issues focusing on the complete maneuver control of AHVs in widespread flight envelop involving the climbing, cruising, re-entry, and inter-shifting regimes stages of the flight trajectory.
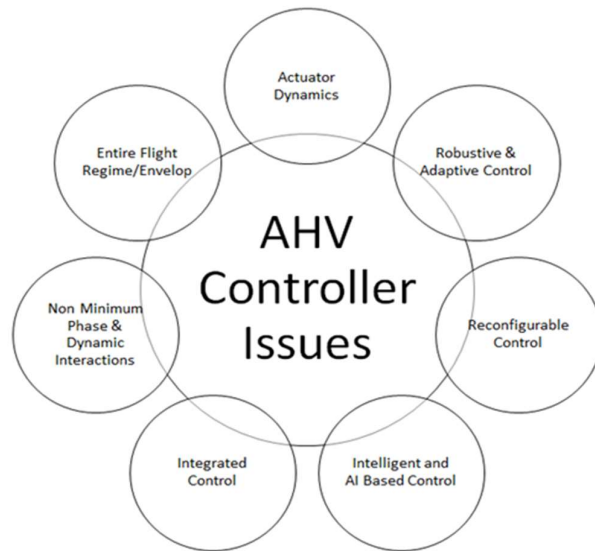
Fig. 2.3 AHV controller issues

The conclusion from the controller design for the AHVs shows that, advanced control methods can be used, and should recognize the change in dynamics and adapt to these changes in the real time application. Advanced control design techniques can be used to design and handle the non-linear complexity of the problem. The adaptive based control technique is preferred for designing the control for the nonlinear flight dynamics. And Intelligent control techniques can be designed to provide a robust flight control using optimization techniques, and guaranteed stability of the system.

The literature survey presents the following *main gaps* which still need to be overcome.

- The dynamic couplings due to integration and interaction problems between systems also need to be solved to the effects of hypersonic speed in any AHV model or control scheme.

- The AHV propulsion, and its interactions for the entire flight regime with Mach number variation provides challenges in the control design.

- The modeling of AHV discussed in the open literature is constrained by the reality for the hypersonic vehicle, dynamics is restricted to flight regime.

- The problems lying in hypersonic flight with large flight envelop and dynamics interaction finds limited research in the open literature.

- Coupling of inputs and outputs, non-minimal phase instability, flexible-modes, and control limitations are common problems in controller design for hypersonic vehicles.

- Bifurcation analysis for the nonlinear AHV model for different flight regimes finds limited study using continuation algorithm.

CHAPTER 3

DEVELOPMENT OF DYNAMIC AHV MODEL

NASA Langley Research Centre developed Generic Hypersonic Vehicle (GHV) simulation model called Winged Cone Configuration in [12] is shown in Fig. 3.1. The model is based on rigid body mass assumption and is used to investigate the hypersonic research improvement and assessment of design concepts, guidance, flight, propulsion, control systems, trajectory optimization, stability and methods for SSTO. The model is integrated with the propulsion system including ramjet and scramjet propulsion system.

3.1 Vehicle Description

The flat Earth approximation is applied for modeling and dynamic simulation of AHV model. The winged cone model is modelled as axis symmetric. The wings and vertical tail is aligned with the center axis of the model. The control surfaces of the model are defined as left elevon, right elevon, canard and rudder. The canard is deployed at subsonic speed to improve longitudinal stability and control. Deflections of the canard are measured in relation to the centerline of the fuselage, with a positive value indicating a downward tilt of the trailing edge. At high sonic velocities (hypersonic) canard fins are placed inside the vehicle body and has negligible impact for high sonic flight velocities. The vertical tail is hinged 25 percent of the chord from the trailing edge and is positioned in the centre of the fuselage. Positive rudder deflections with the trailing edge to the left are considered an elevon deflection about the rudder's hinge line. Gross weight of the vehicle is 300,000 lbs. Also the fuel slosh is ignored and cross coupling of inertia is considered insignificant. Generic AHV model is integrated with propulsion system including ramjet and scramjet propulsion system, and also with rocket engine. The geometric considerations of generic AHV model are specified within Table 3.1.

(a)

(b)
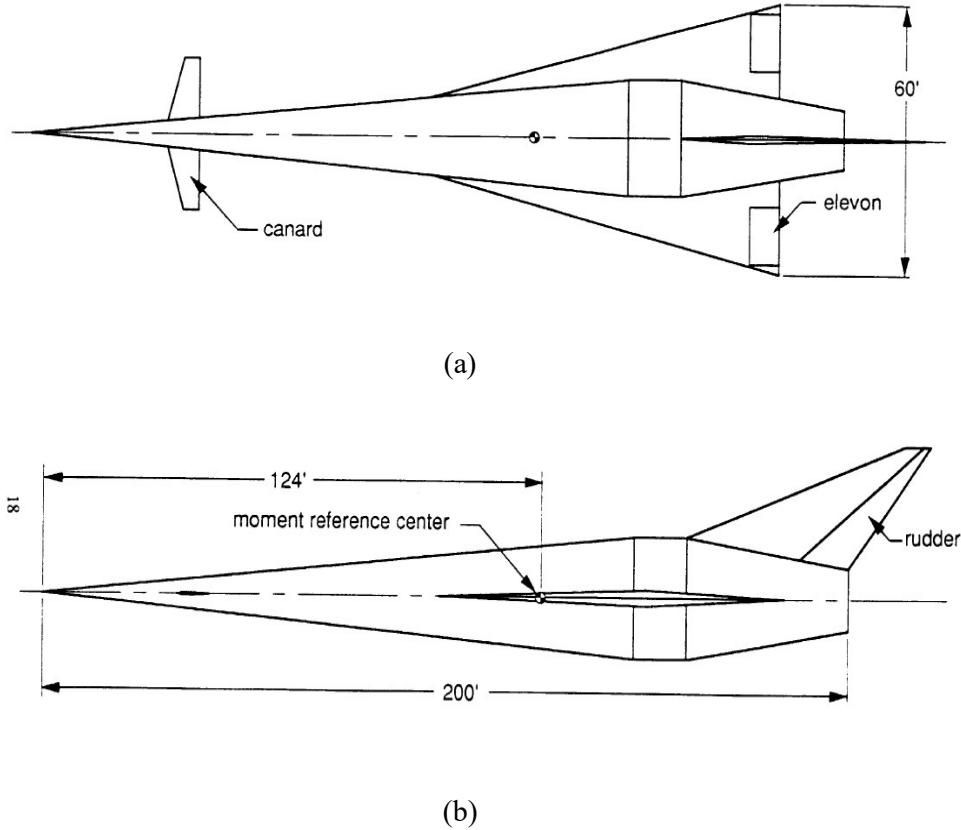
Fig. 3.1 The GHV model (a) top view (b) side view, [12]

Table 3.1 Geometry Parameters

Notation	Parameter	Value	Unit
m	Mass	136080	Kg
S	Wing Reference Area	334.7295	m^2
b	Wing Span	18.2880	m
c	Mean Aerodynamic Chord	24.384	m
x_{mrc}	Moment Reference Centre	37.7952	m
g	Gravity	9.8	m/sec^2
T_{max}	Maximum Thrust	1467900	N
I_{sp}	Specific Impulse	1000	$g\ sec$

3.2 Equation of Motions

For the purposes of the AHV model simulation, a flat Earth approximation is adopted. The aerodynamic and proportional force $F_{A,P}$ as well as the gravitational force mg are incorporated into the governing equations of flight.

The transitional equations in terms of ordinary time derivatives can be represented in body-coordinate as $]^B$ and is given by Eqn. (3.1), as stated in [15]-[16].

$$m\left[\frac{dv_B^V}{dt}\right] + m[\Omega^{BE}]^B[v_B^E]^B = [F_{A,P}]^B + m[g]^B \tag{3.1}$$

The quantity $[g]^B$ is modelled with as $[g]^L = [0 \quad 0 \quad g]$ for the gravitational acceleration. Therefore, Eqn. (3.2) represents the matrix form of the transitional equations.

$$m\left[\frac{dv_B^V}{dt}\right] + m[\Omega^{BE}]^B[v_B^E]^B = [F_{A,P}]^B + m[T]^{BL}[g]^L \tag{3.2}$$

Expressing the relation given by Eqn. (3.2) in coordinate form is obtained using Eqn. (3.3).

$$m\left\{\begin{bmatrix} du/dt \\ dv/dt \\ dw/dt \end{bmatrix}^B + \begin{bmatrix} 0 & -r & q \\ r & 0 & -p \\ -q & p & 0 \end{bmatrix}^B \begin{bmatrix} u \\ v \\ w \end{bmatrix}^B\right\} = \begin{bmatrix} F_{A,P1} \\ F_{A,P2} \\ F_{A,P3} \end{bmatrix}^B + [T]^{BL}\begin{bmatrix} 0 \\ 0 \\ mg \end{bmatrix}^L \tag{3.3}$$

Were,
$$[T]^{BL} = \begin{bmatrix} t_{11} & t_{12} & t_{13} \\ t_{21} & t_{22} & t_{23} \\ t_{31} & t_{32} & t_{33} \end{bmatrix}^{BL}$$

The Eqn. (3.3) in scalar form is expressed using the following Eqn. (3.4)-(3.6).

$$\frac{du}{dt} = rv - qw + \frac{F_{A,P1}}{m} + t_{13}g \tag{3.4}$$

$$\frac{dv}{dt} = pw - ru + \frac{F_{A,P2}}{m} + t_{23}g \tag{3.5}$$

$$\frac{dw}{dt} = qu - pv + \frac{F_{A,P3}}{m} + t_{33}g \tag{3.6}$$

Considering the Eqn. (3.7) transformations can be performed for yaw, pitch and roll (ψ, θ, ϕ respectively) to desired coordinate frame.

$$[T]^{BG} = [T(\phi)]^{BY}[T(\theta)]^{YX}[T(\psi)]^{XG} \tag{3.7}$$

Euler's law determines the degree of freedom (DOF) of rotation by stating that the rate of change of angular momentum over time equals the externally applied moments. The body axis coordinate system is used as a coordinate system because it gives a fixed value for the moment of inertia tensor from [15]-[16] and inertial frame of reference (E), is given by Eqn. (3.8) and Eqn. (3.9).

$$[I_B^B]^B \left[\frac{dw^{BE}}{dt}\right]^B + [\Omega^{BE}]^B [I_B^B]^B [\omega^{BE}]^B = [M_B]^B \tag{3.8}$$

$$\left[\frac{dw^{BE}}{dt}\right]^B = ([I_B^B]^B)^{-1}(-[\Omega^{BE}]^B [I_B^B]^B [\omega^{BE}]^B + [M_B]^B) \tag{3.9}$$

In the case of a flat Earth, the wind and thrust forces, as well as the momentums, are shown using a body coordinate system and are given by Eqn. (3.10) and Eqn. (3.11).

$$[F_{A,P}] = \begin{bmatrix} \bar{q}SC_X + F_P \\ \bar{q}SC_Y \\ \bar{q}SC_Z \end{bmatrix} \tag{3.10}$$

$$[M_B]^B = \begin{bmatrix} \bar{q}SbC_l \\ \bar{q}ScC_m \\ \bar{q}SbC_n \end{bmatrix} \tag{3.11}$$

The nonlinear model of the AHV can be given by the Eq.

$$\dot{u} = rv - qw + \frac{F_{A,X} + F_{P,X}}{m} - g.\sin\theta \tag{3.12}$$

$$\dot{v} = pw - ru + \frac{F_{A,Y}}{m} + g.\cos\theta \tag{3.13}$$

$$\dot{w} = qu - pv + \frac{F_{A,Z}}{m} + g.\cos\theta \tag{3.14}$$

$$\dot{p} = c_1 qr + c_2 pq + c_3 L_a + c_4 N_a \tag{3.15}$$

$$\dot{q} = c_5 pr - c_6(p^2 - r^2) + c_7 M_a \tag{3.16}$$

$$\dot{r} = c_8 pq - c_2 qr + c_4 L_a + c_9 N_a \tag{3.17}$$

$$\dot{\phi} = p + q.\sin\phi.\tan\theta + r.\cos\phi.\tan\theta \tag{3.18}$$

$$\dot{\psi} = q.\sin\phi.\sec\theta + r.\cos\phi.\sec\theta \tag{3.19}$$

$$\dot{\theta} = q.\cos\phi - r.\sin\phi \tag{3.20}$$

$$\dot{h} = u.\sin\theta - v.\sin\phi.\cos\theta - w.\cos\phi.\cos\theta \tag{3.21}$$

The control surfaces of AHV are given by δ_e, δ_a, and δ_r as right elevon, right elevon, and rudder deflection. The elevon (left and right) relation to aileron and elevator deflection is developed using the relation as $\delta_{left\_e} = \delta_a + \delta_e$ and $\delta_{righ\_e} = -\delta_a + \delta_e$.

3.2.1 3DOF Longitudinal Nonlinear Model

The generic AHV model is centered on the theory of rigid model structure combined with flat Earth approximation. Flat Earth approximation is applied in modeling and simulation of AHV model using in [15]. Centres of mass, centres of gravity, and moments of inertia that change over time are incorporated into a simulation model using the equations of motion. Mass of generic AHV, center of gravity location and products of inertia vary as fuel is consumed. Center of gravity moves only along the body x axis as the fuel is consumed. Model configuration of the thrust applied is adjusted with body x axis. And in body y axis and z axis no T force is applied.

The model is modelled to 3DOF AHV model in [16] with the state variables defined as the states as $V, \gamma, q, \theta, R \text{ and } h$. Longitudinal dynamics and kinematic equations of the generic AHV model is given by Eqn. (3.22-3.28).

$$\dot{V} = \frac{1}{m}(T \cos\alpha - \bar{q}SC_D - mg \sin\theta) \tag{3.22}$$

$$\dot{\gamma} = \frac{1}{mV}(T \sin\alpha + \bar{q}SC_L - mg \cos\theta) \tag{3.23}$$

$$\dot{q} = \frac{M}{2I_{yy}} \tag{3.24}$$

$$\dot{\theta} = q \tag{3.25}$$

$$\dot{R} = V \cos\theta \tag{3.26}$$

$$\dot{h} = V \sin\theta \tag{3.27}$$

We can use the relation $\alpha = \theta - \gamma$, to obtain the $\dot{\alpha}$ and is given by the Eqn. (3.28).

$$\dot{\alpha} = q - \left(\frac{1}{mV}\right)(T \sin\alpha + \bar{q}SC_L - mg \cos\theta) \tag{3.28}$$

3.2.2 6DOF Linear Model

The model is based with stiff model structure and flat Earth approximation theory. The AHV model's six degrees of freedom are modelled and simulated using a flat Earth approximation in [15]. Simulation model incorporates time varying center of mass, gravity, and inertia using equations of motion. As fuel is used, the center of gravity shifts exclusively in the x direction of the body. The model's thrust arrangement may be tweaked using the body's x axis. The y and z axes of the body are free of any T (thrust) forces. AHV flight dynamics model in [15] are provided by Eqn. (3.29-3.37).

$$m\dot{u} = rv - qv - g.\sin\theta + F_{ax} + F_{Tx} \qquad (3.29)$$

$$m\dot{v} = pw - rv + g.\cos\theta + F_{ay} \qquad (3.30)$$

$$m\dot{w} = qu - pv + g.\cos\theta + F_{az} \qquad (3.31)$$

$$\dot{p} = c_1 qr + c_2 pq + c_3 L_a + c_4 N_a \qquad (3.32)$$

$$\dot{q} = c_5 pr - c_6(p^2 - r^2) + c_7 M_a \qquad (3.33)$$

$$\dot{r} = c_8 pq - c_2 qr + c_4 L_a + c_9 N_a \qquad (3.34)$$

$$\dot{\phi} = p + q.\sin\phi.\tan\theta + r.\cos\phi.\tan\theta \qquad (3.35)$$

$$\dot{\theta} = q.\cos\phi - r.\sin\phi \qquad (3.36)$$

$$\dot{h} = u.\sin\theta - v.\sin\phi.\cos\theta - w.\cos\phi.\cos\theta \qquad (3.37)$$

The model given by Eqn. (3.29-3.31) are modelled in the wind axis and are represented with V, α and β using the following relations.

$$\dot{V} = \frac{1}{V}(u\dot{u} + v\dot{v} + w\dot{w}) \qquad (3.38)$$

$$\dot{\alpha} = (u\dot{w} - w\dot{u})/(u^2 + w^2) \qquad (3.39)$$

$$\dot{\beta} = ((u^2 + w^2)\dot{v} - v(u\dot{u} + w\dot{w}))/V^2\sqrt{u^2 + w^2} \qquad (3.40)$$

Here the relation between the components are given as $u = V\cos\alpha.\cos\beta$, $v = V.\sin\beta$, $w = V.\sin\alpha.\cos\beta$, $V = |V| = \sqrt{u^2 + v^2 + w^2}$ and, the angles are given by, $\alpha = \tan^{-1}(w/u)$, and $\beta = sin^{-1}(v/V)$. The constants c_1 to c_9 are the inertial constants which are dependent on the moments of inertia in [15]. The AHV model using the above Eqn. (3.38-3.40) and Eqn. (3.32-3.37) are represented by states described as $[V, h, \alpha, \theta, q, T, \beta, \phi, p, r]'$. Here T is the thrust model with engine of the AHV and is discussed in the later section.

3.3 Development of Aerodynamic Model

The aerodynamic model is developed from Appendix A, for the aerodynamics coefficient with the equations used and as stated in [13], to determine the aerodynamic model C_L, C_D, C_m, C_Y, C_l and C_n, are represented by Eqn. (3.41-3.52) for wide flight regime of AHV, and the data generated is given in Appendix A1. MATLAB is used to simulate the data from Appendix A1 by writing a subroutine and performing interpolate. Forces expressed as lift force is given by $L = \bar{q}SC_L$, drag force is given by $D = \bar{q}SC_D$, side force is given by $Y = \bar{q}SC_Y$, the rolling moment given with $L_a = \bar{q}SbC_l$, the pitching moment is given as, $M_a = \bar{q}cSC_m$ and the yawing moment is given by $N_a = \bar{q}SbC_n$. The nonlinear aerodynamic coefficient equations of the 6DOF dynamic simulation model of AHV is given by Eqn. (3.41-3.52),

$$C_L = f(M, \alpha, \delta_e, \delta_a) \qquad (3.41)$$

$$C_L = C_{L,\alpha} + C_{L,\delta e} + C_{L,\delta a} + C_{L,\delta r} \qquad (3.42)$$

$$C_D = f(M, \alpha, \delta_e, \delta_a, \delta_r) \qquad (3.43)$$

$$C_D = C_{D,\alpha} + C_{D,\delta e} + C_{D,\delta a} + C_{D,\delta r} \qquad (3.44)$$

$$C_{mq} = f(M, \alpha, \delta_e, \delta_a, \delta_r) \qquad (3.45)$$

$$C_m = C_{m,\alpha} + C_{m,\delta e} + +C_{m,\delta a} + C_{m,\delta r} + C_{mq}\left(\frac{qc}{2V}\right) \qquad (3.46)$$

$$C_Y = f(M, \alpha, \beta, \delta_e, \delta_a, \delta_r) \qquad (3.47)$$

$$C_Y = C_{Y,\beta}.\beta + C_{Y,\delta e} + C_{Y,\delta a} + C_{Y,\delta r} \qquad (3.48)$$

$$C_l = f(M, \alpha, \beta, \delta_e, \delta_a, \delta_r) \qquad (3.49)$$

$$C_l = C_{l,\beta}.\beta + C_{l,\delta e} + C_{l,\delta a} + C_{l,\delta r} + C_{lp}\left(\frac{pb}{2V}\right) + C_{lr}\left(\frac{rb}{2V}\right) \quad (3.50)$$

$$C_n = f(M, \alpha, \beta, \delta_e, \delta_a, \delta_r) \qquad (3.51)$$

$$C_n = C_{n,\beta}.\beta + C_{n,\delta e} + C_{n,\delta a} + C_{n,\delta r} + C_{np}\left(\frac{pb}{2V}\right) + C_{nr}\left(\frac{rb}{2V}\right) \qquad (3.52)$$

3.3.1 Longitudinal Aerodynamic Model

The aerodynamics model is used from [13] to obtain the aerodynamic coefficient C_L, C_D and C_m as shown in the Fig. 3.2, Fig. 3.3, Fig. 3.4 respectively in variation with the M and α for the winged-cone GHV model for the complete flight regime of the AHV and it includes the different propulsion and engine models. The MATLAB code presented in [15] describes the polynomial for the aerodynamic coefficients C_L, C_D, C_m, C_{mq}, C_{L,δ_e}, C_{D,δ_e} and C_{m,δ_e}. These polynomial equations are used to generate the data points at each M, ranging from $M = 0$ to 24, and for different range of α, with $\alpha = -1, 1, 4$ and 10, and hence all generated data points given in Appendix A1 are used to generate the aerodynamic coefficient plots given in Fig. 3.2, Fig. 3.3, Fig. 3.4. In generation of the aerodynamic coefficient data points the engine model is implemented and is further discussed in section 3.4 of this chapter. The aerodynamic coefficient data is implemented in MATLAB by creating subroutine and interpolation, for the nonlinear simulation of the 3DOF longitudinal AHV model. This aerodynamic data shown in Fig. 3.2 to Fig. 3.4 is used as the aerodynamic model 1 in the 3DOF simulation model of the AHV using interpolation. The lift force is expressed by $L = \bar{q}SC_L$, where lift coefficient is given as $C_L = f(M, \alpha, \delta_e)$, drag force is represented by, $D = \bar{q}SC_D$, where, drag coefficient is expressed with the relation as, $C_D = f(M, \alpha, \delta_e)$ and the pitching moment is given by, $M = \bar{q}cSC_m$, where, pitching moment coefficient is represented by $C_m = f(M, \alpha, \delta_e)$. The linearized equations considered with 3DOF dynamic longitudinal simulation model of AHV is used for the bifurcation method, the reduced aerodynamics model 2 is developed and is given by the Eqn. (3.53-3.55),

$$C_L = C_{L,\alpha}.\alpha + C_{L,\delta e}.\delta_e \qquad (3.53)$$

$$C_D = C_{D,\alpha}.\alpha + C_{D,\delta e} \tag{3.54}$$

$$C_m = C_{m,\alpha}.\alpha + C_{m,\delta e}.\delta_e + C_{mq}\left(\frac{qc}{2V}\right) \tag{3.55}$$

and, $\left(\frac{qc}{2V}\right)$ is the computed non-dimensional pitch rate. The aerodynamic coefficients in longitudinal flight dynamics are most strongly dependent on the aerodynamic angle, angle of attack, Mach number, Reynolds numbers, and control surfaces; and aerodynamic coefficients are also affected by deflections and propulsion systems in [16].
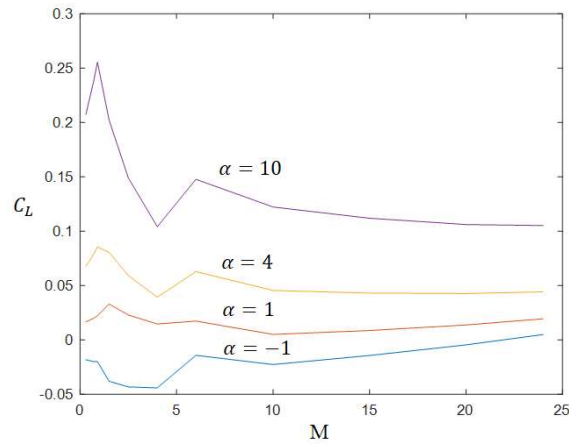
Fig. 3.2 Aerodynamic data of C_L with M
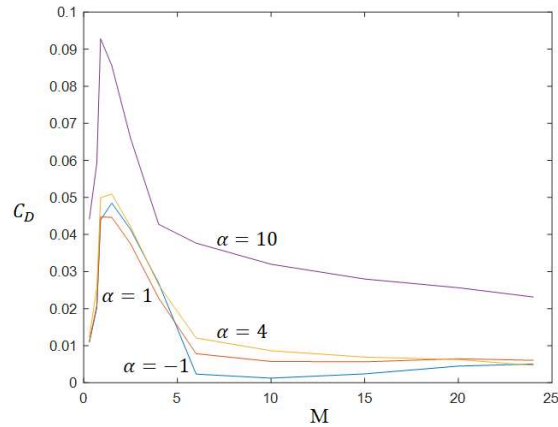
Fig. 3.3 Aerodynamic data of C_D with M
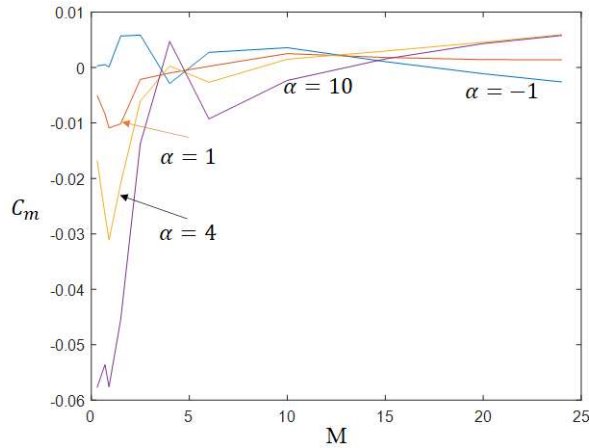
Fig. 3.4 Aerodynamic data of C_m with M

The stability derivatives due to a change in the angle of attack $C_{L,\alpha}$, $C_{D,\alpha}$ and $C_{m,\alpha}$ denotes aerodynamic events at rest; hence, the term is said as "static stability derivatives". The stability derivative $C_{m,\alpha}$ establishes the longitudinal static-stability of the AHV.

3.4 Propulsion Model

The generic AHV engine model operates through the wide flight regime using mixed and combined propulsion system as presented in [16]. The proposed engine model for the required thrust is combined with the hypothetical model of turbojet engine (TE), ramjet and scramjet engine (RSE), and rocket engine (RE), as stated in [16], for different Mach number range is given below in Table 3.2. The different thrust models of the AHV presented in the Eqn. (3.56-3.59) from [16] are used for the 3DOF AHV simulation, considering the thrust with a function in PLA, height, and Mach number for complete regime of AHV flight. The variation of altitude with Mach number and thrust with Mach number using the Eqn. (3.56-3.59) is plotted and is shown in Fig. 3.5 and Fig. 3.6 respectively.

Altitude Variation: The atmospheric model with temperature and air density is required when altitude changes in relation with the corresponding dynamic model output as Mach number. As the atmospheric temperature and air density depends on the altitude variation, therefore the relation between them from [99] is given by the Eqn. (3.60-3.63) respectively.

Table 3.2 Different Engine Model of Generic AHV

Engine Model No.	Engine	Mach No. Range
1	Turbojet	$0 < M \leq 2$
2	Ramjet and Scramjet	$2 < M \leq 6$
3	Rocket	$6 < M \leq 24$

$$Thrust_{TE} = PLA.\left(2.99e05 - 1.00e01.(h) + 1.33e - 04.(h^2) - 6.48e - 10.(h^3) + 3.75e03.(M^3)\right) \tag{3.56}$$

$$Thrust_{RSE} =$$

$$PLA.\left(\begin{matrix} 7.53e02.(M^7) - 1.50e04.(M.^6) + 1.16e05.(M^5) - 4.36e05.(M^4) \\ +8.07e05.(M^3) - 6.97e05.(M^2) + 3.94e05.(M) + 3.93e - 08 \end{matrix}\right) \tag{3.57}$$

For $h < 57000$,

$$Thrust_{RE} = -5.43e04 + 6.64e - 01.(h) + 3.24e05.(PLA) + 3.74e - 01.(h.PLA) \tag{3.58}$$

For $h > 57000$,

$$Thrust_{RE} = -1.64e04 + 3.24e05.(h) + 3.24e05.(PLA) + 21295.(PLA) \tag{3.59}$$
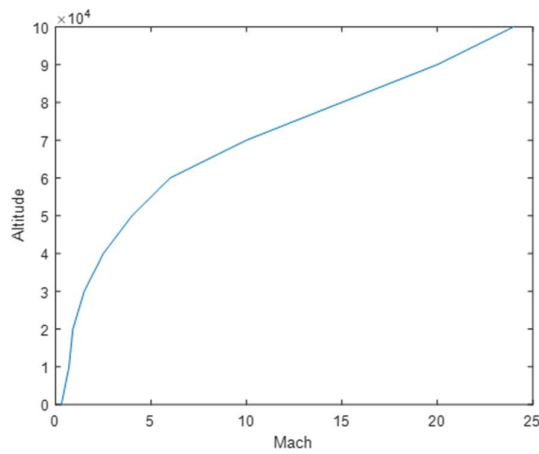
Fig. 3.5 Altitude variation with Mach number
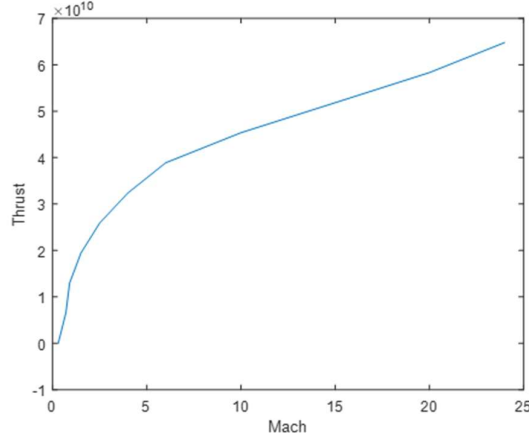
Fig. 3.6 Thrust variation with Mach number

$for\ h < 36089\ ft,$

$$T = T_0(1 - 6.875 \times 10^{-6}h), \quad where\ T_0 = 518.7^0 R \tag{3.60}$$

$for\ h > 36089\ ft, \qquad T = 389.99^0 R \tag{3.61}$

$for\ h < 36089\ ft, \qquad \rho = \rho_0(1 - 6.875 \times 10^{-6}h)^{4.2561} \tag{3.62}$

$$where\ \rho_0 = 2.377 \times 10^{-3}\ slug/(ft^3)$$

$for\ h \geq 36089\ ft, \qquad \rho = 0.2971\rho_0\ e^{-\frac{(h-360\quad)}{20806.7}} \tag{3.63}$

$$where\ \rho_0 = 2.377 \times 10^{-3}\ slug/(ft^3)$$

3.5 Operating Flight Conditions

The aerodynamics coefficient C_{L_α}, C_{D_α} and C_{m_α} are obtained for the different angle of attack with selected value of $\alpha = -1$ and 4 where α is in degrees. Here the coefficients C_{L_α}, C_{D_α} and C_{m_α} are plotted for the complete nonlinear wide flight regime for Mach number, $M = 0\ to\ 24$ and is shown in the Fig. 3.7, Fig. 3.8 and Fig. 3.9 respectively. The stability analysis for the vehicle dynamics presents complicated behaviour to establish complete interpretation for the wide flight regime, and especially when transition takes from the subsonic to different sonic speeds and to high hypersonic speed.

The different cases outlined in the Fig. 3.9 for C_{m_α} corresponds to the different stable and unstable points at different altitude and sonic region for the entire flight regime of the AHV. A negative value for C_m is required for longitudinal

static vehicle stability and, positive and negative C_m value refers nose-up and nose-down pitching moment respectively, and C_m changes with variation in the angle-of-attack, α.
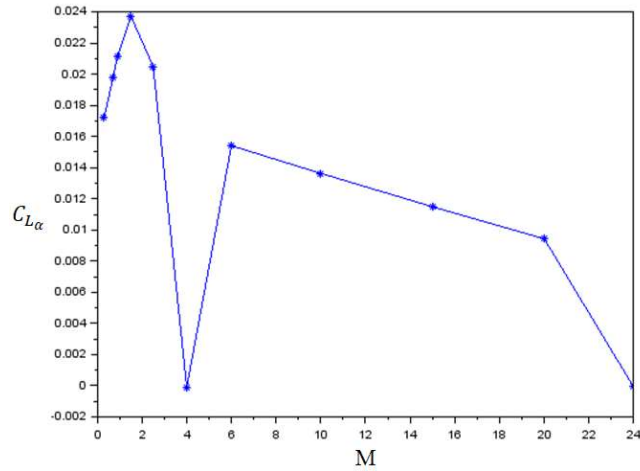
Fig. 3.7 Incremental derivative C_{L_α}
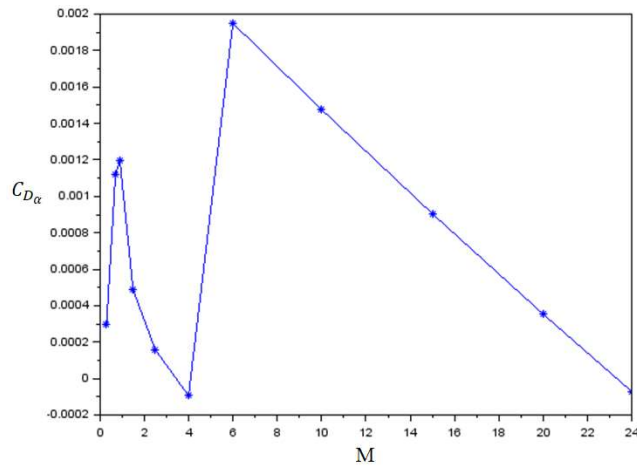
Fig. 3.8 Incremental derivative C_{D_α}

Different cases of C_{m_α} are identified from the Fig. 3.9 and are represented in the Table 3.2. Hence C_{m_α} graph shown in Fig. 3.9 shows the static stability characteristics of the complete dynamic AHV model. The 0.9 M (Case A) is the most stable Mach number as per the C_{m_α} graph as shown in Fig. 3.9, so that the stability corresponds to near about critically stable with no oscillation as shown in the simulation Fig. 4.1, therefore there will be no imaginary part of the eigen values.
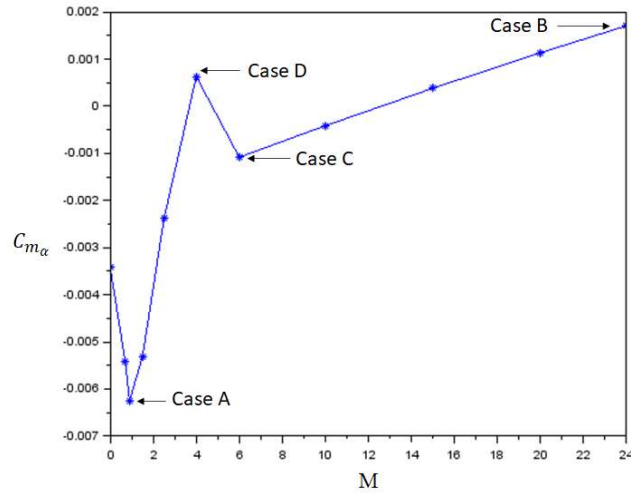
Fig. 3.9 Incremental derivative C_{m_α}

The 24 M (Case B) is the most unstable case having the positive C_{m_α} value. The 6 M (Case C) is the locally second most stable case having the negative C_{m_α} value. And the 4 M (Case D) is the locally second most unstable case having the positive C_{m_α} value. The different Cases highlighted in Table 3.3 for the different Mach number, the lift increment derivatives, drag increment derivatives and pitch increment derivatives for the corresponding Mach number is given in the Table 3.4.

Table 3.3 Mach Number with special stability characteristics

Case No.	Cases	Corresponding M	Sonic Region	Altitude (ft)	Engine
A	Most stable (- C_{m_α} value)	0.9	Subsonic	10000	Turbojet
B	Most unstable (+ C_{m_α} value)	24	High Hypersonic	100000	Rocket
C	Locally 2nd most stable (- C_{m_α} value)	6	Hypersonic	65000	Ramjet and scramjet
D	Locally 2nd most unstable (+ C_{m_α} value)	4	Supersonic	50000	Ramjet and scramjet

Table 3.4 Mach Number with increment derivatives

Mach No.	C_{L_α}	$C_{L_{\delta e}}$	C_{D_α}	$C_{D_{\delta e}}$	C_{m_α}	$C_{m_{\delta e}}$
0.9	0.0252	-0.0032	0.00005	0.00006	-0.0052	0.0024
4	0.0134	0.005	-0.0009	-0.0039	0.0007	0.0006
6	0.0147	-0.0006	0.0013	-0.0006	-0.0011	-0.000005
24	0.0072	-0.002	-0.0009	-0.0007	0.0022	0.0002

The highly nonlinear AHV, complex aerodynamic parameters for the entire flight regimes of the flight, wide flight regime and strong interactive coupling with time variation provides the way for the bifurcation approach to be analyzed and implemented. Also, continuation approaches can outline the topological behavior of the nonlinear dynamic model of AHVs and provide a fruitful analysis of the equilibrium states with the nonlinear fight regimes.

3.6 Validation of Aerodynamic Model

The comparison of the AHV model development with Angle of Attack (α) and Pitch Angle (θ, degree), versus the Mach numbers is shown in Table 3.5 for validation of the results.

Table 3.5 Comparison of the selected Cases for the Aero data for AHV

Cases	Mach No. (M)	Aero Model	Angle of Attack from [12] (α, degree)			Angle of Attack for This work (α, degree)		
			α=1	α=4	α=10	α=1	α=4	α=10
A	0.9	C_L	0.021	0.08	0.23	0.02	0.08	0.23
		C_D	0.02	0.03	0.06	0.02	0.03	0.06
		C_m	-0.01	-0.03	-0.058	-0.01	-0.03	-0.058
B	24	C_L	0.02	0.045	0.11	0.005	0.049	0.11
		C_D	0.005	0.005	0.0225	0.005	0.005	0.024
		C_m	0	0.005	0.005	0	0.005	0.005
C	6	C_L	0.004	0.054	0.15	0.004	0.054	0.15
		C_D	0.008	0.013	0.038	0.008	0.012	0.038
		C_m	0	-2.5	-9	0	-0.004	-0.01
D	4	C_L	0.025	0.049	0.1	0.004	0.048	0.1
		C_D	0.02	0.025	0.044	0.02	0.025	0.044
		C_m	-0.002	0	0.005	-0.002	0	0.005

The comparison of Angle of Attack (α) for the selected cases for the aero model of AHV shows almost overlapping of the data points as shown in Table 3.5.

3.7 Chapter Summary

The chapter presents the development of the dynamic Winged Cone model, GHV (Generic Hypersonic Vehicle) built with NASA Langley Research Centre and is selected for this research and study. The propulsion system is hypothetical proposed with group alignment of turbojet, ramjet and scramjet, and with rocket propulsion system incorporated into the model. Center-of-mass, centre-of-gravity and with moment-of-inertia are included with model motion of equations for simulation. Fuel consumption affects the vehicles weight, centre-of-gravity and the inertia products. X-axis of the body is completely aligned with the vehicle's thrust vector orientation. As a result, there is no thrust force component in the body's (Y and/or Z-axis). Due to this, it is expected that when fuel is spent, the centre of gravity will individually shift beside the body's X axis. Axis symmetrical modelling is used to create the winged cone model and axis of rotation is parallel to the model's wing tips and tail. The AHV control surfaces are elevon (left and right), canard and rudder, and they are tested for elevator deflections in relation to hinge lines and rudder deflections with trailing edge. The canards are either ignored or regarded ineffectual at high AHV speeds. The mathematical modelling of the AHV model uses the flat Earth approximation and the equations-of-motion are determined by using the Newton and Euler equations.

CHAPTER 4

FLIGHT DYNAMIC SIMULATION AND TRIM ANALYSIS

Flight spends most of its time in the longitudinal frame, making longitudinal flight dynamics crucial to flight maneuvers. The entire flight envelop, including velocity in the body-fixed X-plane and Z-plane, is considered to be longitudinal flight, as are the phases of level flight, climbing and descending, and pulling up and down. As a result, the trim and stability analysis should focus primarily on the longitudinal flight dynamics. The stability analysis and nonlinear simulation of the Generic AHV dynamic model are presented in this chapter. In the Bifurcation section, we perform a dynamic analysis of the AHV using the Bifurcation Method, taking into account the eigen values approach, and we analyze the longitudinal modes of the AHV flight. This covers the entire flight envelope for nonlinear simulation in [100] from Mach number M=0 to Mach number M=24.

4.1 Flight Dynamic Nonlinear Simulation of AHV

The aerodynamic analysis of AHV from the Fig. 3.4 shows the stability variation and issues with M and α. Stable region with $M = 0\ to\ 4$, there is increase in the stability from the 0 to 1 M. Due to the increase in the gap, $M = 1\ to\ 4$, decrease in the stability is observed. In the unstable region from $M = 4\ to\ 5$, instability increases and then decreases. The stability region between $M = 5\ to\ 13$, the stability increases approximately for the $M = 5\ to\ 7$ due to the increase in the M and instability increases for the $M = 7\ to\ 13$. The instability increases from $M = 13$ onwards, shows the nonlinear stability. The C_{m_α} graph shown in Fig. 3.9 shows the static stability characteristics of the complete dynamic AHV model.

Trim angle-of-attack graph is shown in the Fig. 4.1 (a) with different elevator deflection (δ_e) i.e., 0, 1 and 2. At $t = 3.5\ sec$ the graph shown in Fig. 4.1 (b) shows the stable dynamics of the AHV at reaching $M = 3\ to\ 5$. The simulation

becomes unstable after $t = 3.6\ sec$, when M is more than $M = 4$ and beyond. At $t = 3.9\ sec$ the system simulation shows the return to stable mode with $M = 5.5$ (more then $M = 5$), as per our system findings earlier for $M = 5\ to\ 13$ dynamics.

The simulation shows small variation of α, approximately $\alpha = 0\ to\ 2$ degree in both stable and unstable mode, whereas there is large variation in pitch angle from $6\ to\ 10$ degrees. This pitching motion corresponds to phugoid motion of the AHV, accompanied by the gain and loss of altitude between, approximated of 40 and 80 meters, respectively. Simulation of dynamic AHV model system at $t = 5.3\ sec$, shows the system crossing $M = 12.5$, hence goes into unstable M region, with sharp nose up and altitude gain; were as α is small, which indicates the phugoid motion going unstable. The stable and unstable M region and qualitative analysis is shown by bifurcation analysis using eigen values in Chapter 5.

In simulation, without oscillation stability cannot be checked. Based on the understanding developed on the preliminary analysis of aerodynamic data about the stability of the vehicle and ability of the simulation result showing any unstable flight region, makes bifurcation analysis mandatory for proper investigation for its stability. However small unstable flight region for any M and any angle of attack may be, but it may result into catastrophic failure of the vehicle upon very small disturbance at that point.

(a)

(b)
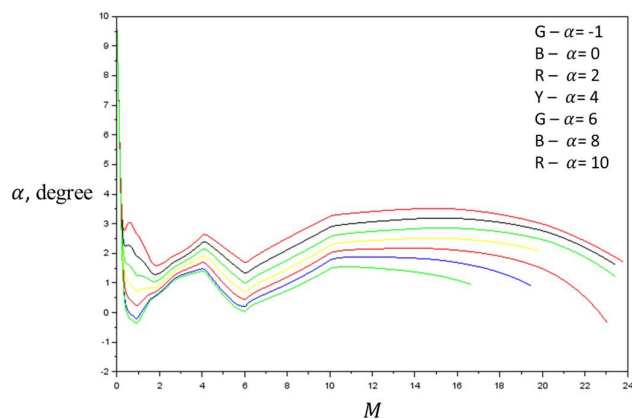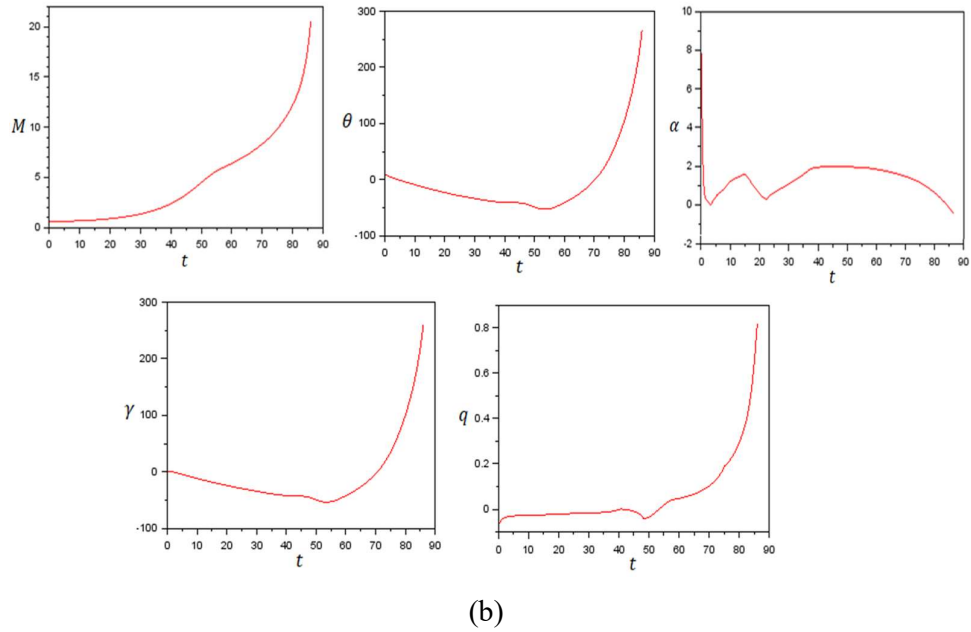
Fig. 4.1. (a) Trim angle of attack graph with different elevator deflection i.e., 0,1 and 2 (b) Simulation of the 3-DOF AHV.

4.2 Validation through Trim Flight Conditions

Validation of developed Generic AHV model is compared in [101] is given in Fig. 4.2 (a) and Fig. 4.3 (a) with the developed AHV model shown in Fig. 4.2 (b) and Fig. 4.3 (b). The comparison of the AHV model development with α and θ (in degrees), versus Mach numbers is shown in Table 3.5 for validation of the results.

(a) Open Literature [101]   (b) Developed Model
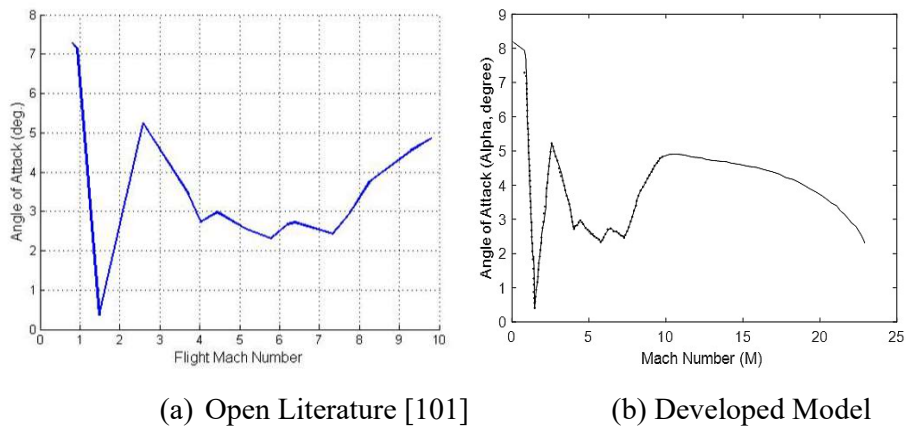
Fig. 4.2 Mach No. (M) Vs Angle of Attack (α, degree)
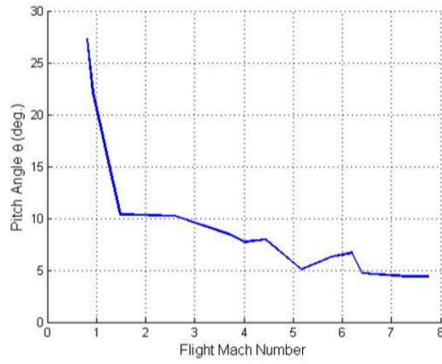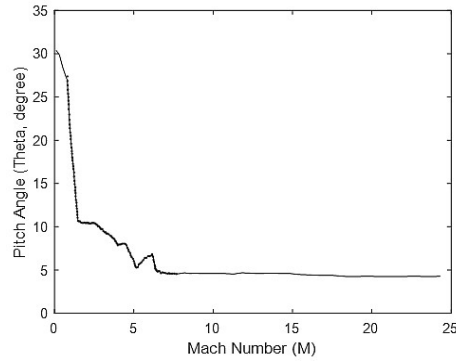
(a) Open Literature [101]   (b) Developed Model

Fig. 4.3 Mach No. (M) Vs Pitch Angle (θ, degree)

The comparison of Angle of Attack (α) for the selected cases for the aero model of AHV shows almost overlapping of the data points as shown in Table 3.5.

4.3 Flight Dynamics Analysis for Different Sonic Velocities

The vehicle dynamics stability study provides challenging behavior to develop comprehensive interpretation for the broad flight envelop, particularly when transition takes place from subsonic to varied sonic velocities and to high hypersonic speeds.

Stability analysis of generic AHV longitudinal dynamics relies heavily on the pitching moment coefficient, and its variation with M for different α are shown with Fig. 4.4 (a) (Fig. 3.4).
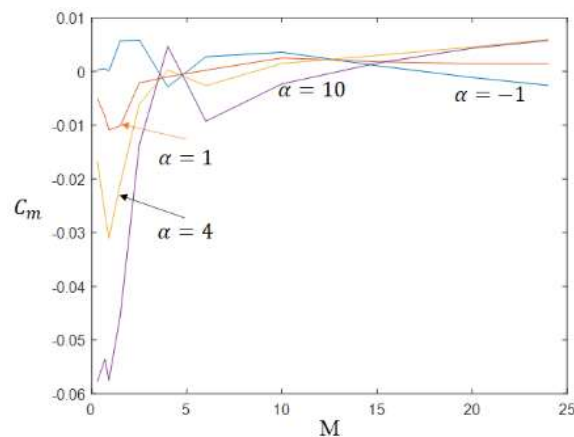
(a)
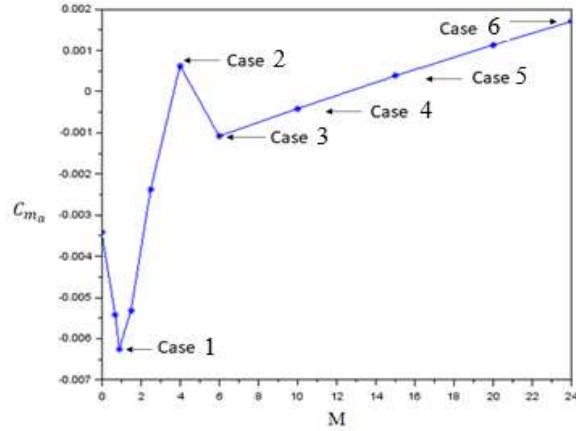
(b)

Fig. 4.4 Aerodynamic coefficient (a) Pitching moment C_m with M

(b) Incremental derivative C_{m_α}

A negative value for C_m is required for longitudinal static vehicle stability; and, positive and negative C_m value refers nose-up and nose-down pitching-moment correspondingly, as C_m changes with the change in α. Aerodynamics incremental derivative C_{m_α} is obtained for the selected angle of attack, α for -1 and 4 degrees for the complete flight envelop ranging M=0 to 24 and is shown in the Fig. 4.4 (b).

Table 4.1 – Different simulation cases for AHV Flight Phase

Cases	Mach Number (M)	Flight Phase
1	0.9	Ascent/Descent
2	4	Ascent/Descent
3	6	Ascent/Descent
4	10	Level
5	15	Level
6	24	Level

Different cases of C_{m_α} are identified from the Fig. 4.4 (b) for the entire flight envelop and are represented in the Table 4.1. These cases represent the different AHV flight phases of ascent, descent and level corresponding to the different Mach numbers. These cases are used for the longitudinal trim analysis and trim AHV simulation considering entire AHV flight envelop.

4.4 Trim Analysis of AHV for Different Operating Conditions

Trim points are often where linear models are created and trim conditions specify the points at which control systems are designed and evaluated. As a result, we can use these trim conditions as an initial point for comparisons between other models and it can be implemented differently based on the actual flight data. Trim analysis is used to minimize a cost function with constraints [102] for nonlinear aircraft models developed considering aerodynamic and propulsion models. It presents a trim algorithm that is implemented for the simulation of the 6DOF aircraft model. It presents a trim algorithm which is implemented for the simulation of the 6DOF aircraft model. Using a bifurcation technique, the authors of [95] analyse the longitudinal dynamics of a parafoil with trim and stability qualities for a four-degrees-of-freedom (DOF) flying model. In order to construct nonlinear flight control laws, a model-based control structure is used for analysis of trim conditions [103]. For various control surface deflections, it displays a trimmed flight analysis performed with outer loop and inner loop equations in the 6DOF aircraft model. For both steady-state straight flight [104] and for turning, pull up, and pull overflight [105], an aircraft's trim analysis is described using equations of motion. This research is focused on developing a generic analytical framework for trim analysis, as well as its application to the trimming of 6 degree-of-freedom (DOF) conventional and unconventional aircraft for control power assessment. The flight maneuvers rely heavily on the longitudinal flight dynamics, which account for the vast majority of the flight time in the longitudinal frame. The full range of motion in flight is considered to be longitudinal flight, which encompasses not just velocity in the body's fixed X and Z planes but also level flight, ascent, descent, and pull-up and pull-down flight. This demonstrates that longitudinal flight dynamics should be prioritized in the trim and stability study. In this study, we examine the Generic AHV dynamic model's stability and do a trim analysis. Chapter 5 presents a dynamic analysis of the AHV flight utilizing the Bifurcation Method, taking into account the eigenvalues approach and longitudinal modes analysis for the entire flight envelope, covering Mach numbers from 0 to 24.

The solution for the trim or equilibrium states is obtained using the longitudinal nonlinear dynamic AHV model provided in Eqn. (3.1-3.7). The model is in one of five possible states, denoted by the variables V, γ, q, θ and α and, with V, γ and θ, and being treated as zero. In this case, the flight is straight, with $\gamma = 0$ for a level flight, $\gamma = $ a positive value for an ascent flight, and $\gamma = $ a negative value for a descent flight, but the nose orientation is constrained to be constant. In order to acquire the trim states necessary to realize these trim criteria for the AHV flight, we set the left-hand side of the Eqn. (3.22-3.25) equal to zero and solve for the right-hand side, which yields the Eqn. (4.1-4.4).

$$0 = (T \cos\alpha - \bar{q}SC_D - mg \sin\theta)/m \tag{4.1}$$

$$0 = (T \sin\alpha + \bar{q}SC_L - mg \cos\theta)/mV \tag{4.2}$$

$$0 = \bar{q}ScC_m/2I_{yy} \tag{4.3}$$

$$q = 0 \tag{4.4}$$

Trim-states are symbolized using * and, are obtained from Eqn. (4.1-4.3) and are given by the following Eqn. (4.5-4.7).

$$C_D^* = (T^* \cos\alpha - mg \sin\theta)/\bar{q}^* S \tag{4.5}$$

$$C_L^* = (mg \cos\theta - T^* \sin\alpha)/\bar{q}^* S \tag{4.6}$$

$$C_m^* = 0 \tag{4.7}$$

In case of climbing condition of flight, from the Eqn. (4.5) we obtain the climb angle and climb rate respectively given by the following Eqn. (4.8-4.9).

$$\sin\gamma^* = (T^* \cos\alpha - \bar{q}^* SC_D^*)/mg \tag{4.8}$$

$$(V\sin\gamma)^* = (T^* \cos\alpha - \bar{q}^* SC_D^*)V^*/mg \tag{4.9}$$

From the Eqn. (4.5), Eqn. (4.10) is formulated for the thrust relation.

$$T^* = (\bar{q}^* SC_D^* + mg \sin\theta)/\cos\alpha \tag{4.10}$$

The trim states obtained are used for the AHV model dynamic simulation by using them as initial conditions or initial parameters for the simulation and for implementing the bifurcation method.

4.5 Simulation of Trim Analysis of AHV

Simulation of the 3DOF generic AHV longitudinal dynamic nonlinear model is carried out and the states V, γ, α, θ, q and h, are obtained at different Mach number and altitude. Here V is replaced by Mach number M and is obtained using $M=V/a$, here a is speed of sound. The simulation is carried out for the trim states or at equilibrium points as discussed above. Here V^* and h^* are considered as constant value, $\gamma^*, \alpha^*, \theta^*$, $q=0$ and T^* is used from the Eqn. (4.17-4.20) depending upon the different Mach number range, and is considered for all different trim or equilibrium points, as considered for the simulation cases, as shown in the Table 4.2. The linear longitudinal AHV model is obtained considering the Eqn. (4.7-4.13) and the state space representation is given by $\dot{x}=Ax+Bu$, were the state is represented as $x=[M,\gamma,\alpha,\theta,q,h]'$ and the input as u=[δ_e , PLA]. The dynamic 3DOF generic AHV longitudinal model simulation is carried out for the different Cases outlined in the Table 4.2 for different Mach number and corresponding altitude. The simulation is carried out for trim condition considering the elevator deflection, δ_e as zero for all Cases shown in the Table 4.2 and magnitude of PLA is considered as incremental value between 0.1 to 1 for all cases. The aerodynamic coefficient with their derivatives from Table 4.3 are used in the simulation for the different Cases.

The dynamic 3DOF generic AHV longitudinal model simulation is carried out for the different cases outlined in the Table 4.2. The simulation is carried out at six different Mach numbers and at corresponding altitude. The simulation cases are shown in Fig. 4.5 to Fig. 4.10.

Table 4.2 – Different simulation cases for 3DOF AHV longitudinal model

Simulation Cases	Mach Number (M)	Altitude (h), ft
1	0.9	10,000
2	4	50,000
3	6	65,000
4	10	10,0000
5	15	10,0000
6	24	10,0000

Table 4.3 – Mach Number with aerodynamic derivatives

Mach No.	C_{L_α}	$C_{L_{\delta e}}$	C_{D_α}	$C_{D_{\delta e}}$	C_{m_α}	$C_{m_{\delta e}}$
0.9	0.0252	-0.0032	0.00005	0.00006	-0.0052	0.0024
4	0.0134	0.005	-0.0009	-0.0039	0.0007	0.0006
6	0.0147	-0.0006	0.0013	-0.0006	-0.0011	-0.000005
10	0.0132	0.001	0.0008	-0.0004	-0.0004	-0.0003
15	0.0115	0.0002	0.0002	-0.0005	0.0006	-0.00007
24	0.0072	-0.002	-0.0009	-0.0007	0.0022	0.0002
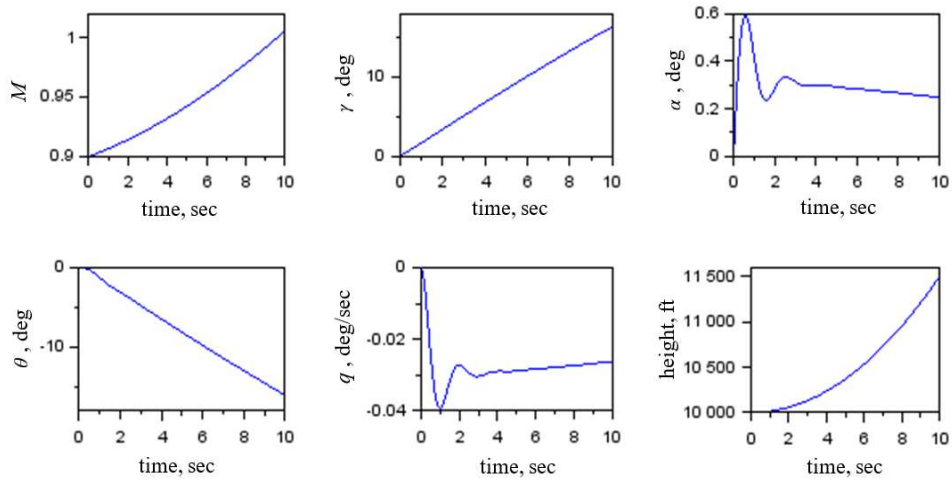
Fig. 4.5 - Dynamic Simulation Case 1 for M = 0.9
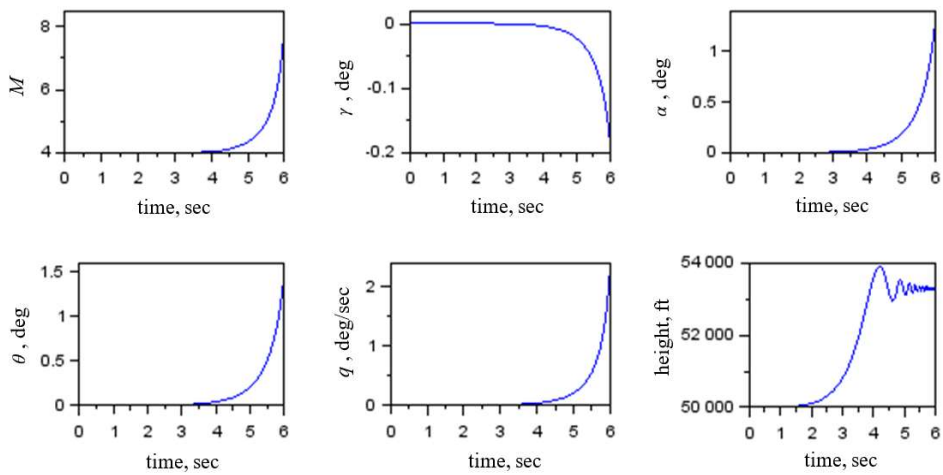
Fig. 4.6 - Dynamic Simulation Case 2 for M = 4
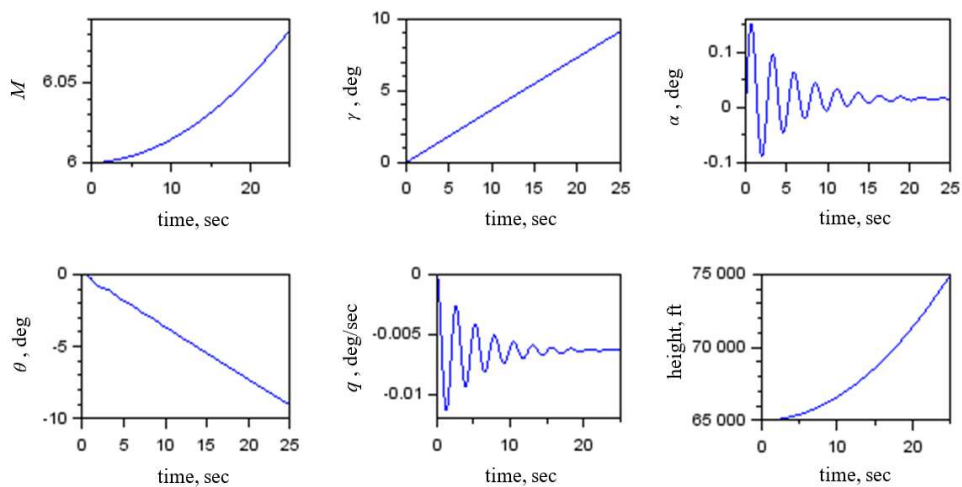
Fig. 4.7 - Dynamic Simulation Case 3 for M = 6
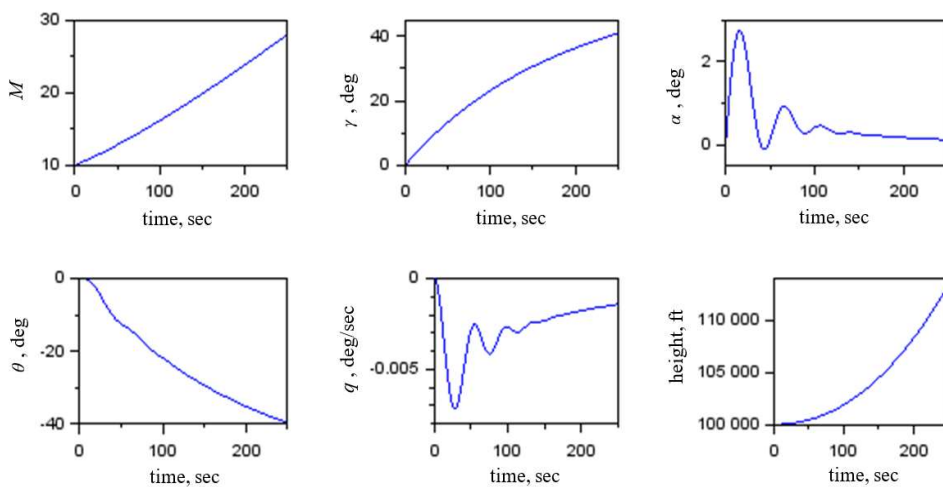
Fig. 4.8 - Dynamic Simulation Case 4 for M = 10
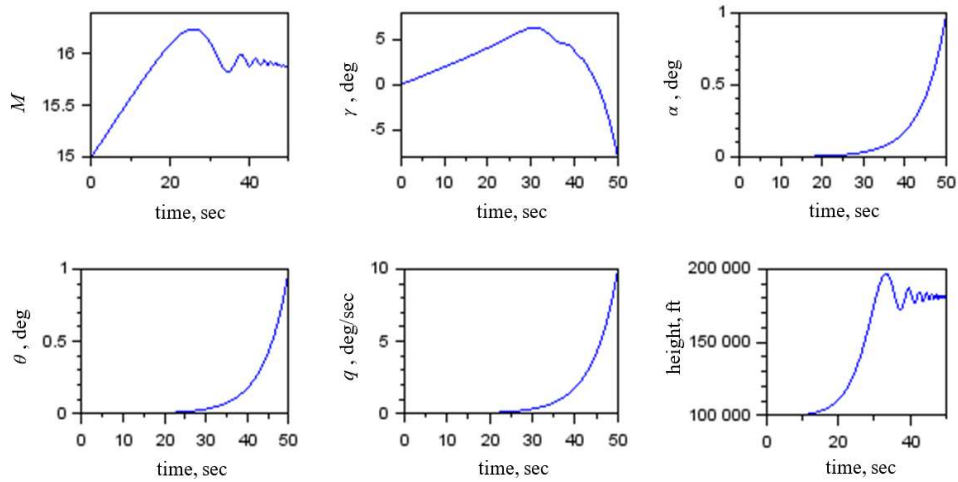
Fig. 4.9 - Dynamic Simulation Case 5 for M = 15
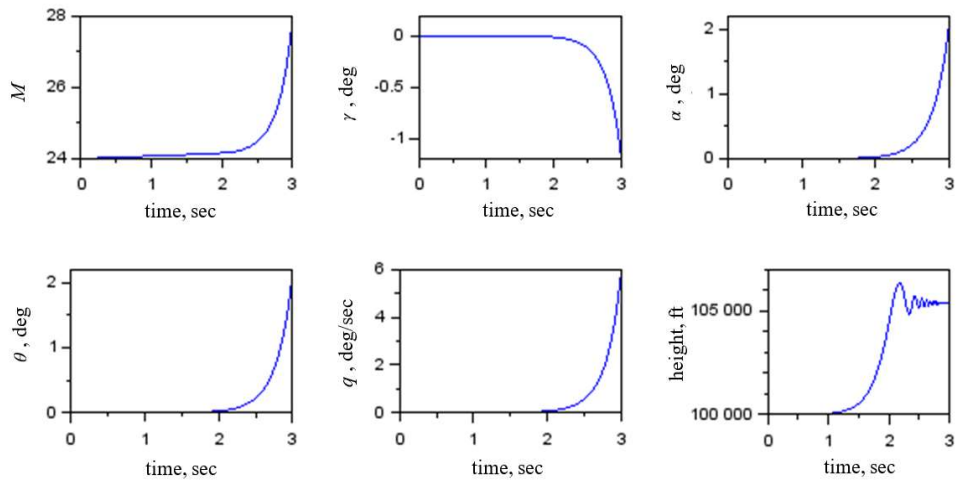
Fig. 4.10 - Dynamic Simulation Case 6 for M = 24

4.6 Flight Dynamic Stability Analysis of Trim Simulation

At varying Mach numbers, the AHV model's dynamic stability is examined. With increasing AHV speed at Mach number M=0.9 and increasing height (Case 1 simulation shown in Fig. 4.5), the angle of attack, α, stabilizes near α =0.25 degrees. Both the flight path angle, γ, and the pitch rate, q, are held steady at around γ=10 degrees and q=0.035, respectively. Dynamic case simulations demonstrate stable behavior, with the angle of attack, α, converging towards the trim point.

For Case 2, when the AHV speed is increased for Mach number M=4, and as altitude is gained, the angle of attack, α, exhibits a breakdown in behavior near

α=5 degrees, as shown in Fig. 4.6; however, the behavior remains constant in height beyond that point. Both the flight path angle (represented by γ) and the pitch rate (shown by q) exhibit breakdown behavior, remaining at a negative heading of γ=-0.2 degrees and trending upwards. Near the equilibrium or trim point, the angle of attack, α, exhibits divergence nature, indicating an unstable dynamic behavior in the simulation.

The simulation results for Case 3 are displayed in Fig. 4.7; they indicate that when the AHV speed is increased for Mach number M=6, and as height is gained, the angle of attack, α, stabilizes near α=0.03 degrees. The pitch rate, q, is kept around q=0.005, while the flight path angle, γ, is kept at γ=10 degrees. Dynamic case simulations demonstrate stable behavior, with the angle of attack, α, converging towards the trim point.

With increasing AHV speed at Mach number M=10 and increasing height, as in Case 4 of the simulation shown in Fig. 4.8, the angle of attack, α, stabilizes near α=0.02 degrees. Both the flight path angle, γ, and the pitch rate, q, are held steady at or near q=0.002. Dynamic case simulations demonstrate stable behavior, with the angle of attack, $α$, converging towards the trim point.

For Case 5, with increasing AHV speed for Mach number M=15 and with the rise in altitude, the angle of attack, α, exhibits breakdown behavior at α=0.5 degrees, as shown in Fig. 4.9; it subsequently demonstrates steady and level flying behavior in height. Breakdown behavior is seen in both the flight path angle, γ, and the pitch rate, q, with the former remaining positive up to γ=5 degrees and the latter being observed at γ=-5 degrees and above. Near the equilibrium or trim point, the angle of attack, α, exhibits divergence nature, indicating an unstable dynamic behavior in the simulation.

Case 6's simulation results are depicted in Fig. 4.10, where the angle of attack, α, exhibits a breakdown behavior near α=1 degrees as the AHV speed increases for Mach number, M=24, and with the gain in altitude, before settling into a pattern of constant and level flying above that altitude. Both the flight path angle, γ, and the pitch rate, q, exhibit breakdown behavior, with the former maintaining a negative heading of γ=-0.5 degrees. Near the equilibrium or trim point, the angle of attack, α, exhibits divergence nature, indicating an unstable dynamic behavior in the simulation.

4.7 Chapter Summary

This chapter details the longitudinal trim and stability assessment of the 3DOF longitudinal AHV model using dynamic simulation. The 3DOF AHV model is simulated and subjected to trim analysis in a variety of scenarios using aerodynamic model analysis of incremental pitching coefficient for the corresponding Mach numbers. Stable simulations are achieved in cases 1, 3, and 4 after a trim simulation is run using the AHV model for all 6 cases for Mach number $M=0.9$, $M=6$ and $M=10$, and for the cases 2, 5 and 6 for Mach number $M=4$, $M=15$ and $M=24$ shows unstable behavior, and the dynamic stability for the simulation cases is shown in Table 4.4. The 3DOF AHV model is then used to implement the bifurcation approach, further validating these cases.

Table 4.4 – Dynamic stability for the simulation cases

Simulation Cases	Mach Number (M)	Stability
1	0.9	Stable
2	4	Unstable
3	6	Stable
4	10	Stable
5	15	Unstable
6	24	Unstable

Comparative study is also carried out using dynamic simulation for trim condition and variable control surface deflection considering the elevator deflection and rudder deflection, δ_e and δ_r, for Cases 1, 3 and 4 shown in the Table 4.2. The 3DOF longitudinal AHV model is considered using the Eqn. (4.7-4.13) and the states represented as $x=[M,\gamma,\alpha,\theta,q,h]'$ and input as $u=[\ \delta_e\ ,\ \delta_r]$.

The dynamic 3DOF longitudinal model simulation is carried out for the different Cases of Case 1, Case 3 and Case 4 as outlined in the Table 4.2 for different Mach number, $M = 0.9$, 6 and 10 for corresponding altitude. The aerodynamic coefficients with their derivatives from Appendix C Table C.1 are used in the simulation for the different Cases 1, 3 and 4, and their dynamic simulation is shown in Appendix C with Fig. C.1-C.4, Fig C.5- C.8 and Fig C.9-C.12 respectively. The α trim comparison is shown in Fig. 4.11 and Fig. 4.12 for the different Cases, Case 1, Case 3 and Case 4.
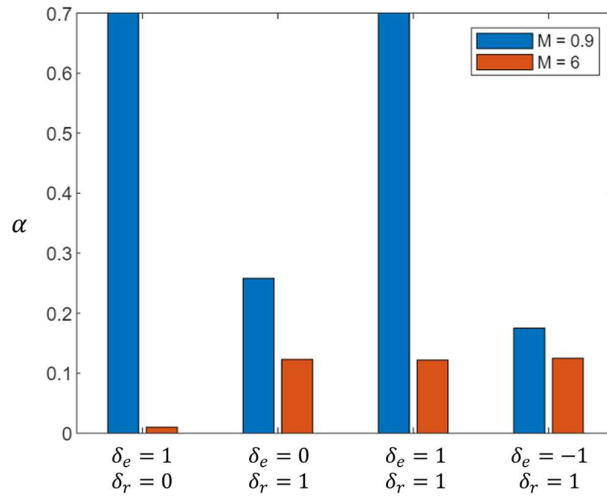
Fig. 4.11 - Dynamic Simulation for α trim, Case 1 and Case 3
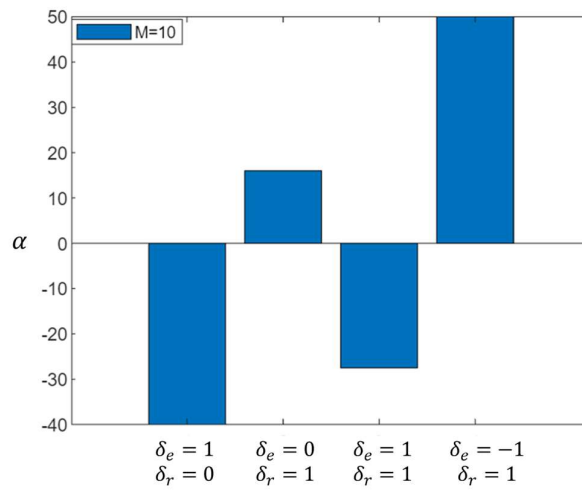
Fig. 4.12 - Dynamic Simulation for α trim, Case 4

CHAPTER 5

BIFURCATION METHOD ANALYSIS

Bifurcation technique involves Continuation Based Algorithm (CBA) using AUTO-07p in [14], uses a nonlinear dynamical system to compute the steady states described using the first order ordinary differential equation (ODE) given by, $\dot{x} = f(x, U)$, here x, U and f are vectors, and of n state variables, m control parameters and nonlinear function respectively. The CBA determines the solution of $\dot{x} = f(x, U)$ by finding the solution of the algebraic nonlinear equations given by, $\dot{x} = f(x, u, p) = 0$ with one parameter is varied $u \in U$ and at the same time keeping other parameters $p \in U$ fixed. Considering the free parameter u is varied in range, and keeping control parameter P fixed using CBA, the bifurcation technique tracks all possible trim states $x*$ in a manner that $f(x *, u, p) = 0$ is fulfilled.

5.1 Bifurcation Software AUTO-07p

Several software programmes exist specifically to examine non-linear dynamical systems, such as MatCont in [106]-[107] and KRIT in [108]. Most people are familiar with the AUTO97 package, a FORTRAN program and AUTO2000, a C program; developed at Concordia University in Canada by a group led by Prof. Eusebius Doedel for bifurcation analysis of non-linear dynamical systems. As of the year 2021, the AUTO-07p in [109] package is the most up to date of these options. Versions of the AUTO package and how to use them are described in [110]-[111]. AUTO-07p is an application written in FORTRAN and designed to run on UNIX. In order to make the AUTO package work on the WINDOWS platform, a group led by Professor Bard Ermentrout at the University of Pittsburgh in the United States created XPPAUT in [112]. Professor Bard Ermentrout's textbook in [113] provides a detailed explanation of this set up in addition to a user's guide. The AUTO in [114] served as

inspiration for the development of a MATLAB system toolbox called the Dynamical System Toolbox in [115]. The team at Concordia University in Canada, led by Professor Doedel, created AUTO, the most well-known software for bifurcation analysis of homogeneous ordinary differential equations.

For this research we are using the latest AUTO-07p in [14] software (open source) to implement the bifurcation analysis of AHV. The guidebook in [14] of AUTO-07p can be used for the installation. The equation-file .f90 file and the constants-file c. file are the two most important input files and these two documents are with the same name. For the continuation calculation, we frequently rely on the c. file. AUTO generates the usual output along with two additional files. Some of the many types of points displayed in the default output are illustrated below.
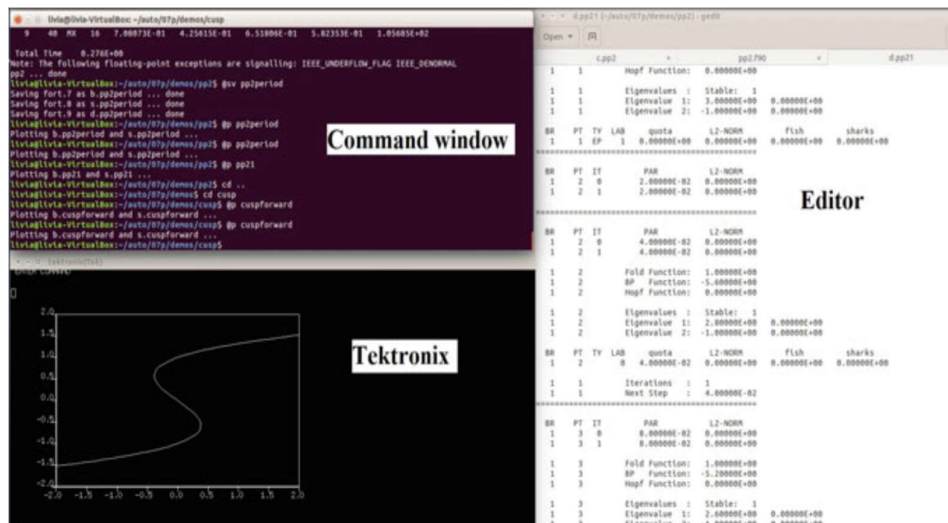
Fig. 5.1 AUTO-07p Command & output window, and editor

There are three distinct file formats that can be generated. The first is the b. file containing the bifurcation diagram, second is the d. file containing the continuation procedures with step size information and with the eigenvalue information of Jacobians, and third the s. file is the solution which includes the solution information. As shown in Fig. 5.1, the AUTO-07p's initial working environment consists of three windows: an editor, a command window, and an output window. The .f90 and c. files are the primary focus of the editor window and it can also be used to access b. and s. files that are generated.

5.2 Bifurcation Diagram for Different Operating Conditions and Control Inputs

The bifurcation analysis can be implemented for the AHVs for varying operative flight conditions and different sonic velocity and control inputs. Applying SBA on an extremely non-linear system could provide novel analysis for the dynamic models of AHVs. Due to the wide flight regimes of the AHVs, continuation technique can provide exceptional analysis for the flight dynamics and control. Implementing SBA to AHVs, the translational and kinematics equations with the variables V, α, q, θ and h can be represented. The importance of Mach number (M) in AHVs is vital due to the different flight regimes of the hypersonic flight, hence $M = $ V/s, were V is velocity and s is speed of sound. Therefore, the states variables and control parameters are, $x = [V \ \alpha \ q \ \theta \ h]'$ and $u = [\delta e]'$, were δe is the elevator deflection. The parameter varied affects directly the α angle of attack of the AHVs and the parameters p in the continuation are fixed during the analysis. The SBA analysis of the AHV dynamic behavior is represented by bifurcation diagram, which helps in the understanding and depicting the flight dynamics. EBA is examined for the level and straight flight at trim conditions, and stability is investigated for the 3DOF longitudinal dynamic model of AHV given by the Eqn. (3.1-3.7).

$$\dot{V} = \frac{1}{m}(T \cos\alpha - \bar{q}SC_D - mg \sin\theta) \tag{5.1}$$

$$\dot{\alpha} = q - \left(\frac{1}{mV}\right)(T \sin\alpha + \bar{q}SC_L - mg \cos\theta) \tag{5.2}$$

$$\dot{q} = M/(2I_{yy}) \tag{5.3}$$

$$\dot{\theta} = q \tag{5.4}$$

$$\dot{h} = V \sin\theta \tag{5.5}$$

Here the aerodynamic model 2 is used for the aerodynamic coefficient C_L, C_D and C_m for the bifurcation analysis of the longitudinal dynamics of AHV. For the Eqn. (5.1-5.5), equilibrium values are obtained equating to 0 for the left hand side of the equation and solving the states $(V, \alpha, q, \theta, h)$. These equilibrium points are required for the bifurcation method for the continuation approach to

start. For simplicity setting $\alpha = \theta = 0$, in Eqn. (5.1-5.5) are solved, to obtain the equilibrium solution with $h = h_0$ and are given by Eqn. (5.6-5.8),

$$T(h_0) = \bar{q}SC_D \tag{5.6}$$

$$V_0 = \bar{q}SC_L/(mg) \tag{5.7}$$

$$M = 0 \tag{5.8}$$

Considering the equilibrium solution in the Eqn. (5.6-5.8) the thrust is equal to the drag, gives the value of thrust at starting equilibrium point, and V_0 is the initial value used in the bifurcation at different equilibrium altitudes setting $h = h_0$, and hence corresponding to $\alpha, q \ and \ \theta$ bifurcation diagram is obtained using the Eqn. (5.2-5.4) in AUTO-07p. The bifurcation diagram is plotted for $\alpha \ and \ \theta$.

The bifurcation diagram for the different cases shown below represents the collection of the different equilibrium points which provides the value of the states relative to the selected parameter. These solution branches are made of different equilibrium points indicating no change in the state variables occurring at the individual points along the curve. The bifurcation diagram is obtained using the AUTO-07p software, where the output shows the numbering which means that, it shows all the equilibrium points for the corresponding range of input variables with the color-coded stability information, where black corresponds to stable and red to unstable. Here negative and positive eigen values corresponds to dynamic system stability and indicate the stable and unstable system behavior. The information is reflected by AUOT-07p by indicating the black color to stable and red color to unstable in the bifurcation diagram.

Bifurcation analysis for the AHV at Mach number, M=0.9 and altitude, h=10000 ft, is carried out and the Bifurcation Diagram obtained is shown in the Fig. 5.2, and it illustrates how the equilibrium solution point shifts between -12^0 and 12^0 deflections when the elevator deflection, δ_e value changes. The AHV stability and bifurcation is examined by focusing on the varying the value of system parameter δ_e and making another parameter, thrust coefficient constant.

Implementing the AUTO-07p code, we observe the numerous bifurcations occurrences for the AHV's states in consideration to the parameter variation.

(a)

(b)

(c)
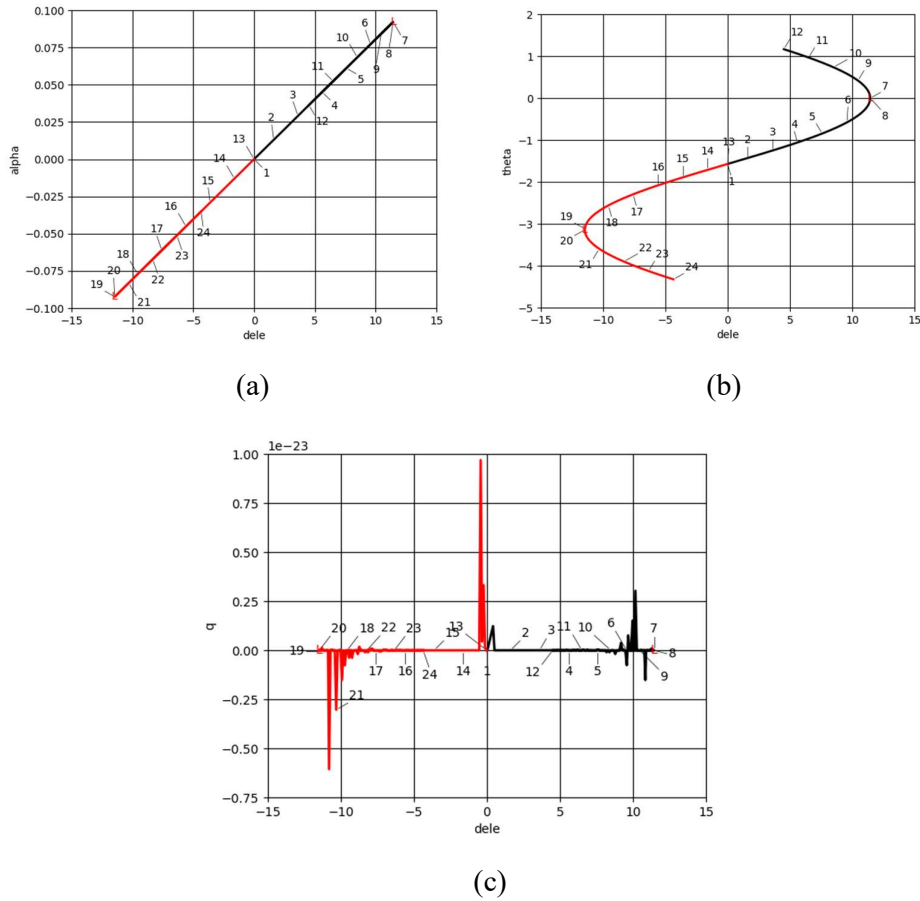
Fig 5.2 Bifurcation Diagram with varying δ_e for M=0.9 (Case A)

Here the angle-of-attack, α given in the Fig. 5.2 (a), when deflected for δ_e from 0^0 to 12^0 degrees, it indicates stable behaviour for the vehicle, and when deflected from 0^0 to -12^0 degrees down it shows stable action.

The pitch angle, θ as shown in the Fig. 5.2 (b), for the elevator deflection, $\delta_{e,} 0^0$ to -12^0 degrees the variation is stable between -4.5 to 1.5 radians and for the -1.5 to -4.25 radians. At each of the 24 possible equilibrium points, AUTO-07p generates result demonstrating stable dynamics for all eigenvalues. For the pitch angle, θ, from the bifurcation diagram, the points 7 and 8 in the Fig. 5.2 (b) show the nose going up, whereas points 19 and 20 show the nose going down. And for the elevator deflection 5^0, the vehicle will have 60^0 nose-down and 60^0 nose-up directional changes at various periods of the vehicle's climb or fall.

75

Table 5.1 – Bifurcation result with forward run in AUTO-07p

BR	PT	TY	LAB	δe (rad)	L2-Norm	α (rad)	θ (rad)	q
1	1	EP	1	0.00000	1.57080	0.00E+00	-1.570E+0	0.00E+00
1	20		2	1.61874	1.42901	1.30E-02	-1.428E+0	2.90E-29
1	40		3	3.61065	1.25028	2.91E-02	-1.25E+0	9.51E-31
1	60		4	5.60149	1.06042	4.51E-02	-1.059E+0	-2.70E-29
1	80		5	7.58995	0.84797	6.11E-02	-8.46E-01	1.42E-27
1	100		6	9.57201	0.58508	7.71E-02	-5.79E-01	-1.191E-26
1	120		7	11.4416	0.09220	9.22E-02	-3.05E-03	4.91E-27
1	121	LP	8	11.4416	0.09215	9.22E-02	1.38E-05	5.74E-28
1	140		9	10.4622	0.42539	8.43E-02	4.17E-01	7.73E-29
1	160		10	8.48822	0.73837	6.84E-02	7.35E-01	-2.00E-27
1	180		11	6.50178	0.96809	5.24E-02	9.67E-01	-4.068E-27
1	200	EP	12	4.51178	1.16626	3.63E-02	1.17E+00	-2.19E-28

Table 5.2 – Bifurcation Result with backward run in AUTO-07p

BR	PT	TY	LAB	δe (rad)	L2-Norm	α (rad)	θ (rad)	q
1	1	EP	1	0.00E+00	1.57E+00	0.00E+00	-1.57E+00	0.00E+00
1	20		2	-1.62E+00	1.71E+00	-1.30E-02	-1.71E+00	9.76E-29
1	40		3	-3.61E+00	1.89E+00	-2.91E-02	-1.89E+00	3.47E-29
1	60		4	-5.60E+00	2.08E+00	-4.51E-02	-2.08E+00	7.11E-28
1	80		5	-7.59E+00	2.30E+00	-6.11E-02	-2.29478	-3.05E-27
1	100		6	-9.57E+00	2.56E+00	-0.077102	-2.55934	-9.77E-27
1	120		7	-1.15E+01	3.12E+00	-0.092300	-3.11735	-3.23E-26
1	121	LP	8	-1.15E+01	3.14E+00	-0.092327	-3.14158	-3.20E-29
1	140		9	-1.03E+01	3.59E+00	-0.083054	-3.59342	-3.03E-24
1	160		10	-8.34E+00	3.90E+00	-0.067136	-3.89795	-1.03E-25
1	180		11	-6.35E+00	4.13E+00	-0.051132	-4.12518	-1.55E-26
1	200	EP	12	-4.36E+00	4.32E+00	-3.51E-02	-4.32E+00	4.09E-27

The pitch rate, q as shown in the Fig. 5.2 (c), for the elevator deflection, δ_e, 0^0 to -12^0 degrees the variation is stable and when deflected δ_e from 0^0 to 12^0

degrees, it also indicates stable behaviour for the vehicle, with ranging in a stable magnitude for the δ_e change.

Table 5.3 – Eigen values for M=0.9 using Bifurcation in AUTO-07p

BR	PT	TY	Iteration	TY Details	Eigen values	Stability
1	1	EP	1	Hopf Function: 1.19248E+00	-3.05831E-02	Stable:3
					-1.19248E+00, 3.12365E+00	
					-1.19248E+00, -3.12365E+00	
1	121	LP	5	Fold Function: 1.54337E-04	-4.08777E-07	Stable: 3
				Fold Function: -2.83356E-01	-1.20756E+00, 3.12940E+00	
				Fold Function: -3.89938E-03	-1.20756E+00, -3.12940E+00	
				BP Function: -6.02481E-02		
				Hopf Function: -1.20756		
1	200	EP	3	Fold Function: -9.95546E-01	2.79319E-02	Stable: 2
				BP Function: -6.35212E-01	-1.22165E+00, 3.13491E+00	
				Hopf Function: -1.22165E	-1.22165E+00, -3.13491E+00	

Running the AUTO-07p code for the bifurcation of AHV using CBA, we obtain the bifurcation diagram as shown in Fig. 5.2. We obtain the simulation results of forward run and backward run for the implemented bifurcation method and is shown in Table 5.1 and Table 5.2 respectively. These tabular results show the bifurcation diagram data points for different run with iterations, indicating the different values of α, θ and q. Here BR, PT, TY and LAB are the Bifurcation Result, Bifurcation Point, Bifurcation Type and Labelled Solution respectively. Here for different range (1 to 200) of PT's, the forward and backward run are carried out with different iterations and corresponding L_2 NORM values for the different selected parameters are determined. It shows that the result is obtained for 200 different points with different iterations and step size at each AUTO-07p run and LP bifurcation type is obtained at 121 run; this indicates the presence of bifurcation point as fold for the ordinary differential equation present in the AHV dynamics. The eigen values determined from the forward and backward run are shown in the Table 5.3 for the corresponding PT for 1, 121 and 200. This shows the different eigen values with respective to the different iteration and the stability of the AHV with the Bifurcation TY. It shows the presence of Hopf function at PT 1 and Iteration 1; and Fold, BP and Hopf

function at PT 121, 200 and Iteration 5, 3; with the eigen values with each iteration. The stability information can be determined with the corresponding each iteration with the eigen values. Considering the trim condition and iteration 1 the eigen values with the dynamic stability information is shown in the Table 5.4 indicating the AHV stability information at the given Mach Number. It shows that there are three eigen values with one eigen value with real number and the two eigen values with complex in nature, as shown in the Table 5.4; and the corresponding damping ratio and the frequency at the given Mach Number is determined indicating the short period mode behaviour of the AHV. For the eigen values considered the pole-zero plot is obtained and is shown in the Fig. 5.3, which outlines the stable behaviour of the AHV at the Mach Number, M=0.9, as all the poles lies at the LHS plane of the stability axis. Thus, it can be said that using the Bifurcation Method the AHV's dynamically stability can be determined and at M=0.9 it is dynamically stable.

Table 5.4 – Dynamic stability using Bifurcation analysis for

Mach Number, $M = 0.9$

Mach No. (M)	Eigen values	Damping Ratio (ζ)	Frequency (ω_n)	Stability
0.9	-3.05831E-02 -1.19248E+00, 3.12365E+00 -1.19248E+00, -3.12365E+00	0.356	3.342	Dynamically Stable
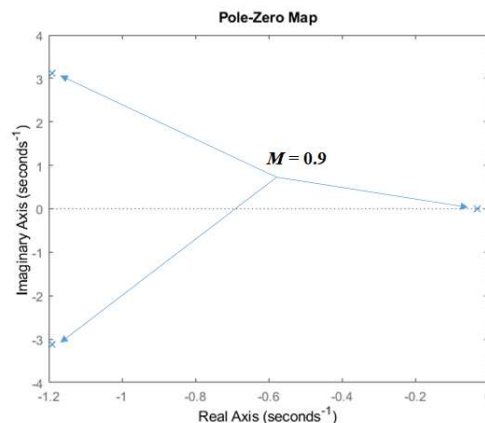
Fig. 5.3 Pole-zero plot for Mach Number, $M = 0.9$

Considering the simulation carried out for the AHV at the Mach Number, M=0.9 it shows, most stable behavior for it, using the Bifurcation Method; and their bifurcation diagrams are nonlinear in nature but are mirror images in the

vertical plane and about $\delta_e = 0^0$. This shows that for the different Mach number of the AHV's flight can be considered to determine the dynamical stability of the vehicle ranging from Mach number, M=0 to 24.

The bifurcation diagram with varying δ_e for M=0.9 (Case A) shown in Fig. 5.2 (a), shows the α variation with equilibrium solution point to change in the different values of δe ranging from -12^0 to 12^0 deflection. Here α is stable for the region of δe deflection from 0^0 to 12^0 and unstable for the δe deflection from 0^0 to -12^0. Similar Fig. 5.2 (b) shows the θ variation from -4.5 to 1.5 radians with the different values of δe ranging from -12^0 to 12^0 deflection corresponding to stable θ region from -1.5 to 1.5 and unstable θ region from -1.5 to -4.25 radians.

The bifurcation diagram with varying δ_e for M=24 (Case B) shown in Fig. 5.4 (a), shows the α variation with equilibrium solution point to change in the different values of δe ranging from -16^0 to 16^0 deflection. Here α is stable for the region of δe deflection from 0^0 to 16^0 and unstable for the δe deflection from 0^0 to -16^0. Similar Fig. 5.4 (b) shows the θ variation from 0.65 to -3.65 radians with the different values of δe ranging from -16^0 to 16^0 deflection corresponding to stable θ region from 0 to -3.65 and unstable θ region from -1.5 to 0.65 radians.

For the bifurcation diagram with varying δ_e for M=6 (Case C) shown in Fig. 5.5 (a), shows the α variation with equilibrium solution point to change in the different values of δe ranging from -20^0 to 20^0 deflection. Here α is stable for the region of δe deflection from 0^0 to 20^0 and unstable for the δe deflection from 0^0 to -20^0. Similar Fig. 5.5 (b) shows the θ variation from -1.1 to -2 radians with the different values of δe ranging from -20^0 to 20^0 deflection corresponding to stable θ region from -1.65 to -2 and unstable θ region from -1.65 to -1.25 radians.

For the bifurcation diagram with varying δ_e for M=4 (Case D) shown in Fig. 5.6 (a), shows the α variation with equilibrium solution point to change in the different values of δe ranging from -5^0 to 5^0 deflection. Here α is unstable for the complete region of δe deflection from -5^0 to 5^0. Similar Fig. 5.6 (b) shows the θ variation from -7.5 to 4.5 radians with the different values of δe ranging

from -5^0 to 5^0 deflection corresponding to stable θ region from -1.5 to -7.5 and unstable θ region from -1.5 to 4.5 radians.

The bifurcation diagram with varying δ_e for M=10 (level flight at 100000 ft) shown in Fig. 5.7 (a), shows the α variation with equilibrium solution point to change in the different values of δe ranging from -15.5^0 to 15.5^0 deflection. Here α is stable for the region of δe deflection from 0^0 to -12^0 and unstable for the δe deflection from 0^0 to -12^0. Similar Fig. 5.7 (b) shows the θ variation from -1 to -2.25 radians with the different values of δe ranging from -15.5^0 to 15.5^0 deflection corresponding to stable θ region from -1.56 to -2.25 and unstable θ region from -1.56 to -1 radians.

(a)   (b)
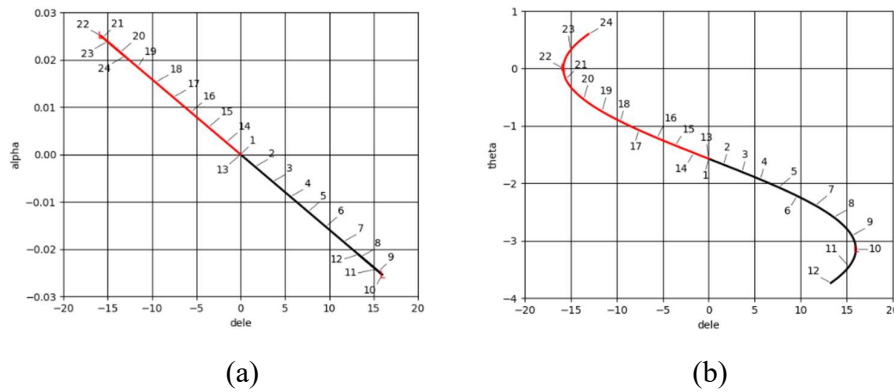
Fig. 5.4 Bifurcation diagram with varying δ_e for M=24 (Case B)

(a)   (b)
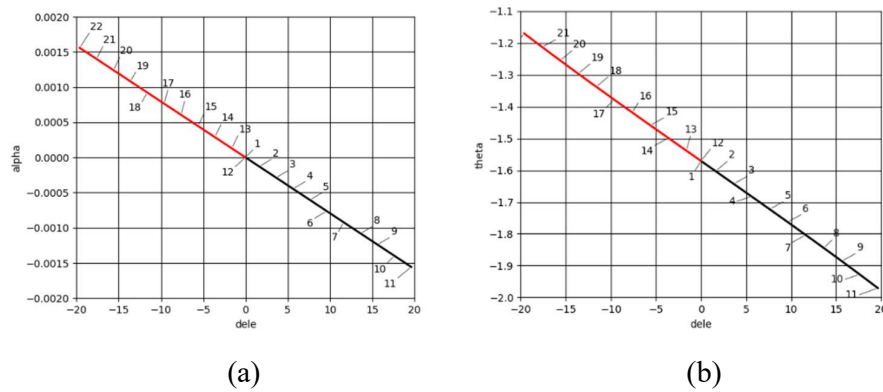
Fig. 5.5 Bifurcation diagram with varying δ_e for M=6 (Case C)

(a)　　　　　　　　　　　　　　　(b)
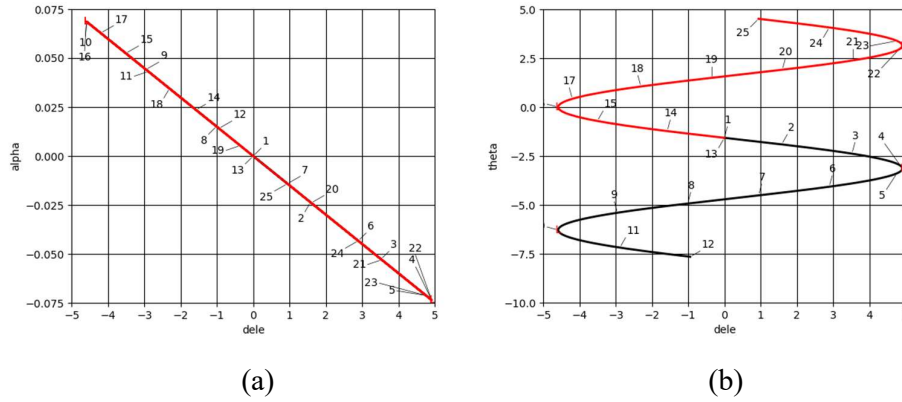
Fig. 5.6 Bifurcation diagram with varying δ_e for M=4 (Case D)

(a)　　　　　　　　　　　　　　　(b)
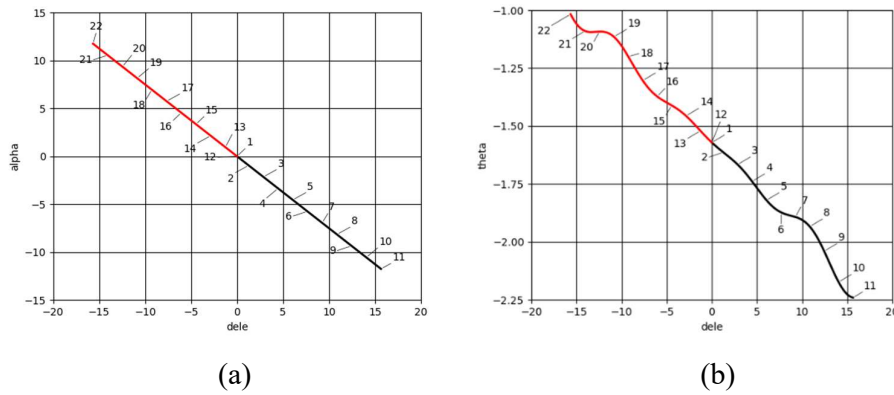
Fig. 5.7 Bifurcation diagram with varying δ_e for M=10

5.3 Flight Dynamic Analysis for Different Operating Conditions using Bifurcation Method

Using the bifurcation method to demonstrate global stability presents a chance to improve vehicle control design parameters. The technique provides quantitative data on global stability and suggests ways to control the aircraft's nonlinear behaviour. The technique uses CBA (Continuation-Based-Algorithm) to study the nonlinear-dynamical models considering ODE (Ordinary-Differential-Equation) of first order and determine the steady states and different equilibrium points, by using the software AUTO-07p [14]. To identify all trim states for an ODE expressed as a function of states variables and control parameters given by, $\dot{x}=f(x,u)$, the solution of the nonlinear equation is specified by, $\dot{x}=f(x,u,p)=0$, where p is a constraint held constant while the next parameter u is varied. CBA is an implementation of the standard Bifurcation

Analysis (SBA) technique. By taking both the variable and constant parameters into account, the continuation algorithm generates all possible solutions with trim states for the system and calculates the specifics of the local stability at each trim state. 'Bifurcation Points' are used to describe or illustrate transitions in the branch stability of the trim state's solution. These 'Bifurcation Points' prominently display the occurrence or behavior of an unstable dynamical system by indicating the instant at which the eigenvalues of the system migrate from the left half to the right half of the complex plane, indicating instability. SBA is used to the nonlinear dynamic model of the 3DOF longitudinal AHV to accomplish the approach. The dynamic model represented for the 3DOF AHV model simulation is used for the method implementation, and the state variables are given by $x=[M,\gamma,\alpha,\theta,q,h]'$. Because of these simplifications, the state variable evaluated for the analysis is $x=[\alpha,\theta,q]'$, where, h, and M are constants and where q is assumed to vary by only very small amounts. When applied to the AHV, SBA yields a bifurcation diagram containing eigen values for each scenario, illuminating the avionics' dynamical behaviour in flight. The eigen values derived from the bifurcation analysis can be used to investigate the longitudinal dynamic model's stability. Depending on these eigen values, the system's behaviour could be stable or unstable. Table 5.5 displays the eigen values obtained via the bifurcation method for the various Mach number cases. Fig. 5.8 displays the pole-zero map obtained from the eigen values in order to comprehend the system stability behaviour. Cases 1, 3, and 4 exhibit stable conduct as evidenced by the poles plot, while Cases 2, 5, and 6 exhibit unstable behaviour as evidenced by the poles lying on the RHS-plane.

Table 5.5 – Calculated Eigen values via the Bifurcation Approach

Simulation Cases	Mach Number (M)	Eigen Values	Stability
1	0.9	-0.0305831, -1.192±j3.123	Stable
2	4	1.69283, -0.009158, -2.49717	Unstable
3	6	-0.006419, -0.021±j2.501	Stable
4	10	-0.00523866, -0.0086±j0.073	Stable
5	15	0.123599, -0.003423, -0.150586	Unstable
6	24	3.11523, -0.002149, -3.19905	Unstable
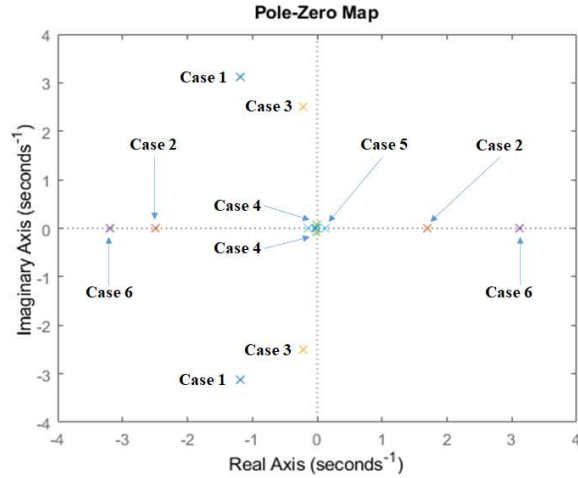
Fig. 5.8 - System Poles plot for the simulation cases

The corresponding longitudinal modes for the simulation cases 1, 3 and 4 are obtained and is shown in the Table 5.6. For cases 1 and 4 at Mach number $M=0.9$ and $M=10$ its shows short period behavior for the AHV flight, and for case 3 at Mach number $M=6$ its shows long period or phugoid behavior for the AHV flight.

Table 5.6 – Simulation cases with longitudinal modes

Cases	Mach Number	Frequency (rad/sec)	Damping Ratio	Periods (sec)	Numbers of cycles to damp to half amplitude of the respective modes
1	0.9	0.35665	0.3817	17.6081	2.8506, short period
2	4	-	-	-	-
3	6	0.00846	0.0084	742.2356	128.6150, long period
4	10	0.11803	0.1188	53.2044	9.1551, short period
5	15	-	-	-	-
6	24	-	-	-	-

The cases 2, 5 and 6 at Mach number $M=4$, $M=15$ and $M=24$ indicates unstable or instability behavior for the AHV flight. This unstable Mach number for the AHV flight can be made stable with the design of suitable control design methods, and hence the entire flight envelops of the AHV from Mach number $M=0$ to 24 can have a stable flight.

5.4 Chapter Summary

The topological behavior of the generic AHV model provides the quantitative assessment of the equilibrium states for the entire wide flight regimes of the

dynamic AHV model with high altitude and Mach number. The static and dynamic stability and global stability of the AHV model using Bifurcation Analysis is carried out. And the flight dynamics and stability analysis for the generic AHV model using 3-DOF dynamic simulation model is presented with the Bifurcation Method. The analysis shows that the Bifurcation Method is a powerful tool to analyze the stability regions with the different equilibrium points of the chosen parameters.

Bifurcation analysis of Longitudinal dynamics for Generic AHV model considering CBA has been implemented for AHV dynamics at Mach Number, M=0.9, for different choices of elevator deflection and with the aim to observe the control effects. Bifurcation technique is implemented with the 3DOF longitudinal AHV model using the AUTO-07p platform for the different elevator deflection, δ_e= -12^0 and 12^0. The Bifurcation Diagram obtained for the data points with different forward and backward runs with the different iterations, shows the parameter values of α, θ and q. The forward and backward run shows the presence of Hopf function at PT 1 with iteration 1, and Fold, BP and Hopf function at PT 121, 200 and iteration 5, 3; with the eigen values with each iteration. The stability information is determined with the corresponding iteration of the eigen values, showing the dynamic stability information. The eigen values determined indicate the short period mode behaviour of the AHV indicating the stable behaviour at the Mach Number. The Method shows the AHV's dynamically stability determined at M=0.9 is stable. This shows that for the different Mach Number of the AHV's flight, Bifurcation is promising method to determine the dynamical stability of the vehicle for the Mach number ranging from M=0 to 24. Finally, the paper outlines Bifurcation Methodology application intended for the investigation of the dynamic stability of the Generic AHV.

Trim analysis eigen values are calculated and related poles are established for all cases using the bifurcation approach, confirming that Cases 1, 3, and 4 are stable whereas Cases 2, 5, and 6 are unstable. Cases 1 and 4 exhibit short-period behavior, as seen by the AHV's longitudinal modes, while case 3 exhibit long-period, or phugoid, behavior. The given bifurcation analysis results show a possible method for identifying stable trim points.

CHAPTER 6

CLOSE LOOP SIMULATION OF AHV

The complications and difficulties with hypersonic vehicles' aerodynamics explain the many aerodynamic phenomena that occur at various altitudes and high speeds of flight. The AHV hypersonic flight has issues due to the huge flight envelope and the dynamical interaction within the many hypersonic flight regimes. This necessitates the use of dynamic analysis of the AHV and flight dynamics analysis with stability analysis. This chapter presents the linear model analysis with the linearized aerodynamic coefficient and covers the full AHV flight regime. Nonlinear dynamic AHV model is also presented with the nonlinear aerodynamic coefficient data. The linearized AHV model is used with the linear aerodynamic model, thrust engine model and atmospheric model to develop the linear 6DOF dynamic AHV model for simulation. With the developed linear model, stability is analyzed with the classical control method like root locus to understand the dynamic behavior of the zero poles location and hence stability, and controller design approaches can be implemented. Further state feedback approach is used to analysis open loop and closed loop response of the linear 6DOF dynamic AHV model, indicating the closed loop stability of the AHV. The control design is carried out using the linear state feedback control law design using pole placement, and controllers like PI, PD and PID are used for the controller development for AHVs. The linear controller is designed for the AHV for different control inputs and stability is analysed.

6.1 Flight Dynamics Analysis for Different Control Inputs

The AHV's linear aerodynamics model incorporates the various propulsion and engine models and is obtained over the entire flight regime. The linearized equations are taken into account while designing the controller and stability analysis for the AHV's 6DOF dynamic simulation model.

Considering the nonlinear AHV model given by Eqn. (3.29-3.37) and Eqn. (3.38-3.40) are linearized using small disturbance theory in [99] and with steady and wing level flight, and with no sideslip is considered as reference condition with steady and perturbated. The linearized model derived here with the longitudinal and lateral dynamics model are decoupled from each other. The linear model obtained here is considered for the case of level and straight flight at fixed velocity and altitude considering the bank angle zero. The linear AHV model is expressed with the state space design approach and the model is represented by Eqn. (6.1-6.2), and here A_n is the normal acceleration of the AHV.

$$\dot{X} = AX + BU \tag{6.1}$$

$$Y = CX + DU \tag{6.2}$$

The state space variables are given by Eqn. (6.3-6.5).

$$X = [V \ h \ \alpha \ \theta \ q \ T \ \beta \ \phi \ p \ r]' \tag{6.3}$$

$$U = [PLA \ \delta a \ \delta e \ \delta r]' \tag{6.4}$$

$$Y = [A_n \ q \ \alpha]' \tag{6.5}$$

6.2 Linear Aerodynamic Model

The nonlinear aerodynamic coefficient of AHV is given by Eqn. (3.41-3.52), are linearized for the 6DOF linear model simulation considering at Mach number, $M = 5$. The linearized equations for the dynamic simulation of linear AHV model is obtained using analytical method considering fixed point for linearization and ignoring the higher terms, the reduced and the linearized model is obtained by Eqn. (6.6-6.11).

$$C_L = C_{L,\alpha}.\alpha + C_{L,\delta e}.\delta_e \tag{6.6}$$

$$C_D = C_{D,\alpha}.\alpha + C_{D,\delta e}.\delta_e \tag{6.7}$$

$$C_m = C_{m,\alpha}.\alpha + C_{m,\delta e}.\delta_e + C_{mq}\left(\frac{qc}{2V}\right) \tag{6.8}$$

$$C_Y = C_{Y,\beta}.\beta + C_{Y,\delta a}.\delta_a + C_{Y,\delta r}.\delta_r \qquad (6.9)$$

$$C_l = C_{l,\beta}.\beta + C_{l,\delta a}.\delta_a + C_{l,\delta r}.\delta_r + C_{lr}\left(\frac{rb}{2V}\right) + C_{lp}\left(\frac{pb}{2V}\right) \qquad (6.10)$$

$$C_n = C_{n,\beta}.\beta + C_{n,\delta a}.\delta_a + C_{n,\delta r}.\delta_r + C_{nr}\left(\frac{rb}{2V}\right) + C_{np}\left(\frac{pb}{2V}\right) \qquad (6.11)$$

and $\left(\frac{qc}{2V}\right)$ is non-dimensional pitch rate. The linear aerodynamic coefficient model obtained is used for the 6DOF linear simulation for the AHV model. Aerodynamics coefficient, dynamics, as stated in [13], [116], are implemented to develop aerodynamic model of total lift coefficient, drag coefficient, pitching moment coefficient, side force coefficient, rolling moment coefficient, yawing moment coefficient as C_L, C_D, C_m, C_Y, C_l and C_n respectively, and is given using Eqn. (6.6-6.11) considering entire flight envelop of AHV. Interpolation is performed by creating subroutines of the aerodynamic data and the aerodynamic coefficients are determined. Aerodynamic force represented with lift force is described with $L = \bar{q}SC_L$, drag force represented with $D = \bar{q}SC_D$, side force expressed with $Y = \bar{q}SC_Y$, the rolling moment as $L_a = \bar{q}SbC_l$, the pitching moment is expressed as $M_a = \bar{q}ScC_m$, and yawing moment is given by $N_a = \bar{q}SbC_n$. Here $\bar{q}$, S, b, c is the dynamic pressure, reference area, span and mean aerodynamic chord respectively. The linear aerodynamic coefficient equations of the 6DOF dynamic simulation model of AHV is given by Eqn. (6.6-6.11). Here the control surfaces of AHV are given by δ_e, δ_a, and δ_r as elevator, aileron, and rudder deflection. The elevon (left and right) relation to aileron and elevator deflection is developed using the relation as $\delta_{left\_e}=\delta_a+\delta_e$ and $\delta_{right\_e}=-\delta_a+\delta_e$. The increment derivatives are given by the notation $C_{L,\alpha}$ and $C_{L,\delta e}$ for lift, and similarly expressed for drag, pitching moment, side force, rolling moment and yawing moment, and here V is AHV free stream velocity.

6.3 AHV Model Simulation

The linear AHV model developed in [16] is used for the 6DOF modelling and simulation, to obtain the transient response for the Y given by Eqn. (6.5). The linear aerodynamic model is used for the simulation. The thrust model with engine dynamics with ramjet/scramjet engine considering Eqn. (3.63) is used

for the simulation for Mach number, $M = 5$ and $h = 65000\,ft$. The thrust engine model in [16] is used over broad variation of the flight envelopes. The proposed propulsion incorporates theoretical ramjet and scramjet engine. Considering 6DOF model, AHV engine dynamics using Eqn. (3.57) is implemented with Mach number, height and with PLA (pilot-lever-angle), and a function with selected flight envelop of M=5. Mach number with related altitude changes, need the use of an atmospheric model that includes temperature and density data. As the temperature and density of the air are affected by the height disparity, the relation is given by Eqn. (3.63) for height, $h\geq36089\,ft$ (11000 m).

The dynamic model for simulation using Eqn. (3.38-3.40) and Eqn. (3.32-3.37) are used to obtain the AHV model given by the states $[V, h, \alpha, \theta, q, T, \beta, \phi, p, r]^T$. Considering the nonlinear AHV model given by Eqn. (3.38-3.40) and Eqn. (3.32-3.37) are linearized using small disturbance theory in [99], and with steady and wing level flight and with no sideslip, is considered as reference condition with steady and perturbated state. The linearized model derived here with the longitudinal and lateral dynamics model are decoupled from each other. The linear model obtained here is considered for the case of level and straight flight at fixed velocity and altitude considering the bank angle as zero. The linear AHV model is expressed with the state space design approach in [100] and the model is represented by Eqn. (6.1-6.2), and here A_n is the normal acceleration of the AHV; pitch rate and angle of attack are given by q and α. The states, input and output are given by Eqn. (6.3-6.5).

The state variables given by Eqn. (6.3) are determined for the M=5 and the state space model matrices are obtained as **A**, **B**, **C**, and **D**. This model is obtained considering the level and straight AHV flight for considered velocity as M=5 and height of 65000 ft (19812 m) considering the banking angle of zero. The model obtained is decoupled from the longitudinal and lateral system interactions. The linearized model **A**, **B**, **C**, and **D** is obtained for the AHV model considering trimmed for M=5 and height of 65000 ft (19812 m).

$$A = \begin{bmatrix}
0 & 0 & -6.238 & -0.0312 & 0 & 0 & 0 & 0 & 0 & 0 \\
0.0002 & 0 & -4.851 & 4.851 & 0 & 0 & 0 & 0 & 0 & 0 \\
0 & 0 & -0.0002 & 0 & 0.001 & 0 & 0 & 0 & 0 & 0 \\
0 & 0 & 0 & 0 & 0 & 0 & 0 & 0 & 0 & 0 \\
0 & 0 & -0.0125 & 0 & 0 & 0 & 0 & 0 & 0 & 0 \\
0 & 0 & 0 & 0 & 0 & 0 & 0 & 0 & 0 & 0 \\
0 & 0 & 0 & 0 & 0 & 0 & -0.0001 & 0 & 0 & -0.001 \\
0 & 0 & 0 & 0 & 0 & 0 & 0 & 0 & 0.001 & 0.0002 \\
0 & 0 & 0 & 0 & 0 & 0 & -0.0023 & 0 & 0 & 0 \\
0 & 0 & 0 & 0 & 0 & 0 & 0.0005 & 0 & 0 & 0
\end{bmatrix}$$

$$B = \begin{bmatrix}
36.92 & -0.0029 & 0 & 0.0016 \\
0 & 0 & 0 & 0 \\
-0.0003 & 0.0001 & 0 & 0 \\
0 & 0 & 0 & 0 \\
0 & 0.0018 & 0 & 0 \\
0 & 0 & 0 & 0 \\
0 & 0 & 0 & 0.0001 \\
0 & 0 & 0 & 0 \\
0 & 0 & -0.0056 & 0.0047 \\
0 & 0 & 0 & -0.0021
\end{bmatrix}$$

$$C = \begin{bmatrix}
0.0003 & -0.0524 & -12.48 & 0 & 0 & 0 & 0 & 0 & 0 & 0 \\
0 & 0 & 0 & 0 & 1 & 0 & 0 & 0 & 0 & 0 \\
0 & 0 & 57.3 & 0 & 0 & 0 & 0 & 0 & 0 & 0
\end{bmatrix}$$

$$D = \begin{bmatrix}
0 & -0.0107 & 0 & -0.0107 \\
0 & 0 & 0 & 0 \\
0 & 0 & 0 & 0
\end{bmatrix}$$

6.3.1 Open Loop Simulation of AHV

The open loop dynamic simulation is carried out for the output state space model given by Eqn. (6.5) and for the corresponding inputs from aileron and rudder deflections using Eqn. (6.4). Considering the linearized model of the AHV given by Eqn. (6.3-6.5), the 6DOF linear model simulation using [100] is carried out. From the Fig. 6.1-6.4 show the transient response of the AHV model given by Eqn. (6.1-6.2).
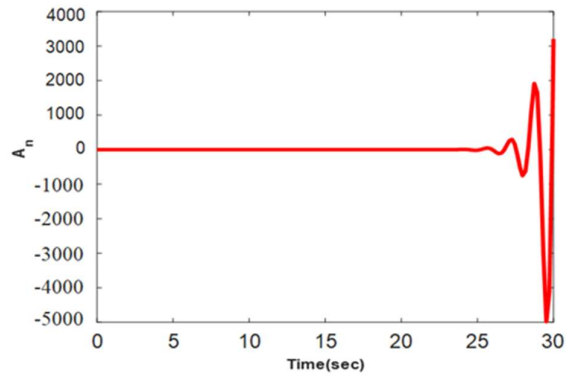
(a)
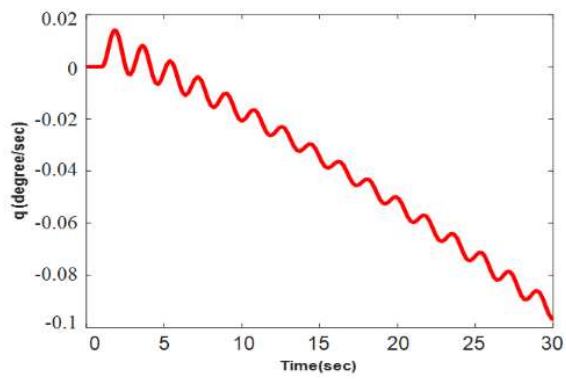
(b)
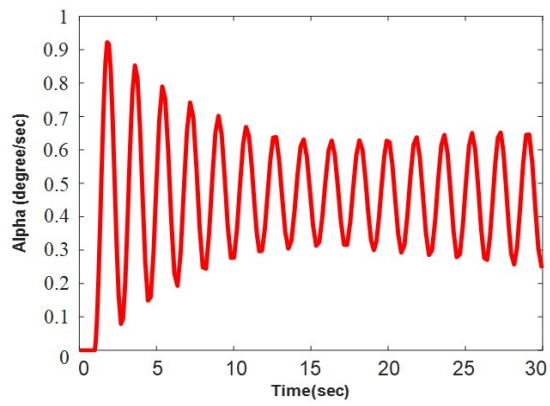
(c)

Fig. 6.1 Response for elevator deflection δ_a
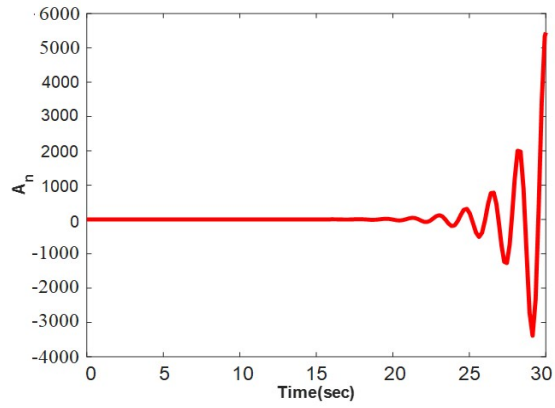
(a)
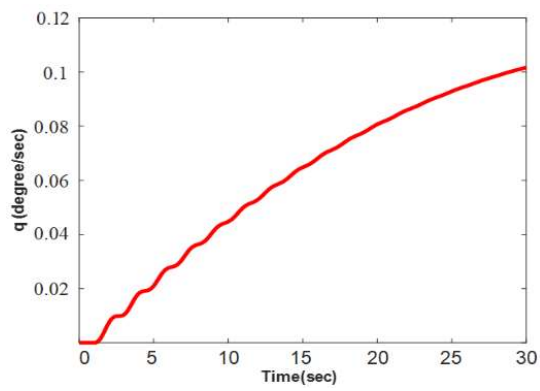
(b)
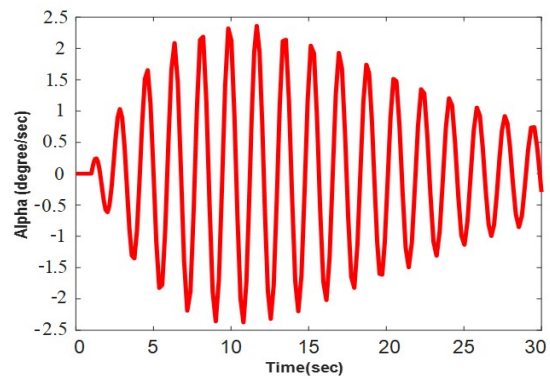
(c)

Fig. 6.2 Response for rudder deflection δ_r
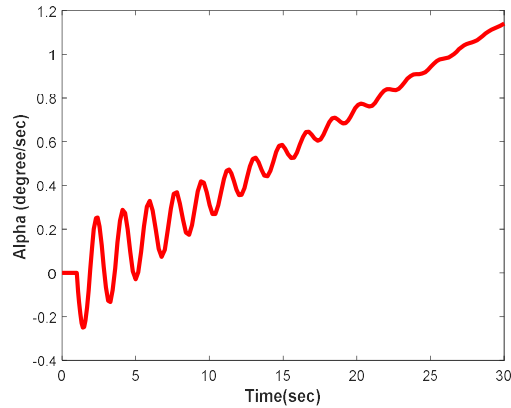
Fig. 6.3 Transient response for PLA
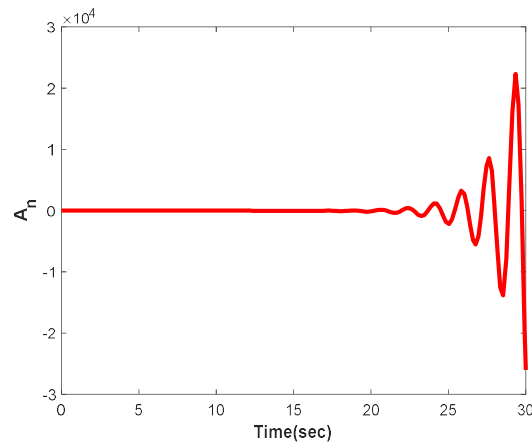
Fig. 6.4 Transient response for PLA

6.3.2 Open Loop Model Analysis

Considering the linearized model of the AHV given by Eqn. (6.3-6.5), the model trim is obtained at Mach number, $M = 5$ and at altitude $h = 65000, ft$ at level flight. The linearized AHV model is developed for linear time invariant control design applicability. The open loop dynamic analysis shows the stability concerns using Bounded Input Bounded Output (BIBO) condition in [117] for the simulated flight behaviour. For the δ_a deflection, A_n shows unstable behaviour and, α and q remain stable for the considered flight condition as shown in Fig. 6.1. Similarly, for the δ_r deflection, A_n, q and α results in the unstable behaviour of the AHV flight as shown in Fig. 6.2. Therefore, AHV flight for the considered state must be stabilised for the δ_a and δ_r deflection, using controller design and closed loop analysis for all outputs. The stability

analysis of the linear model is carried. In Fig. 6.5 the pole zero plot shows that the model has poles and zeros on the RHS plane and occurrence of non-minimum phase, which results in the unstable of the system, this suggests designing a controller to make the stable behaviour of the AHV model at the flying flight condition. As a result of these nonminimum phases in [118]-[119], which render the system unstable, the AHV model flight circumstances for the anticipated level flight at M=5 Mach number are unstable.
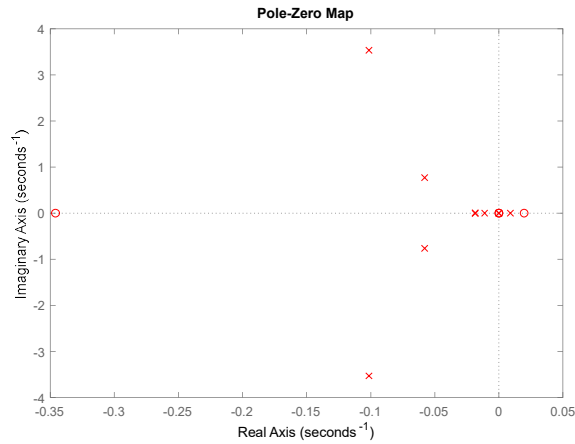
Fig. 6.5 Pole zero plot
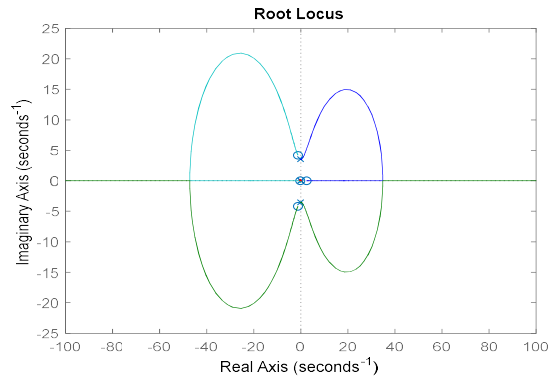
Fig. 6.6 Root locus plot of A_n for δa deflection
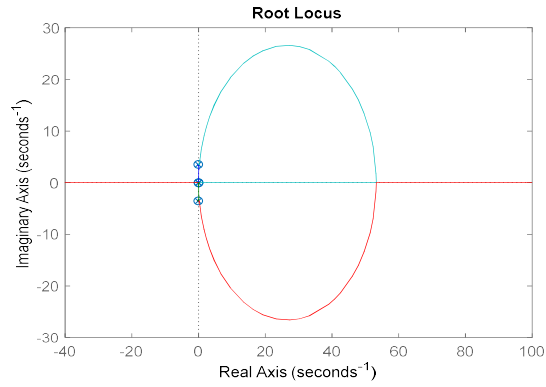
Fig. 6.7 Root locus plot of A_n for δr deflection
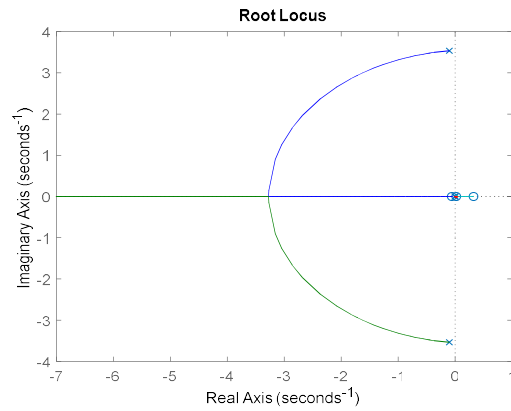
Fig. 6.8 Root locus plot of q for δa deflection
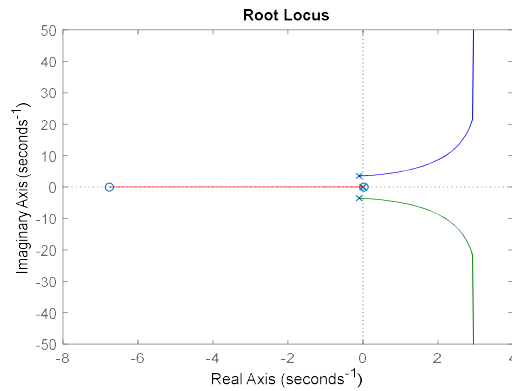
Fig. 6.9 Root locus plot of q for δr deflection

For the AHV model represented by Eqn. (6.1-6.2), root locus is obtained corresponding to the different input and output. It is observed that for the δa

deflection, A_n results in unstable behaviour of the AHV at the corresponding flight condition as shown in Fig. 6.6. Similarly, for the δr deflection A_n, q and α results in the unstable behaviour of the AHV flight is shown in Fig. 6.7, Fig. 6.9 and Fig. 6.11. It is also observed that for the δa deflection, α and q remain stable for the given AHV flight and is shown in Fig. 6.6, Fig. 6.8 and Fig. 6.10. So, it becomes necessary for the unstable states, the controller design and closed loop analysis can be performed for the AHV flight to be stable for all the states and outputs.
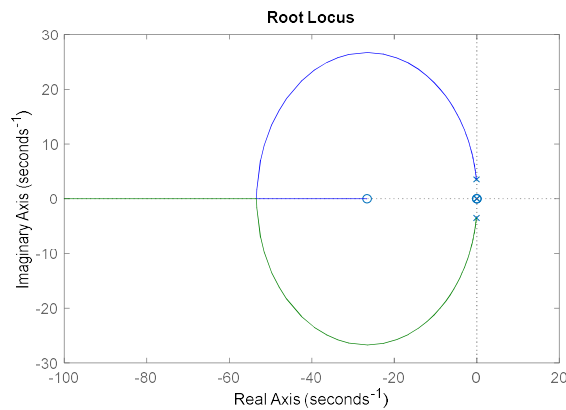
Fig. 6.10 Root locus plot of α for δa deflection
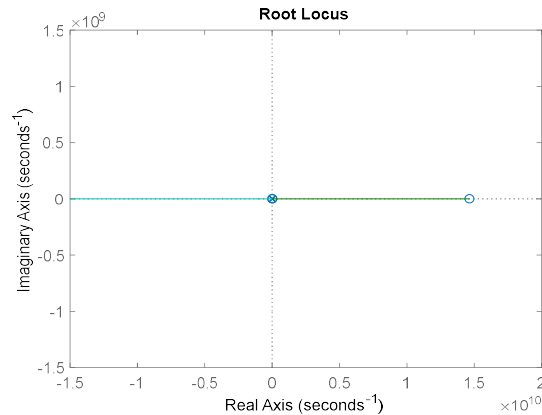
Fig. 6.11 Root locus plot of α for δr deflection

6.4 Closed Loop Control Design

The controller design aspects for the AHVs from the control law design point of view using state feedback approach in [120] is presented here. There is a

strong correlation between the closed-loop stability of Linear Time Invariant (LTI) system and location of the system's poles. As a result, while designing a closed-loop system, the poles placed should have reasonable and anticipated performance. The pole-placement method uses state feedback or output feedback to locate the poles at the required location. Pole placement is critical in system design since system performance is directly related to pole placements. There are two primary steps that must be followed. The placement or assignment of poles is the initial stage, followed by the determination of feedback using gain values. The system's control is required and adequate for the state feedback-based strategy using closed-loop pole placement method.

Controllability is a critical quality to test before we can use our state-space controller design methodologies in [121]-[122]. There must be a controllability attribute in order for us to influence the system's current state. The system's closed loop poles may be located anywhere on the s-plane. The controllability matrix given by Eqn. (6.12) must be satisfied for the system to be fully state controllable,

$$P = [B \quad AB \quad A^2B \quad \dots \quad A^{n-1}B] \tag{6.12}$$

and should have rank n. The number of rows in a matrix determines its rank (or columns) and the system has n state variables, were n is state variables count.

State-space method with state feedback technique offers more appropriate control design constraints considering movement with complete closed-loop pole autonomously to one another. A controller with full-state feedback creates the input vector $u(t)$, and accordingly the control-law is designed with state-space representation. Considering the control law design using state feedback method, the LTI system state model expressed with Eqn. (6.1-6.2), indicating open-loop dynamics representation needs controller design. For the state feedback based design control law using state model is expressed using Eqn. (6.13),

$$u(t) = -Kx(t) + r(t) \tag{6.13}$$

where the dimension of K is $m \times n$, and to accomplish required system attributes with feedback approach the state-run equations is expressed using Eqn. (6.14),

$$\dot{x}(t) = (A - BK)x(t) + Br(t) \tag{6.14}$$

and the block diagram depiction of Eqn. (6.14), is represented and given by Fig.
6.12.
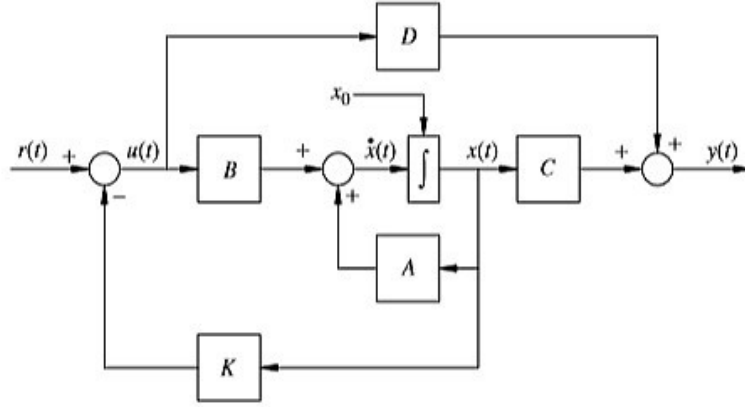
Fig. 6.12 Model closed-loop state feedback control

Transfer function from state space representation is presented and given by Eqn.
(6.15),

$$G = C(sI - A)^{-1}B + D \tag{6.15}$$

with the characteristics polynomial for the system is expressed and provided
using Eqn. (6.16).

$$|sI - (A - BK)| = 0 \tag{6.16}$$

Considering a symmetric set of n complex values given by $(\mu_1, \mu_2, \ldots, \mu_n)$,
indicating considered closed-loop eigenvalues of the system, hence desired
closed-loop characteristics polynomial is given by Eqn. (6.17).

$$\alpha(s) = (s - \mu_1)(s - \mu_2)\ldots(s - \mu_n)$$

$$= s^n + \alpha_{n-1}s^{n-1} + \ldots + \alpha_2 s^2 + \alpha_1 s^1 + \alpha_0 \tag{6.17}$$

For determining the state feedback gain **K**, Ackermann's formula is used and
considering closed-loop characteristics polynomial $\alpha(s)$, and the gain of the
state-feedback is expressed using Eqn. (6.18),

$$K = [0 \quad 0 \quad \ldots \quad 0 \quad 1]P^{-1}\alpha(A) \tag{6.18}$$

where **P** gives controllability matrix and controllable pair (**A**, **B**) and α(**A**) gives
$n \times n$ matrix given by Eqn. (6.19).

$$\alpha(A) = A^n + \alpha_{n-1}A^{n-1} + \ldots + \alpha_2 A^2 + \alpha_1 A^1 + \alpha_0 I \tag{6.19}$$

The state-feedback can be designed with the gain matrix for achieving desirable closed-loop eigenvalues and can be implemented as shown in Fig. 6.13, using state-space model demonstration with desired control.

Linear state feedback control law design with pole placement is used in the control design for the AHV model and controller is implemented and is compared to those obtained with other controllers like proportional-integral (PI) controller and proportional-integral derivative (PID) in [123]. State realization using feedback version for the feedback-based controller design are realized using Eqn. (6.15) and is modelled using closed-loop state equation with pole positioning to achieve the required performance attributes.

The control design is carried out using linear state feedback control law design using pole placement, and comparison with other controllers like PI, PD and PID is performed. The linear model given by Eqn. (6.1-6.2) represents the open loop system which are required for controller design. Using the feedback control law design using state feedback is given by Eqn. (6.13). The desired performance characteristics of the model for the closed loop state equation using pole placement is given by Eqn. (6.1-6.2) and Eqn. (6.20).
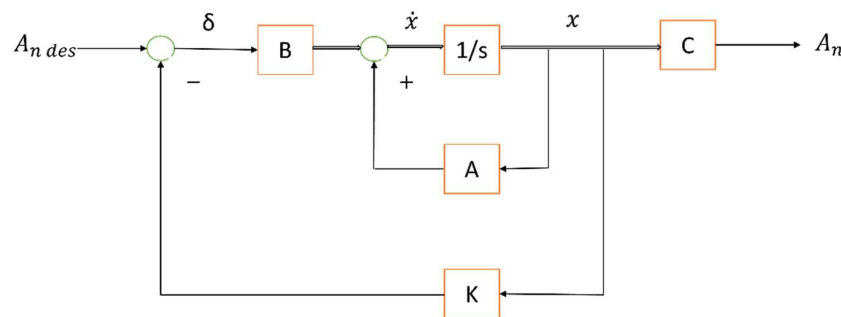
Fig. 6.13 State model representation with desired control

$$K = \begin{bmatrix} -0.1014 + 3.5328i \\ -0.1014 - 3.5328i \\ -0.0089 + 0.0000i \\ -0.0111 + 0.0000i \\ -0.0580 + 0.7680i \\ -0.0580 - 0.7680i \\ -0.0184 + 0.0068i \\ -0.0184 - 0.0068i \\ 0.0000 + 0.0000i \\ 0.0000 + 0.0000i \end{bmatrix} \qquad (6.20)$$

The gain value K for the AHV closed loop performance is determined using pole placement and is given by Eqn. (6.20). The control law design is implemented in MATLAB with the state feedback approach as shown in the Fig. 6.12. In MATLAB, the state feedback technique is used to implement the control law design as shown in Fig. 6.14. The aileron and rudder desired deflection is controlled using the controller for the AHV linear model using feedback design and corresponding deflection in terms of controller response is obtained. AHV model is simulated using MATLAB software for dynamic simulation. The dynamic response for AHV model is performed with different controller implementation using the block diagram as illustrated with Fig. 6.13 and Fig. 6.14.
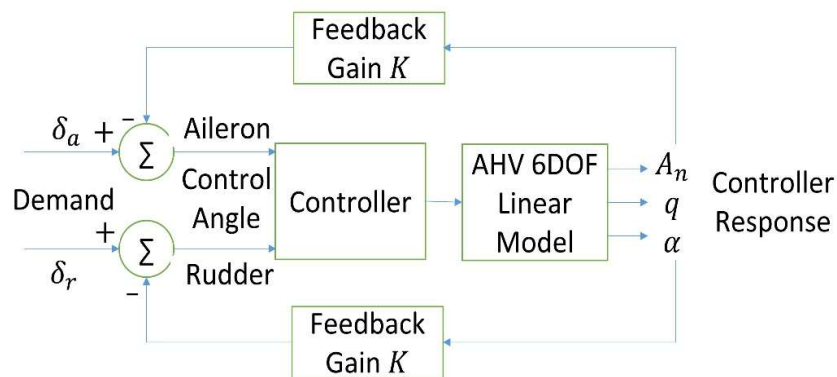
Fig. 6.14 Feedback with controller design

6.5 Closed Loop Simulation and Results

The AHV 6DOF linear model is used for the control design considering state feedback development using pole placement. AHV model given by Eqn. (6.1-6.5) is used for the open loop simulation, with the linear aerodynamic coefficients using Eqn. (3.41-3.52) and the propulsion engine model by Eqn. (3.57) is incorporated in the simulation, and the state feedback with pole placement using Eqn. (6.16) and Eqn. (6.20), is used for the dynamic stability implementation. The linear AHV state space model output given by Eqn. (6.5) is simulated for the control to be implemented for the corresponding input given by Eqn. (6.4). Closed loop simulation is performed for the output A_n, and a comparison for open and closed loop is shown in Fig. 6.15. The open-loop and closed-loop response analysis of AHV is shown in Fig. 6.15 and illustrates the

stability with closed loop design and hence shows convergence in the output generated via the use of the pole placement design and state feedback technique.

The dynamic simulation of the AHV model is carried out using the MATLAB software. The 6DOF linear AHV model simulation is performed with the initial parameters and the system parameters in [64]. The open loop and closed-loop response analysis of AHV model are given by the Fig. 6.15, indicating the convergence of the output is obtained by the state feedback approach using the pole placement design.
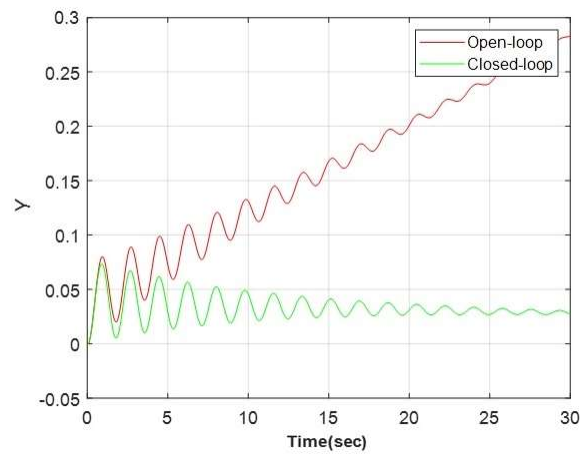
Fig. 6.15 Output response of Y for open and closed loop

Fig. 6.16 represents the controller design implementation for output A_n, and for δ_a deflection PI controller generates better response time due to less overshoot to PID and for δ_r deflection PI controller gives better response and fast settling time in comparison to PID.
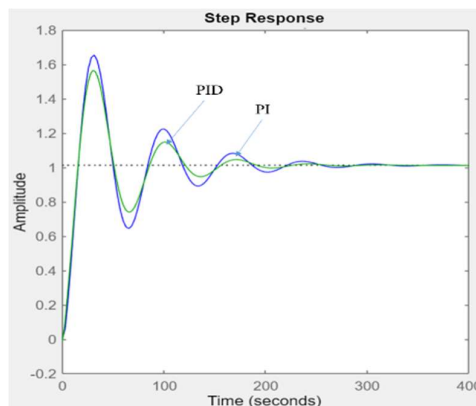
(a)
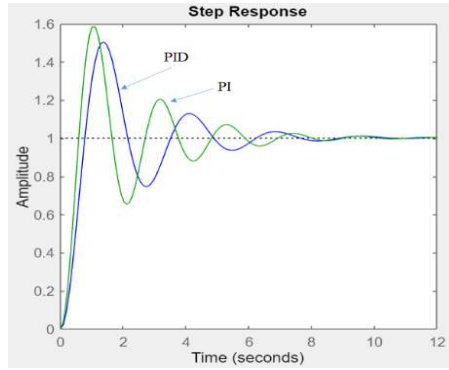
(b)

Figure 6.16. Response to controller design for output A_n for

(a) δ_a deflection and (b) δ_r deflection

Fig. 6.17 shows the controller design for output q, and for δ_a deflection PID controller generates better response and faster settling time and for δ_r deflection PID controller gives better response and fast settling time.
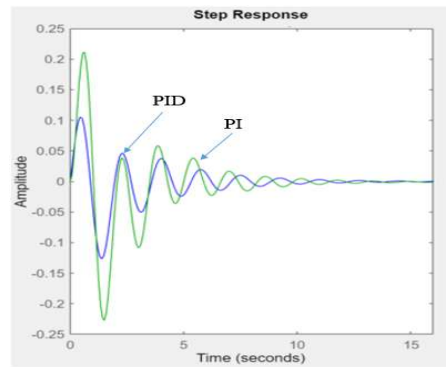
(a)
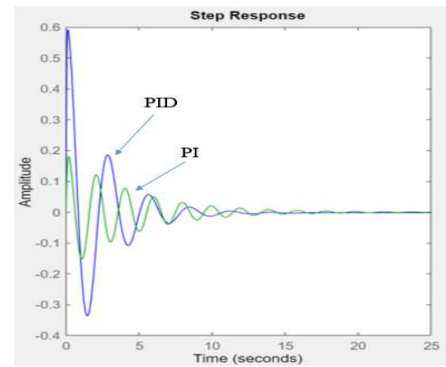
(b)

Fig. 6.17. Response to controller design for output q for

(a) δ_a deflection and (b) δ_r deflection

101

Fig. 6.18 shows the controller design for output α, and for δ_a deflection PID controller generates better and fast response with faster settling time, and for δ_r deflection PID controller shows fast response with fast settling time.
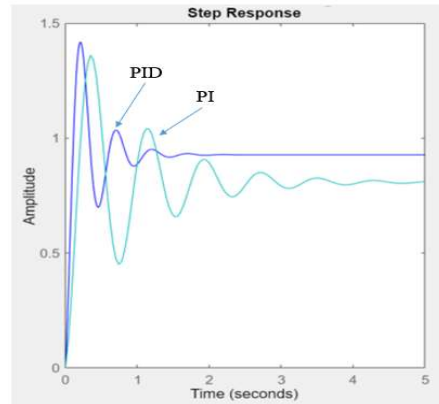
(a)
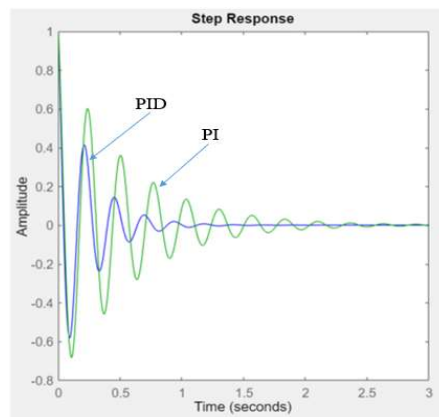
(b)

Fig. 6.18. Response to controller design for output α for

(a) δ_a deflection and (b) δ_r deflection

Validation of the results is shown using comparison of implemented controller with other AHV works carried out in the open literature is presented in Table 6.1. The comparison of implemented controller with other AHV works carried out in the open literature is presented in Table 6.1 and shows that the controller design for the selected Mach number, M=5 provides better response in comparison to other designs.

Table 6.1 Comparison of Results with earlier works

Work	Responses for δ_a deflection and δ_r deflection, Stability of A$_n$, q, α is Stable					
	Stability of A$_n$, q, α	t_r	t_s	M_p	PI	PID
This work, M=5	Stable	1s	3s	6-9%	Slow	Fast
[124]	Stable	Fast	Fast	6-7%	Combined	
[125], M=7	Stable	0.02s	3s	5-7%	-	PID+ PSO
[126], M=4 to 7	Stable	-	3.36s	43.4%	-	PID
[127]	Stable	4s	9s	9.4%	-	PID

The PID design presented here finds better control design in comparison to [124], [125]. The control design presented for the system matrices **A**, **B**, **C**, and **D** from Eqn. (6.3-6.5) finds difficulty as controller order is of higher order and it's difficult to reduce and then design the control law.

6.6 Chapter Summary

The AHV 6DOF dynamic linear model is used for the analysis and control design for this study. The model uses linear aerodynamic model with ramjet and scramjet engine for the propulsion model. The linear model developed is considered for the steady and wing level flight condition operating at level and straight flight condition for considered velocity M=5 and altitude of 65000 *ft* (19812 *m*). The linear model is developed as state space model with states as *x*, with inputs given by *u* as δ_a and δ_r and the output *y* given as A$_n$, *q* and *α.* as the normal acceleration, pitch rate and angle of attack of AHV. The model obtained is decoupled from the longitudinal and lateral system interactions and state space system matrices A, B, C, and D is obtained for the AHV model using mathematically modelling.

This linear model is analysed for the open loop dynamic simulation for the state space developed model of the AHV for the different inputs δ_a and δ_r deflection. The pole-zero plot of the model shows nonminimum phase for the poles and zeros, which results in system unstability. Hence, control design is implemented using state feedback architecture for the AHV dynamic model. The dynamic stability of the model is investigated, and state feedback control using pole

placement is implemented to attain the stability of the model. The open-loop and closed-loop response analysis of AHV shows the stability with closed loop design and convergence is seen using the pole placement design and state feedback technique. The state feedback technique is implemented in MATLAB for the control law design using control system design tool. The aileron and rudder desired deflection is controlled using the controller for the linear model using feedback design. The dynamic response for AHV model is obtained for different controller implementation for the output A_n, q and α. For the output's PI and PID controller is designed and is compared for better responses for the δ_a deflection and δ_r deflection. The PI controller gives better response and fast settling time in comparison to PID for A_n. And PID controller generates better response and faster settling time for δ_r deflection for q. And PID controller design for output α, generates better and fast response with faster settling time, and shows better response with fast settling time for δ_r and δ_a deflection respectively in comparison to the other designs.

The dynamic AHV model analysed for the level flight M=5 Mach number for the δ_a and δ_r deflection shows unstable behaviour for the A_n, α and q with the considered flight condition. The pole-zero location show occurrence of nonminimum phase for the considered flight state leading to unstable dynamics, resulting in control design. Repsonses to controller design for the δ_a and δ_r deflection shows that PID gives better response and faster settling time for the considered flight condition at M=5 Mach number and in comparison to other designed controllers.

CHAPTER 7

CONCLUSION AND FUTURE RESEARCH

This chapter presents the conclusion of this research work and presents the future scope of this research for the Air-Breathing Hypersonic Vehicle.

7.1 Introduction

The hypersonic technology development of the different vehicles from the 1930's to till date, shows that vehicles like X-15, X-20, X-30 have created a benchmark for the upcoming vehicle design and developments. From the 1990s the pace of hypersonic vehicle development increased, and it resulted in new research and different initiatives like Hyper-X, X-51, HTV-3X, SKYLON and HIFiRE. Literature shows that dynamic models like Winged cone, Road Runner and X-43A, are completely established models available to public for research and these models can be used in the investigation of flight dynamics and control systems. Other programs are in progress stage and can provide a prospective for the control design. The key technologies under development for the hypersonic flight like the aerodynamics, propulsion systems, scramjets, hybrid propulsion systems, materials, airframe integrated system design and others need a breakthrough over the coming decades to achieve the new developments for the AHVs.

The crucial technology in AHVs is model development with design constraints for the control law and control system design for the AHVs, is facing adequately number of challenges, and substantial remains a concern in achieving AHVs flight realistic. The controller design for the AHVs shows that, advanced control methods can be used to adapt the dynamic changes in the real time application. Advanced control design methods and adaptive control methods can be used for designing the controller for the nonlinear flight dynamics, and intelligent control techniques can be designed to provide a robust flight control using optimization techniques, and guaranteed stability of the system. Bifurcation Method

approach is used for the stability analysis of the non-linear AHV dynamic models with wide flight regimes ranging from Mach 0 to 25. Non-linear behaviour and topological behaviour are analysed using Bifurcation Method for the dynamic models, and it shows all critical points and where equilibrium results in change in the stability of the AHV.

7.2 Summary of Research Findings

The topological behaviour of the generic AHV model provides the quantitative assessment of the equilibrium states for the entire wide flight regimes of the dynamic AHV model with high altitude and Mach number. The static, dynamic and global stability study of AHV model using Bifurcation Analysis is presented. And the flight dynamics and stability analysis for the generic AHV model using 3-DOF dynamic simulation model is presented with the Bifurcation Method. The analysis shows that the Bifurcation Method is a powerful tool to analyse the stability regions with the different equilibrium point of the chosen parameters.

The research presents the nonlinear modeling, simulation and aerodynamic model development with dynamic 3-DOF longitudinal AHV model. Dynamic simulation is carried out with zero elevator deflection. The nonlinear aero data model is developed for C_L, C_D and C_m with the entire flight regime of hypersonic flight to Mach number M, from $M = 0.9\ to\ 24$. The dynamic stability investigation with selected $M = 0.9, 4, 6$ and 24, is presented considering the bifurcation analysis. This study provides eigen values, based on which the stability analysis is provided. It is seen that at the Mach number, $M = 0.9\ and\ 6$ shows short period mode and $M = 4\ and\ 24$, shows the long period mode presence. Results presented here with the bifurcation analysis shows a promising method for stability analysis for various trim points under consideration.

Bifurcation analysis of Longitudinal dynamics for Generic AHV model considering CBA has been implemented for AHV dynamics at Mach Number, M=0.9, for different choices of elevator deflection and with the aim to observe the control effects. Bifurcation technique is implemented with the 3DOF longitudinal AHV model using the AUTO-07p platform for the different

elevator deflection, δe= -120 and 120. The Bifurcation Diagram obtained for the data points with different forward and backward runs with the different iterations, shows the parameter values of α, θ and q. The forward and backward run shows the presence of Hopf function at PT 1 with iteration 1, and Fold, BP and Hopf function at PT 121, 200 and iteration 5, 3; with the eigen values with each iteration. The stability information is determined with the corresponding iteration of the eigen values, showing the dynamic stability information. The eigen values determined indicate the short period mode behaviour of the AHV indicating the stable behaviour at the Mach Number. The Method shows the AHV's dynamically stability determined at M=0.9 is stable. This shows that for the different Mach Number of the AHV's flight, Bifurcation is promising method to determine the dynamical stability of the vehicle for flight range between M=0 to 24. The research outlines Bifurcation Methodology application implementation to study the different stability behaviour for Generic AHV.

This study details the dynamic modelling and simulation of a 3 degree-of-freedom (3DOF) longitudinal AHV model, as well as the construction of a bifurcation approach for assessing the model's stability. Different aerodynamic model analyses of incremental pitching coefficient at different Mach numbers are used in a simulation-based 3DOF AHV trim analysis. Trim simulation is carried out using the AHV model, with stable results achieved for Cases 1, 3, and 4 at Mach numbers M=0.9, M=6, and M=10, and unstable results achieved for Cases 2, 5, and 6 at Mach numbers M=4, M=15, and M=24. The 3DOF AHV model is used to implement the bifurcation approach for case validation. The eigen values and poles are calculated using the bifurcation method for each scenario, confirming that scenarios 1, 3, and 4 are stable whereas scenarios 2, 5, and 6 are unstable. The longitudinal modes of the AHV shows that cases 1 and 4 shows short period behaviour and case 3 shows long period or phugoid behaviour. The given bifurcation analysis results show a possible method for identifying stable trim points.

This research presents the linear control design for the linear 6DOF dynamic model for the AHV with decoupled dynamics. State feedback control via pole placement is introduced, and the dynamic stability of the model is analyzed with the help of the root locus method. The closed loop stability analysis provides

suitable linear control design with PI, PD and PID, and their response suggests PI as valid controller design for the AHV flight at Mach number, $M = 5$.

7.3 Contributions of this Research

The research presents the historical developments of AHV during the last six decades to present, followed by the dynamic models used from 1990's to present for the model development, simulation and control design, and then presents the literature review of the controller design for the AHV's highlighting the different control techniques with the controller issues, and finally highlights the ongoing AHV developments and their future work progress from different nations. The research shows that, the hypersonic vehicles like X-15, X-20, X-30 have created a benchmark and foundation for the next generation vehicle design for the initiatives like Hyper-X, X-51, HTV-3X, SKYLON and HIFiRE. Dynamic models of AHV's like Winged cone, Road Runner and X-43A, are completely established models available to public for research and these models could be employed in investigation of AHV dynamics and control design. Control design for the AHVs shows that, advanced control methods can be implemented considering the dynamic changes in the real time application with intelligent adaptive control method and to provide a robust flight control using optimization techniques, to achieve guaranteed stability of the AHV's hypersonic flight.

The AHV (Air-breathing Hypersonic Vehicle) offers an appealing concept for routine, low-cost access to space. For low-cost transport and tourism on Earth as well as in the near future in space, it finds extensive use in both civilian and military applications. In recent years, the benefits and potential of Hypersonic has got international attention, resulting in an expansion of Hypersonic Technology on a global scale with prospective military and civilian applications. The use of AHVs can provide long-distance travelling at cruising speed and cheap cost in Low Earth Orbit. As NASA's Program has progressed over the years, the need for good quality at a reasonable cost to enter space has reawakened interest in Hypersonic Vehicles (HVs). SSTO (Single Stage To Orbit) flights using AHV technology can be used for a variety of military and commercial purposes, with tremendous potential for space tourism. This

research provides a way forward to achieve and a small contribution to the Air-breathing Hypersonic Vehicle research programs to accomplish the dreams of human to reach in space.

The impending applications of AHV technology to SSTO flights in achieving LEO with cost effective Space missions, military missions and commercial usage, will open new gateways for immense prospects with space tourism in coming decades.

7.4 Limitations and Future Research

The developments in Hypersonic Technology, a safe, affordable, and efficient hypersonic travel to Space is now within reach. The analysis of the AHV's nonlinear dynamical model using the Bifurcation Method is presented here. It demonstrates how the Bifurcation Method may be applied to the study of nonlinear dynamics and stability for three degrees of freedom along the longitudinal axis of a generic hypersonic vehicle. The dynamic stability study for Mach Number, M=0.9, and the equilibrium states throughout the entire broad flight envelope are presented in the Bifurcation study of AHV. Here, we use the AUTO-07p software platform to show how the Bifurcation Technique and Continuation method may be used to analyse the dynamics and control of an AHV in flight. For the AHV dynamic model, AUTO-07p is used to implement the Bifurcation Methodology throughout a range of flight situations involving elevator deflection, δ_e. For the different Mach Number of the AHV's flight, Bifurcation is promising method to determine the dynamical stability of the vehicle for the Mach number ranging from $M=0$ to 24, and post stall analysis can be carried out for the different angle of attack as future work using the Bifurcation Method.

The development over the half of the century to achieve hypersonic atmospheric flight and access to space in the coming decade can lead to the operational hypersonic aircraft. The key developments and research over the years of the hypersonic vehicles X-15, X-43A, HyFly, X-51 and many others have resulted the key technologies and several approaches that have laid the foundation for the development platform for the Falcon HTV-3X as a fully integrated system.

The development for the AHV technology over the last six decades and the future roadmap [128] outlined in the Fig. 7.1 shows the combined building block approach from the scramjet flight, ground propulsion, combined cycle flight and airframe testbeds to full scale development capability. The supporting component research and technology of different testbeds and demonstration can lead to the full-scale development of the AHV in the coming decades and hence easy access to space can be achieved with the advance safety measures.
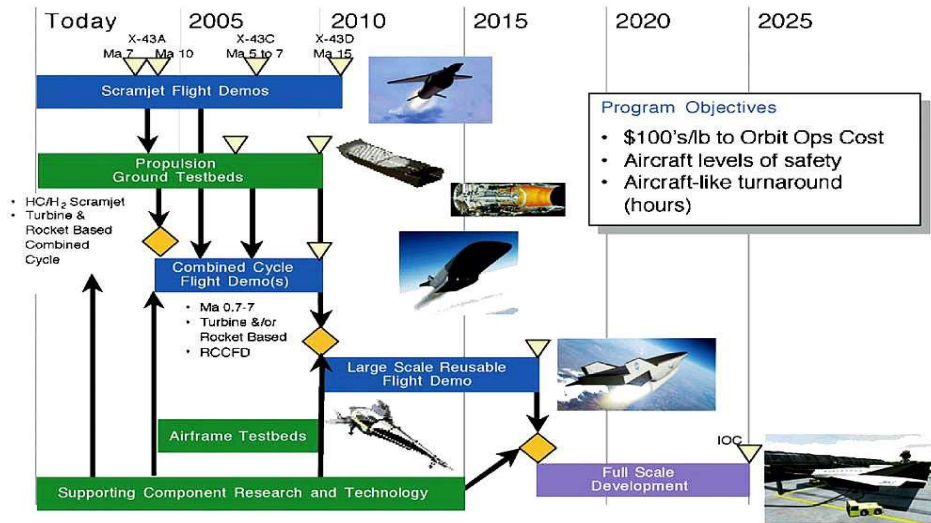
Fig. 7.1 Roadmap of building block approach of AHV access to space [128]

Achieving hypersonic flight in near future will be complex and challenging, and influence of political sides will play an important role in its success. The coming decades will prove and outcast the research and development of AHVs with the involvement of the private players into the field and high interest of the Nations to achieve the Hypersonic Technology.

REFERENCES

[1]   Hallion, R. P. (2005), The History of Hypersonics: Back to the Future-Again and Again. *43rd AIAA Aerospace Sciences Meeting and Exhibit*, AIAA, Reno, Nevada.

[2]   Fry, R. S. (2011), The U.S. Navy's Contribution to Airbreathing Missile Propulsion Technology. *Centennial of Naval Aviation Forum "100 Years of Achievement and Progress",* AIAA, Virginia Beach, VA.

[3]   Colville, J., Starkey, R. and Lewis, M. (2005), Extending the Flight Mach Number of the SR-71 Inlet. *AIAA/CIRA 13th International Space Planes and Hypersonics Systems and Technologies Conference*, AIAA, Capua, Italy.

[4]   Erbland, P. J. (2004), Current and Near-Term RLV/Hypersonic Vehicle Programs. *RTO AVT Lecture Series on "Critical Technologies for Hypersonic Vehicle Development", RTO-EN-AVT-116*, von Kármán Institute, Rhode-St-Genèse, Belgium.

[5]   Bertin, J. J. and Cummings, R. M. (2003), Fifty years of hypersonics: where we've been, where we're going. *Progress in Aerospace Sciences*, Elsevier, 39 (6-7), 511-536.

[6]   Hank, J., Murphy, J. and Mutzman, R. (2008), The X-51A Scramjet Engine Flight Demonstration Program. *15th AIAA International Space Planes and Hypersonic Systems and Technologies Conference*, AIAA, Dayton, Ohio.

[7]   Guicheteau, P. (1998), Bifurcation Theory A Tool for Nonlinear Flight Dynamics. *Philosophical Transactions of the Royal Society of London, Series A: Mathematical, Physical and Engineering Sciences,* 356 (1745), 2181-2201.

[8]   Paranjape, A. and Ananthkrishnan, N. (2012), The Bifurcation and Continuation Method from an Aerospace Systems Design Point of View. *AIAA Atmospheric Flight Mechanics Conference*, AIAA, Minneapolis, Minnesota.

[9] Goman, M. G., Zagainov, G. I. and Khramtsovsky, A. V. (1997), Application of Bifurcation Methods to Nonlinear Flight Dynamics Problems. *Progress in Aerospace Sciences*, Elsevier, 33 (9-10), 539-586.

[10] Thomas, S., Kwatny, H. G. and Chang, B. C. (2005), Bifurcation Analysis of Flight Control Systems. *16th Triennial World Congress*, IFAC, Elsevier, Czech Republic.

[11] Goman, M. G. and Khramtsovsky, A. V. (1998), Application of continuation and bifurcation methods to the design of control systems. *Philosophical Transactions of the Royal Society of London, Series A: Mathematical, Physical and Engineering Sciences*, 356 (1745), 2277-2295.

[12] Shaughnessy, J. D., Pinckney, S. Z., Mcminn, J. D., Cruz, C. I. and Kelley, M. L. (1990), Hypersonic vehicle simulation model: Winged-cone configuration. *NASA Langley Research Center*, NASA-TM-102610, United States.

[13] Keshmiri, S., Colgren, R., and Mirmirani, M. (2005), Development of an Aerodynamic Database for a Generic Hypersonic Air Vehicle. *AIAA Guidance, Navigation and Control Conference and Exhibit*, San Francisco, California.

[14] Doedel, E. J., Champneys, A. R., Fairgrieve, T. F., Kuznetsov, Y. A., Sandstede, B., and Xang, X. (2007), AUTO-07p: Continuation and Bifurcation Software for Ordinary Differential Equations. Ver. AUTO-07p 2007, Department of Computer Science, Concordia University, Montreal, Canada.

[15] Keshmiri, S., Colgren, R., and Mirmirani, M. (2007), Six DOF Nonlinear Equations of Motion for a Generic Hypersonic Vehicle. *AIAA Guidance, Navigation and Control and Co-located Conferences*, Hilton Head, South Carolina.

[16] Keshmiri, S., Colgren, R., and Mirmirani, M. (2006), Six-DOF Modelling and Simulation of a Generic Hypersonic Vehicle, for Control and Navigation Purposes. *AIAA Guidance, Navigation and Control Conference and Exhibit*, Keystone, Colorado.

[17] Ananthkrishnan, N. and Sinha, N. K. (2001), Level Flight Trim and Stability Analysis Using Extended Bifurcation and Continuation Procedure. *Journal of Guidance, Control, and Dynamics*, AIAA, 24 (6), 1225-1228.

[18] Sziroczak, D. and Smith, H. (2016), A review of design issues specific to hypersonic flight vehicles. *Progress in Aerospace Sciences,* Elsevier*,* 84, 1-28.

[19] NASA (1961). X-15 landing on lakebed, NASA Photo No. E-7469. Retrieved from. https://www.dfrc.nasa.gov/Gallery/Photo/X-15/HTML/E-7469.html

[20] Launius, R. (2003), Hypersonic Flight: Evolution From X-15 To Space Shuttle. *AIAA/ICAS International Air and Space Symposium and Exposition: The Next 100 Years*, AIAA, Dayton, Ohio.

[21] Johnston, E. W. (1965), Current and Advanced X-15. *Journal of Aircraft*, AIAA, 2 (6), 493-498.

[22] Wiswell, R. L. (1997), X-15 Propulsion System. *33rd AIAA Joint Propulsion Conference and Exhibit*, AIAA, Seattle, WA, USA.

[23] Walker, J. A. and Weil, J. (1996), The X-15 Program. NASA 19630022960.

[24] Xolleman, E. C. and Adkins, E. J. (1964), Contributions of the X-15 Program to Lifting Entry Technology. *Journal of Aircraft*, AIAA, 1 (6), 360-370.

[25] Tishkoff, J. M. (2016), Dyna-Soar: What Might Have Been. *54th AIAA Aerospace Sciences Meeting*, AIAA, San Diego, California, USA.

[26] Rana, L. and Chudoba, B. (2014), Sizing the Boeing X-20 Dyna-Soar to Mission Utilizing the 1965 US Air Force Systems Command Space Planners Guide. *AIAA SPACE 2014 Conference and Exposition*, AIAA, San Diego.

[27] M. Conner (2016, Feb). Rockwell X-30, NASA Photo. Retrieved from. https://www.nasa.gov/centers/armstrong/history/experimental_aircraft/X-30.html.

[28] Waldman, B. J. and Harsha, P. T. (1991), The First Year of Teaming - A Progress Report. *3rd AIAA International Aerospace Planes Conference*, AIAA, Orlando, FL, U.S.A.

[29] Parks, S. and Waldman, B. (1990), Flight Testing Hypersonic Vehicles - The X-30 and Beyond. *2nd AIAA International Aerospace Planes Conference*, AIAA, Orlando, FL, USA.

[30] Longstaff, R. and Bond, A. (2011), The SKYLON Project. *17th AIAA International Space Planes and Hypersonic Systems and Technologies Conference*, AIAA, San Francisco, California.

[31] Mehta, U. B., Aftosmis, M. J., Bowles, J. V. and Pandya, S. A. (2015), Skylon Aerodynamics and SABRE Plumes. *20th AIAA International Space Planes and Hypersonic Systems and Technologies Conference*, AIAA, Glasgow, Scotland.

[32] Conner, M. (2016, March). X-43A (Hyper-X), NASA Photo X-43 ED99-45243-01. Retrieved from. https://www.nasa.gov/centers/armstrong/history/experimental_aircraft/X-43A.html

[33] Voland, R. T., Huebner, L. D. and McClinton, C. R. (2006), X-43A Hypersonic Vehicle Technology Development. *Acta Astronautica, Elsevier*, 59 (1-5), 181-191.

[34] McClinton, C., Rausch, V., Sitz, J. and Reukauf, P. (2001), Hyper-X Program Status. *10th AIAA/NAL-NASDA-ISAS International Space Planes and Hypersonic Systems and Technologies Conference*, AIAA, Kyoto, Japan.

[35] Jenkins, D. R., Landis, T. and Miller, J. (2003), American X-Vehicles An Inventory- X-1 to X-50 Centennial of Flight Edition. *Monographs in Aerospace History No. 31*, NASA SP-2003-4531, Washington, DC.

[36] Tang, M. and Chase, R. (2008), The Quest for Hypersonic Flight with Air-Breathing Propulsion. *15th AIAA International Space Planes and Hypersonic Systems and Technologies Conference*, AIAA, Dayton, Ohio.

[37] Walker, S., Tang, M., Morris, S. and Mamplata, C. (2008), Falcon HTV-3X - A Reusable Hypersonic Test Bed. *15th AIAA International Space*

Planes and Hypersonic Systems and Technologies Conference, AIAA, Dayton, Ohio.

[38] Barnstorff, K. (2010, May). X-51A Makes Longest Scramjet Flight, NASA Photo X-51A b-800. Retrieved from. https://www.nasa.gov/topics/aeronautics/features/X-51A.html

[39] Yost, M. F., Choi, Y., Lerner, E. W. and Driscoll, J. F. (2019), Performance of a Generic X-51 Waverider - Thrust, Drag, and Trim Computed Using the MASIV Reduced Order Model. *AIAA Propulsion and Energy 2019 Forum*, AIAA, Indianapolis, IN.

[40] HyShot VII (HIFiRE 8) - Sustained Mach 8 Scramjet Powered Flight. Retrieved from. http://hypersonics.mechmining.uq.edu.au/hifire

[41] Bolender, M., Staines, J. and Dolvin, D. (2012), HIFiRE 6: An Adaptive Flight Control Experiment. *50th AIAA Aerospace Sciences Meeting including the New Horizons Forum and Aerospace Exposition*, AIAA, Nashville, Tennessee.

[42] Kimmel, R. L., Adamczak, D. W., Borg, M. P., Jewell, J. S., Juliano, T. J., Stanfield, S. A. and Berger, K. T. (2019), First and Fifth Hypersonic International Flight Research Experimentation's Flight and Ground Tests. *Journal Of Spacecraft And Rockets,* 56 (2), 1-11.

[43] Bin, X. and Ke, S. Z. (2015), An overview on flight dynamics and control approaches for hypersonic vehicles. *Science China Information Sciences & Springer-Verlag*, Berlin, Heidelberg, 58, 1-19.

[44] Fidan, B., Mirmirani, M. and Ioannou, P. (2003), Flight Dynamics and Control of Air-Breathing Hypersonic Vehicles: Review and New Directions. *AIAA International Space Planes and Hypersonic Systems and Technologies*, Virginia.

[45] Bolender, M. A. (2009), An Overview on Dynamics and Controls Modelling of Hypersonic Vehicles. *American Control Conference*, USA.

[46] Schmidt, D., Mamich, H., and Chavez, F. (1991), Dynamics and control of hypersonic vehicles - The integration challenge for the 1990's. *3rd International Aerospace Planes Conference*, AIAA, Orlando, U.S.A.

[47] Marrison, C., and Stengel, F. (1998), Design of robust control systems for a hypersonic aircraft. *Journal of Guidance, Control, and Dynamics*, AIAA, 21, 58–63.

[48] Parker, J. T., Serrani, A., Yurkovich, S., Bolender, M. A. and Doman, D. B. (2007), Control-Oriented Modeling of an Air-Breathing Hypersonic Vehicle. *Journal of Guidance, Control, And Dynamics*, AIAA, 30 (3), 856-869.

[49] Javaid, K. H. and Serghides, V. C. (2005), Airframe-propulsion Integration Methodology for Waverider Derived Hypersonic Cruise Aircraft Design Concepts. *Journal of Spacecraft & Rockets,* AIAA, 42 (4), 1201-1211.

[50] Bolender, M., and Doman, D. (2005), A Non-Linear Model for The Longitudinal Dynamics of A Hypersonic Air-Breathing Vehicle. *AIAA Guidance, Navigation, and Control Conference and Exhibit*, San Francisco.

[51] Frendreis, S., Skujins, T. and Cesnik, C. (2009), Six-Degree-of-Freedom Simulation of Hypersonic Vehicles. *AIAA Atmospheric Flight Mechanics Conference*, Chicago, Illinois.

[52] Huifeng, L., Ping, L. and Dajun, X. (2011), Control-oriented Modeling for Air-breathing Hypersonic Vehicle Using Parameterized Configuration Approach. *Chinese Journal of Aeronautics*, Elsevier, 24 (1), 81-89.

[53] Wiese, D. P., Annaswamy, A. M., Muse, J. A. and Bolender, M. A. (2013), Adaptive Control of a Generic Hypersonic Vehicle, *AIAA Guidance, Navigation, and Control (GNC) Conference*, Boston.

[54] Vick, T. J. (2014), Geometry Modeling and Adaptive Control of Air-Breathing Hypersonic Vehicles. University of Cincinnati.

[55] Dalle, D. J., Torrez, S. M., Driscoll, J. F., Bolender, M. and Bowcutt, K. G. (2014), Minimum-Fuel Ascent of a Hypersonic Vehicle Using Surrogate Optimization. *Journal of Aircraft*, AIAA*,* 51 (6), 1973-1986.

[56] Gao, H., Si, Y. L., Li, H. Y., Hu, X., and Wang, C. H. (2009), Modeling and Control of an Air-breathing hypersonic Vehicle. *Proceedings of the 7th Asian Control Conference*, Hong Kong, China.

[57] Schmidt, D. K. (1992), Problems in Control System Design for Hypersonic Vehicles. *IFAC Proceedings*, 25 (22), 89-96.

[58] Liu, Y., Ban, X. I., Huang, X. L. and Pengo, H. J. (2013), Gain Scheduling Output Feedback Controller Design for Hypersonic Vehicle with Actuator Saturation. *Proceedings of the 32nd Chinese Control Conference*, Xi'an, China.

[59] Ghersin, A. S. and Perra, R. S. S. (2002), LPV Control of a 6-DOF Vehicle. *IEEE Transactions on Control Systems Technology*, 10 (6), 883-887.

[60] Hu, X., Wu, L. G., Hu, C. H. and Gao, H. (2012), Adaptive Sliding Mode Tracking Control for A Flexible Air-Breathing Hypersonic Vehicle. *Journal of the Franklin Institute*, 349 (2), 559-577.

[61] Qi, R. Y., Huang, Y. H., Jiang, B. and Tao, G. (2012), Adaptive backstepping control for a hypersonic vehicle with uncertain parameters and actuator faults. *Journal of Systems and Control Engineering*, 227 (1), 51-61.

[62] Xu, B., Gao, D. X. and Wang, S. X. (2011), Adaptive neural control based on H$_\infty$ for hypersonic flight vehicles. *Science China Information Sciences*, 54 (3), 511-520.

[63] Gao, D. X. and Sun, Z. Q. (2011), Fuzzy tracking control design for hypersonic vehicles via T-S model. *Science China Information Sciences*, 54 (3), 521-588.

[64] Bolender, M. and Doman, D. (2007), Nonlinear longitudinal dynamical model of an air-breathing hypersonic vehicle. *Journal of Spacecraft & Rockets*, AIAA, 44, 374-387.

[65] Fiorentini, L., Serrani, A. & Bolender, M. (2009), Nonlinear robust adaptive control of flexible air-breathing hypersonic vehicles. *Journal of Guidance, Control & Dynamics*, AIAA, 32, 401-416.

[66] Shaughnessy, J. D., McMinn, J. D., Gregory, I. M., Chowdhry, R. S. (1994), Hypersonic Vehicle Model and Control Law Development Using H$_\infty$ and μ Synthesis. *NASA Technical Memorandum*-4562.

[67] Wang, Q. and Stengel, R. F. (2000), Robust nonlinear control of a hypersonic aircraft. *Journal of Guidance, Control, and Dynamics*, AIAA, 23 (4), 577-585.

[68] Parker, J., Serrani, A., and Yurkovich, S. (2007), Control-oriented modeling of an air-breathing hypersonic vehicle. *Journal of Guidance, Control, and Dynamics*, AIAA, 30, 856-869.

[69] Williams, T., Bolender, M. A. and Doman, D. B. (2006), An aerothermal flexible mode analysis of a hypersonic vehicle. *Proceedings of the 2006 AIAA Atmosphere Keystone, Flight Mechanics Conference and Exhibit*, AIAA, Colorado.

[70] Yao, Z. H., Bao, W., Chang, J., Yu, D. and Tang, I. (2009), Modelling for couplings of an airframe-propulsion integrated hypersonic vehicle with engine safety boundaries. *Proceedings of the Institution of Mechanical Engineers, Part G: Journal of Aerospace Engineering*, 224, 43-55.

[71] Davidson, J., Lalhnan, F., McMinn, J. D. (1999), Flight control law for NASA's hyper-X research vehicle. *Guidance, Navigation, and Control Conference and Exhibit*, AIAA, Portland, OR, U.S.A.

[72] Xu, H. J., Ioannou, P. A., and Mirmirani, M. (2004), Adaptive sliding mode control design for a hypersonic flight vehicle. *Journal of Guidance, Control and Dynamics*, AIAA, 27 (5), 829-838.

[73] Ito, D., Ward, D., and Valasek, J. (2001), Robust dynamic inversion controller design and analysis for the X-38. *Guidance, Navigation, and Control Conference*, AIAA, Montreal, Canada.

[74] Wallner, E. M. and Well, K. H. (2001), Nonlinear flight control design for the X-38 using CMAC neural networks. *Guidance, Navigation, and Control Conference and Exhibit*, AIAA, Montreal, Canada.

[75] Xu, H. J., Mirmirani, M., and Ioannou, P. A. (2003), Robust neural adaptive control of a hypersonic aircraft. *Guidance, Navigation, and Control Conference*, AIAA, Austin, Texas, USA.

[76] Kokotovic, P. V. (1992), The joy of feedback: nonlinear and adaptive. *IEEE Control System Magazine*, 12 (7), 7-12.

[77] Swaroop, D., Hedrick, J. K., Yip, P. P., and Gerdes, J. C. (2000), Dynamic surface control for a class of nonlinear systems. *IEEE Transactions on Automatic Control*, 45 (10), 1893-1899.

[78] Bongsob, S., Howell, A. and Hedrick, J. K. (2001), Dynamic surface control design for a class of non-linear systems. *Proceedings of 40th IEEE Conference on Decision and Control*, Orlando, Florida.

[79] Gao, D. X., Sun, Z. Q. and Du, T. R. (2007), Dynamic Surface Control for Hypersonic Aircraft Using Fuzzy Logic System. *Proceedings of IEEE International Conference on Automation and Logistics*, Jinan, China.

[80] Lee, T. and Kim, Y. (2001), Nonlinear Adaptive Flight Control Using Backstepping and Neural Networks Controller. *Journal of Guidance, Control and Dynamics*, AIAA, 24 (4), 675-682.

[81] Swaroop, D., Gerdes, J. C., Yip, P. P., and Hedrick, J. K. (1997), Dynamic surface control of nonlinear systems. *Proceedings of the American Control Conference*, Albuquerque, New Mexico.

[82] Kanellakopoulos, I., Kokotovic, P. V., and Morse, A. S. (1991), Systematic design of adaptive controllers for feedback linearizable systems. *IEEE Transactions on Automatic Control*, 36 (11), 1241-1253.

[83] Carroll, J. V. and Mehra, R. K. (1982), Bifurcation Analysis of Nonlinear Aircraft Dynamics. Journal of Guidance, Control, and Dynamics, AIAA, 5 (5), 529-536.

[84] Guicheteau, P. (1998), Bifurcation Theory A Tool for Nonlinear Flight Dynamics. *Philosophical Transactions of the Royal Society of London, Series A: Mathematical, Physical and Engineering Sciences*, 356 (1745), 2181-2201.

[85] Goman, M. G. and Khramtsovsky, A. V. (1998), Application of Continuation and Bifurcation Methods to the Design of Control Systems. *Philosophical Transactions of the Royal Society of London, Series A: Mathematical, Physical and Engineering Sciences*, 356, 2277-2295.

[86] Paranjape, A. and Ananthkrishnan, N. (2012), The Bifurcation and Continuation Method from an Aerospace Systems Design Point of View. *AIAA Atmospheric Flight Mechanics Conference*, Minneapolis, Minnesota, USA.

[87] Pashilkar, A. A. and Pradeep, S. (2001), Computation of Flight Mechanics Parameters Using Continuation Techniques. *Journal of Guidance, Control, and Dynamics*, AIAA, 24 (2), 324-329.

[88] Khatri, A. K. and Singh, J. (2014), Aircraft Design Using Constrained Bifurcation and Continuation Method. *Journal of Aircraft*, AIAA, 51 (5), 1647-1652.

[89] Thomas, S., Kwatny, H. G. and Chang, B. C. (2005), Bifurcation Analysis of Flight Control Systems. *16th Triennial World Congress, IFAC*, Elsevier, Czech Republic.

[90] Goman, M. G. and Khramtsovsky, A. V. (1998), Application of continuation and bifurcation methods to the design of control systems. *Philosophical Transactions of the Royal Society of London, Series A: Mathematical, Physical and Engineering Sciences*, 356 (1745), 2277-2295.

[91] Khatri, A. K., Singh, J. and Sinha, N. K. (2012), Aircraft Maneuver Design Using Bifurcation Analysis and Sliding Mode Control Techniques. *Journal of Guidance, Control, and Dynamics*, AIAA, 35 (5), 1435-1449.

[92] Littleboy, D. M. and Smith, P. R. (1998), Using Bifurcation Methods to Aid Nonlinear Dynamic Inversion Control Law Design. *Journal of Guidance, Control, and Dynamics*, AIAA, 21 (4), 632-638.

[93] Sinha, N. K. (2002), Applications of Bifurcation Methods to F-181HARV Open-loop Dynamics in Landing Configuration. *Defence Science Journal*, 52 (2), 103-115.

[94] Prakash, O., Daftary, A. and Ananthkrishnan, N. (2005), Bifurcation analysis of parafoil-payload system flight dynamics. *Atmospheric Flight Mechanics Conference and Exhibit*, AIAA, San Francisco, California, USA.

[95] Prakash, O., Daftary, A. and Ananthkrishnan, N. (2005), Trim and Stability Analysis of Parafoil/Payload System Using Bifurcation Methods. *18th AIAA Aerodynamic Decelerator Systems Technology Conference and Seminar*, Munich, Germany.

[96] Su, E., Min, C. and Xiao, Z. (2017), Research on Multi-model of Hypersonic Vehicle based on Bifurcation Theory. *21st AIAA International Space Planes and Hypersonics Technologies Conference*, Xiamen, China.

[97] Jeppu, N., Jeppu, Y. and Murthy, N. (2015), Arguing formally about flight control laws. *International Conference on Industrial Instrumentation and Control (ICIC)*, IEEE, COEP, Pune, India.

[98] Jeppu, Y. (2013), "Flight Control Software: Mistakes Made and Lessons Learned." *IEEE Software*, 30 (3), 67-72.

[99] Roskam, J. and Lan, C. T. (2000). *Airplane Aerodynamics and Performance*. Darcorporation, Lawrence, Kansas, Revised Edition.

[100] Stevens, B. L. and Lewis, F. L. (1992). *Aircraft Control and Simulation*. Wiley, New York, 2nd Edition.

[101] Keshmiri, S., Colgren, R., and Mirmirani, M. (2006), Modeling and Simulation of a Generic Hypersonic Vehicle using Merged Aerodynamic Models. *14th AIAA/AHI Space Planes and Hypersonic Systems and Technologies Conference*, Canberra, Australia.

[102] Marco, A. D., Duke, E. L. and Berndt, J. S. (2007), A General Solution to the Aircraft Trim Problem. *AIAA Modeling and Simulation Technologies Conference and Exhibit*, Hilton Head, South Carolina, USA.

[103] Miller, G., Jacques, D. and Pachter, M. (2003), Aircraft Trim Control. *AIAA Guidance, Navigation, and Control Conference and Exhibit*, Austin, Texas, USA.

[104] Chudoba, B. and Cook, M. V. (2003), Trim Equations of Motion For Aircraft Design: Steady State Straight-Line Flight. *AIAA Atmospheric Flight Mechanics Conference and Exhibit*, Austin, Texas, USA.

[105] Chudoba, B. and Cook, M. V. (2003), Trim Equations of Motion For Aircraft Design: Turning Flight, Pull-Up and Push-Over. *AIAA Atmospheric Flight Mechanics Conference and Exhibit*, Austin, Texas, USA.

[106] Retrieved from. https://sourceforge.net/projects/matcont/files/matcont/.

[107] Dhooge, A. W., Govaerts, W. and Kuznetsov, A. Y. (2003), Matcont: Matlab Package for Numerical Bifurcation Analysis of ODEs. *ACM Transaction*, Math Software, 29, 141-164.

[108] Goman, M. G. and Khramtsovsky, A. V. (2008), Computational framework for investigation of aircraft nonlinear dynamics. *Advances in Engineering Software*, Elsevier, 39 (3), 167-177.

[109] Retrieved from. http://indy.cs.concordia.ca/auto/.

[110] Doedel, E. J., Fairgrieve, T. F., Champneys, A. R., Sandstede, B., Kuznetsov, Y. A., Wang, X. (1998), Auto97: Continuation and Bifurcation Software for Ordinary Differential Equations (with HomCont). Technical Report for Concordia University, Montreal, QC, Canada. Retrieved from. http://citeseerx.ist.psu.edu/viewdoc/summary?doi=10.1.1.44.9955

[111] Doedel, E., Keller, H. B., Kernevez, J. P. (1991), Numerical analysis and control of bifurcation problems. *International Journal of Bifurcation and Chaos,* 1 (3), 493-520.

[112] Retrieved from. http://www.math.pitt.edu/~{}bard/xpp/xpp.html

[113] Ermentrout, B. (2002), Simulating, Analyzing, and Animating Dynamical Systems. A Guide to XPPAUT for Researchers and Students. *SIAM*, Philadephia, PA, USA.

[114] Coetzee, E. B., Krauskopf, B., Lowenberg, M. H. (2010), The Dynamical Systems Toolbox: Integrating AUTO into MATLAB. *Proceedings of the 16th U.S. National Congress of Theoretical and Applied Mechanics*, State College, PA, USA.

[115] Retrieved from. https://www.mathworks.com/matlabcentral/fileexchange/32210-dynamical-systems-toolbox

[116] Singh, R., Prakash, O., Joshi, S., and Jeppu, Y. (2022), Longitudinal Trim and Stability Analysis of Generic Air-Breathing Hypersonic Vehicle using Bifurcation Method. *INCAS Bulletin*, 14 (3), 111-123.

[117] Unser, M. (2020), A Note on BIBO Stability. *IEEE Transactions on Signal Processing*, 68, 5904-5913.

[118] Oppenheimer, M. W., and Doman, D. B. (2006), Control of an unstable, nonminimum phase hypersonic vehicle model. *IEEE Aerospace Conference*, MT, USA.

[119] Xu, B., Wang, X., and Shi, Z. (2021), Robust Adaptive Neural Control of Nonminimum Phase Hypersonic Vehicle Model. *IEEE Transactions on Systems, Man, and Cybernetics: Systems*, 51, 1107-1115.

[120] Urakawa, Y. (2021), Application of Limited Pole-Placement Method to State Feedback System. *IEEE International Conference on Mechatronics*, Kashiwa, Japan.

[121] Williams II, R. L., Lawrence, D. A. (2007), *Linear State-Space Control Systems*, New Jersey, John Wiley & Sons.

[122] Michiel, H., Ionescu, C. M., Depraetere, B., Stockman, K., and Derammelaere, S. (2021), Hardware and control co-design enabled by a state-space formulation of cascaded, interconnected PID controlled systems. *7th International Conference on Optimization and Applications (ICOA)*, Wolfenbüttel, Germany.

[123] Wang, L. (2020), *Implementation of PID Controllers, PID Control System Design and Automatic Tuning using MATLAB/Simulink*, Wiley-IEEE Press.

[124] Hu, Z. B., Deng, L. X., and Li, B. B. (2015), Design of Air-Breathing Hypersonic Vehicle Control System. *Applied Mechanics and Materials*, Trans. Tech Publications Ltd., Switzerland, 719, 324-29.

[125] Amrutha, K. and Kumar, R. H. (2018), PID Tracking Controller for Air-Breathing Hypersonic Vehicle. *International Conference on Emerging Trends and Innovations in Engineering And Technological Research*, IEEE, Ernakulam, India.

[126] Li, J., Li, D., Wu, G., and Liu, K. (2022), Flight-Propulsion Integration Dynamic Analysis and Adaptive Control of the Hypersonic Vehicle at Wide-Range Mach Numbers. *IEEE Access*, 10, 6954-6965.

[127] Zhang, Y., and Sheng, G. (2019), Design of Fuzzy Neural Network PID Controller for Hypersonic Vehicle. *Chinese Automation Congress (CAC)*, Hangzhou, China.

[128] Moses, P. L., Rausch, V. L., Nguyen, L. T., & Hill, J. R. (2004), NASA hypersonic fight demonstrators - overview, status, and future plans. *Acta Astronautica*, Elsevier, 55, 619-630.

APPENDIX A

AHV Aerodynamic Model Data Generation

The aerodynamic coefficients of the AHV is generated using the aerodynamic equations given by [13] using MATLAB and are given below and are used in the AHV modeling and simulation.

Table A.1

α	-1	1	4	10
M	$C_{L,\alpha}$	$C_{L,\alpha}$	$C_{L,\alpha}$	$C_{L,\alpha}$
0.3	-0.018297169	0.0166991	0.06762333	0.207304831
0.7	-0.020004771	0.019808539	0.078826588	0.237821465
0.9	-0.020009696	0.022212133	0.08553757	0.255647812
1.5	-0.038046197	0.03303119	0.080517511	0.20236353
2.5	-0.043225858	0.022926329	0.059178313	0.149064336
4	-0.04412589	0.014638497	0.039302282	0.1041236
6	-0.014222008	0.017310178	0.062810272	0.147721312
10	-0.022666584	0.005081602	0.045480736	0.12226
15	-0.014376709	0.008641477	0.043068736	0.1119475
20	-0.004556884	0.013731302	0.042635936	0.10613
24	0.004940828	0.019445014	0.044255008	0.105252688

Table A.2

α	-1	1	4	10
M	$C_{D,\alpha}$	$C_{D,\alpha}$	$C_{D,\alpha}$	$C_{D,\alpha}$
0.3	0.010948266	0.011163619	0.012444198	0.04415793
0.7	0.020227468	0.02095402	0.02581343	0.05923374
0.9	0.043923569	0.044730889	0.04991365	0.09284453
1.5	0.048491413	0.044637912	0.050920647	0.08554807
2.5	0.041371981	0.037512305	0.042159237	0.06600876
4	0.026863349	0.022842588	0.026393963	0.04275877
6	0.002346163	0.007841117	0.012093798	0.03767423
10	0.001256723	0.005751677	0.008639238	0.031975
15	0.002413348	0.005658302	0.006934301	0.02799531
20	0.004498873	0.006493827	0.006263638	0.02564
24	0.005059249	0.006054203	0.004694934	0.02314845

Table A.3

α	-1	1	4	10
M	$C_{m,\alpha}$	$C_{m,\alpha}$	$C_{m,\alpha}$	$C_{m,\alpha}$
0.3	0.000303381	-0.005047015	-0.01681	-0.05767
0.7	0.00052382	-0.008384308	-0.0266	-0.05357
0.9	9.86E-05	-0.010894128	-0.03113	-0.05762
1.5	0.005692055	-0.010146226	-0.02089	-0.04545
2.5	0.005857435	-0.002145266	-0.00607	-0.01374
4	-0.002869432	-0.000986622	0.000279	0.004722
6	0.002746997	0.000238299	-0.00266	-0.00928
10	0.003574237	0.002511939	0.001507	-0.00232
15	0.001070549	0.001816252	0.002984	0.001558
20	-0.001118163	0.001435539	0.004559	0.004324
24	-0.002592747	0.001407355	0.00594	0.005787

Table A.4

α	-5	-1	4	10
M	$C_{m,q}$	$C_{m,q}$	$C_{m,q}$	$C_{m,q}$
0.3	-1.12505	-1.12505	-1.12505	-1.12505
0.7	-1.25005	-1.25005	-1.25005	-1.25005
0.9	-1.31255	-1.31255	-1.31255	-1.31255
1.5	-0.44481174	-0.79390233	-0.79852	-0.79826
2.5	-0.28299252	-0.60039559	-0.59342	-0.60115
4	-0.25868612	-0.48087063	-0.48735	-0.615
6	0.02869321	-0.32726331	-0.34397	-0.46735
10	0.10335625	-0.24736507	-0.26315	-0.39365
15	0.12004375	-0.22202757	-0.23797	-0.38474
20	0.08273125	-0.24835007	-0.26591	-0.43715
24	0.02055829	-0.30004623	-0.31995	-0.51666

Table A.5 $C_{L,\delta e}$ for $\alpha = -1$

δ_e	-20	-10	0	10	20
M	$C_{L,\delta e}$	$C_{L,\delta e}$	$C_{L,\delta e}$	$C_{L,\delta e}$	$C_{L,\delta e}$
0.3	0.0590744	0.0290498	-0.002311	-0.0331131	-0.055049
0.7	0.06582282	0.0321325	-0.002979	-0.0376041	-0.063426
0.9	0.06909906	0.0336187	-0.003355	-0.039902	-0.067691
1.5	0.03998671	0.0173909	-0.003607	0.01948981	0.038657
2.5	0.01973249	0.0034184	-0.016478	0.00253716	0.0124391
4	0.0085639	0.0089535	-0.006862	0.00360073	-0.007686
6	0.0070419	0.0034704	-0.000101	-0.0036726	-0.007244

10	0.0063403	0.0031244	-9.15E-05	-0.0033074	-0.006523
15	0.0054633	0.0026919	-7.95E-05	-0.0028509	-0.005622
20	0.0045863	0.0022594	-6.75E-05	-0.0023944	-0.004721
24	0.0038847	0.0019134	-5.79E-05	-0.0020292	-0.004001

Table A.6 $C_{L,\delta e}$ for $\alpha = -4$

δ_e	-20	-10	0	10	20
M	$C_{L,\delta e}$	$C_{L,\delta e}$	$C_{L,\delta e}$	$C_{L,\delta e}$	$C_{L,\delta e}$
0.3	0.07420601	0.0379849	0.0007722	-0.035595	-0.062875
0.7	0.08150173	0.0413282	0.001556	-0.0365133	-0.065403
0.9	0.08562174	0.0428057	0.0015528	-0.0373303	-0.067273
1.5	0.04746074	0.0230857	0.0006949	0.02280146	0.0414245
2.5	0.02396952	0.0078545	-0.012567	0.00523732	0.0134711
4	0.00575197	0.010609	-0.003904	0.00457715	-0.010861
6	0.0081409	0.0043429	0.0005449	-0.0032531	-0.007051
10	0.0076013	0.0041249	0.0006485	-0.0028279	-0.006304
15	0.0069268	0.0038524	0.000778	-0.0022964	-0.005371
20	0.0062523	0.0035799	0.0009075	-0.0017649	-0.004437
24	0.0057127	0.0033619	0.0010111	-0.0013397	-0.003691

Table A.7 $C_{L,\delta e}$ for $\alpha = 10$

δ_e	-20	-10	0	10	20
M	$C_{L,\delta e}$	$C_{L,\delta e}$	$C_{L,\delta e}$	$C_{L,\delta e}$	$C_{L,\delta e}$
0.3	0.08941146	0.0431799	-0.00181	-0.0443692	-0.07721
0.7	0.10060761	0.0447903	-0.004452	-0.0458184	-0.08087
0.9	0.09557987	0.0445565	-0.008142	-0.0493487	-0.084835
1.5	0.06343123	0.034115	0.0091963	0.03110144	0.0526985
2.5	0.02746606	0.0132619	-0.006253	0.00913354	0.0165205
4	-0.00141554	0.0034666	-0.00292	-0.0013506	-0.014575
6	0.0094597	0.0053899	0.0013201	-0.0027497	-0.00682
10	0.0091145	0.0053255	0.0015365	-0.0022525	-0.006042
15	0.008683	0.005245	0.001807	-0.001631	-0.005069
20	0.0082515	0.0051645	0.0020775	-0.0010095	-0.004097
24	0.0079063	0.0051001	0.0022939	-0.0005123	-0.003319

Table A.8 $C_{m,\delta e}$ for $\alpha = -1$

δ_e	-20	-10	0	10	20
M	$C_{m,\delta e}$	$C_{m,\delta e}$	$C_{m,\delta e}$	$C_{m,\delta e}$	$C_{m,\delta e}$
0.3	-0.03297319	-0.016425	0.00067743	0.01749009	0.03305639

0.7	-0.03855385	-0.0194971	0.00029355	0.01997042	0.03857338
0.9	-0.04130971	-0.0210809	2.70E-05	0.02116193	0.0413595
1.5	-0.00549776	-0.0027421	1.3625E-05	0.00276932	0.00552501
2.5	-0.00537547	-0.0026794	1.6575E-05	0.0027126	0.00540862
4	-0.00519202	-0.0025855	0.000021	0.00262751	0.00523402
6	-0.00494744	-0.0024603	0.0000269	0.00251407	0.00500124
10	-0.00445826	-0.0022098	0.0000387	0.00228718	0.00453566
15	-0.00384679	-0.0018967	0.00005345	0.00200357	0.00395369
20	-0.00323532	-0.0015836	0.0000682	0.00171996	0.00337172
24	-0.00274614	-0.0013331	0.00008	0.00149307	0.00290614

Table A.9 $C_{m,\delta e}$ for $\alpha = 4$

δ_e	-20	-10	0	10	20
M	$C_{m,\delta e}$	$C_{m,\delta e}$	$C_{m,\delta e}$	$C_{m,\delta e}$	$C_{m,\delta e}$
0.3	-0.03812239	-0.0196516	-0.0006729	0.01798912	0.0353978
0.7	-0.04254847	-0.021706	-0.0004956	0.02045564	0.04042703
0.9	-0.04499088	-0.0228588	-0.0005159	0.0216154	0.04305194
1.5	-0.00632329	-0.0033363	-0.0003493	0.00263766	0.00562464
2.5	-0.00623302	-0.0033008	-0.0003687	0.0025635	0.00549567
4	-0.0060976	-0.0032477	-0.0003977	0.00245225	0.0053022
6	-0.00591706	-0.0031767	-0.0004364	0.00230393	0.00504426
10	-0.00555596	-0.0030349	-0.0005138	0.00200728	0.00452836
15	-0.00510459	-0.0028576	-0.0006106	0.00163647	0.00388349
20	-0.00465322	-0.0026803	-0.0007073	0.00126566	0.00323862
24	-0.00429212	-0.0025384	-0.0007847	0.00096901	0.00272272

Table A.10 $C_{m,\delta e}$ for $\alpha = 10$

δ_e	-20	-10	0	10	20
M	$C_{m,\delta e}$	$C_{m,\delta e}$	$C_{m,\delta e}$	$C_{m,\delta e}$	$C_{m,\delta e}$
0.3	-0.04248405	-0.0212691	6.26E-05	0.02092828	0.04065812
0.7	-0.04833456	-0.0232817	0.00040908	0.02307777	0.04569537
0.9	-0.04970235	-0.0249178	0.00028081	0.0240719	0.04655268
1.5	-0.00731393	-0.0040494	-0.0007849	0.00247967	0.0057442
2.5	-0.00726208	-0.0040465	-0.000831	0.00238458	0.00560013
4	-0.0071843	-0.0040422	-0.0009001	0.00224194	0.00538402
6	-0.0070806	-0.0040365	-0.0009924	0.00205176	0.00509588
10	-0.0068732	-0.004025	-0.0011768	0.0016714	0.0045196
15	-0.00661395	-0.0040107	-0.0014074	0.00119595	0.00379925
20	-0.0063547	-0.0039963	-0.0016379	0.0007205	0.0030789
24	-0.0061473	-0.0039848	-0.0018223	0.00034014	0.00250262

Table A.11 $C_{D,\delta e}$ for $\alpha = -1$

δ_e	-20	-10	0	10	20
M	$C_{D,\delta e}$	$C_{D,\delta e}$	$C_{D,\delta e}$	$C_{D,\delta e}$	$C_{D,\delta e}$
0.3			-0.00118	-0.0023598	0.0104032
0.7			-4.75E-05	-0.0024261	0.0077493
0.9			0.0006952	-0.0024911	0.0057655
1.5			-2.13E-05	0.00148197	0.0057776
2.5			-3.49E-05	0.00128493	0.00513
4			-0.000156	0.00076381	0.0035574
6			-0.000144	0.00021957	0.0019761
10			-0.000409	-2.38E-05	0.001754
15			-0.000604	-0.0001923	0.0016121
20			-0.000648	-0.0002101	0.0016209
24			-0.000575	-0.0001158	0.0017365

Table A.12 $C_{D,\delta e}$ for $\alpha = 4$

δ_e	-20	-10	0	10	20
M	$C_{D,\delta e}$	$C_{D,\delta e}$	$C_{D,\delta e}$	$C_{D,\delta e}$	$C_{D,\delta e}$
0.3			0.0010107	-0.0019039	0.0102063
0.7			0.0005091	-0.0070183	-0.001709
0.9			0.0007606	-0.0093959	-0.008556
1.5			7.63E-05	0.00010796	0.0029132
2.5			0.0001093	0.00023391	0.0029023
4			3.16E-05	0.0001882	0.0023193
6			3.10E-05	0.00023597	0.0018338
10			-0.000234	-0.0001132	0.0014005
15			-0.000429	-0.0004138	0.000995
20			-0.000473	-0.0005636	0.000741
24			-0.0004	-0.0005748	0.0006467

Table A.13 $C_{D,\delta e}$ for $\alpha = 10$

δ_e	-20	-10	0	10	20
M	$C_{D,\delta e}$	$C_{D,\delta e}$	$C_{D,\delta e}$	$C_{D,\delta e}$	$C_{D,\delta e}$
0.3			-0.001413	-0.0040304	0.0143224
0.7			0.0009027	-0.0122136	-0.013909
0.9			0.0043875	-0.0152103	-0.034563
1.5			0.0001897	-0.001586	-0.000708
2.5			0.0001522	-0.001117	0.0001906
4			-0.000182	-0.0007217	0.0009846
6			0.0004538	0.00046859	0.0018775

10			0.0001893	-6.67E-06	0.0011942
15			-5.79E-06	-0.0004642	0.0004795
20			-5.01E-05	-0.0007699	-8.03E-05
24			2.29E-05	-0.0009052	-0.000417

Table A.14

α	-1	4	10
M	$C_{Y,\beta}$	$C_{Y,\beta}$	$C_{Y,\beta}$
0.3	-0.49	-0.49	-0.49
0.7	-0.51	-0.51	-0.51
0.9	-0.52	-0.52	-0.52
1.5	-0.497509598	-0.510225353	-0.510178163
2.5	-0.454304835	-0.457897936	-0.461856258
4	-0.69995643	-0.700432091	-0.759052243
6	-0.530000244	-0.528688293	-0.580557915
10	-0.420624142	-0.421551473	-0.4696026
15	-0.367970755	-0.370691563	-0.4096081
20	-0.352333323	-0.357981784	-0.3877646
24	-0.337413659	-0.348414111	-0.375612075

Table A.15

α	-1	4	10
M	$C_{l,\beta}$	$C_{l,\beta}$	$C_{l,\beta}$
0.3	-0.09755	-0.09755	-0.09755
0.7	-0.10255	-0.10255	-0.10255
0.9	-0.10505	-0.10505	-0.10505
1.5	-0.122263742	-0.121908721	-0.122064535
2.5	-0.119564261	-0.120155868	-0.119895892
4	-0.054431274	-0.057944506	-0.062547784
6	-0.036382048	-0.039889496	-0.043967875
10	-0.02162665	-0.0249722	-0.0289004
15	-0.016208154	-0.019358379	-0.023138319
20	-0.013326742	-0.016289472	-0.019965
24	-0.012398801	-0.015217172	-0.018840741

Table A.16

α	-1	4	10
M	$C_{n,\beta}$	$C_{n,\beta}$	$C_{n,\beta}$
0.3	0.12495	0.12495	0.12495

0.7	0.14995	0.14995	0.14995
0.9	0.16245	0.16245	0.16245
1.5	0.186162934	0.184874633	0.184226077
2.5	0.119786938	0.120837827	0.118576656
4	0.14881386	0.149843409	0.127697128
6	0.039243466	0.039424406	0.028913214
10	-0.02835737	-0.02946127	-0.03902097
15	-0.06059489	-0.06285485	-0.06952738
20	-0.07130017	-0.07413045	-0.07831064
24	-0.08055409	-0.0834256	-0.08666

Table A.17

α	-1	4	10
M	$C_{l,p}$	$C_{l,p}$	$C_{l,p}$
0.3	-0.1375	-0.1375	-0.1375
0.7	-0.1425	-0.1425	-0.1425
0.9	-0.145	-0.145	-0.145
1.5	-0.1499914	-0.14998252	-0.14991435
2.5	-0.13751894	-0.13746269	-0.13742725
4	-0.11505553	-0.11718957	-0.13027708
6	-0.07821943	-0.07864883	-0.09761488
10	-0.04967828	-0.0520096	-0.0739
15	-0.03825828	-0.0430696	-0.06919
20	-0.03284588	-0.0402512	-0.07124
24	-0.03046255	-0.04002515	-0.07536832

Table A.18

α	-1	4	10
M	$C_{n,p}$	$C_{n,p}$	$C_{n,p}$
0.3	0.185	0.185	0.185
0.7	0.193	0.193	0.193
0.9	0.197	0.197	0.197
1.5	0.174999575	0.174999575	0.174999575
2.5	0.164999375	0.164999375	0.164999375
4	0.1299992	0.1299992	0.1299992
6	0.08393888	0.08393888	0.08393888
10	0.049	0.049	0.049
15	0.0306875	0.0306875	0.0306875
20	0.018	0.018	0.018
24	0.01108352	0.01108352	0.01108352

Table A.19

α	-1	4	10
M	$C_{l,r}$	$C_{l,r}$	$C_{l,r}$
0.3	0.27	0.27	0.27
0.7	0.28	0.28	0.28
0.9	2.85E-01	0.285	0.285
1.5	0.250531966	0.25946533	0.269513675
2.5	0.191285726	0.199814283	0.209388715
4	0.131718317	0.139642191	0.148519896
6	0.088618503	0.095740847	0.103715984
10	0.058770033	0.064305481	0.070566
15	0.04827377	0.051855906	0.056142875
20	0.058498503	0.060161001	0.062663
24	0.070755861	0.070906895	0.072116696

Table A.20

α	-1	4	10
M	$C_{n,r}$	$C_{n,r}$	$C_{n,r}$
0.3	-1.31995	-1.31995	-1.31995
0.7	-1.37495	-1.37495	-1.37495
0.9	-1.40245	-1.40245	-1.40245
1.5	-1.44893934	-1.44893029	-1.44749232
2.5	-1.20008234	-1.19823884	-1.19806549
4	-0.95040632	-0.95622604	-1.01651342
6	-0.68597321	-0.69337297	-0.73412612
10	-0.49178235	-0.4950648	-0.531153
15	-0.42358551	-0.4217654	-0.45226925
20	-0.41789194	-0.41101824	-0.436212
24	-0.45442839	-0.44354709	-0.46469024

Table A.21 $C_{l,\delta a}$ for $\alpha = -1$

δ_e	-20	-10	0	10	20
M	$C_{l,\delta a}$	$C_{l,\delta a}$	$C_{l,\delta a}$	$C_{l,\delta a}$	$C_{l,\delta a}$
0.3	-0.01362102	-0.006011	0.0006703	0.00790596	0.0144517
0.7	-0.01507192	-0.006905	0.0004978	0.00861932	0.0162126
0.9	-0.01574555	-0.007376	0.000363	0.00895175	0.0171407
1.5	-0.00239636	-0.000879	0.0004068	0.00146042	0.002282
2.5	-0.00242621	-0.000909	0.0003765	0.00142978	0.002251
4	-0.00246577	-0.000949	0.0003363	0.0013891	0.0022098
6	-0.00250876	-0.000992	0.0002926	0.00134471	0.0021645

10	-0.00256133	-0.001045	0.0002389	0.00128968	0.0021075
15	-0.00256438	-0.001047	0.0002354	0.00128418	0.0020989
20	-0.00249781	-0.00098	0.0003024	0.001349	0.0021598
24	-0.00239443	-0.000875	0.0004069	0.00145148	0.0022588

Table A.22 $C_{l,\delta a}$ for $\alpha = 4$

δ_e	-20	-10	0	10	20
M	$C_{l,\delta a}$	$C_{l,\delta a}$	$C_{l,\delta a}$	$C_{l,\delta a}$	$C_{l,\delta a}$
0.3	-0.01856455	-0.009041	-0.000579	0.00831497	0.01641
0.7	-0.01988219	-0.009736	-0.000668	0.00893449	0.0179707
0.9	-0.02060926	-0.010122	-0.000751	0.00923646	0.0188856
1.5	-0.00280538	-0.001285	2.64E-06	0.00105815	0.0018813
2.5	-0.00283914	-0.001317	-2.77E-05	0.00102864	0.001852
4	-0.0028856	-0.00136	-6.79E-05	0.00098938	0.0018123
6	-0.00293975	-0.001407	-0.000112	0.00094639	0.0017671
10	-0.00302131	-0.00147	-0.000165	0.00089249	0.0017034
15	-0.00307314	-0.001488	-0.000169	0.00088527	0.0016739
20	-0.00306927	-0.00144	-0.000102	0.00094489	0.0017001
24	-0.00302608	-0.001353	2.66E-06	0.00104071	0.0017612

Table A.23 $C_{l,\delta a}$ for $\alpha = 10$

δ_e	-20	-10	0	10	20
M	$C_{l,\delta a}$	$C_{l,\delta a}$	$C_{l,\delta a}$	$C_{l,\delta a}$	$C_{l,\delta a}$
0.3	-0.02339649	-0.01062	0.0002699	0.01091403	0.0202424
0.7	-0.02558012	-0.011323	0.0004172	0.01170205	0.0224466
0.9	-0.02518862	-0.011832	0.0005029	0.01226155	0.0227526
1.5	-0.00297225	-0.001447	-0.000156	0.00090145	0.0017245
2.5	-0.0030156	-0.001482	-0.000186	0.00087205	0.0016923
4	-0.0030823	-0.001531	-0.000226	0.00083151	0.0016424
6	-0.00317434	-0.001589	-0.00027	0.00078407	0.0015727
10	-0.00336912	-0.001684	-0.000324	0.00071193	0.0014226
15	-0.00363264	-0.001759	-0.000327	0.00066436	0.001215
20	-0.00391842	-0.001788	-0.00026	0.00066414	0.0009851
24	-0.00416308	-0.001776	-0.000156	0.00069805	0.0007851

Table A.24 $C_{n,\delta a}$ for $\alpha = -1$

δ_e	-20	-10	0	10	20
M	$C_{n,\delta a}$	$C_{n,\delta a}$	$C_{n,\delta a}$	$C_{n,\delta a}$	$C_{n,\delta a}$
0.3	-0.00100531	-0.0001703	-2.06E-21	0.00017035	0.00100531

0.7	-0.00092184	-0.0001286	-2.06E-21	0.0001286	0.00092184
0.9	-0.00088013	-0.0001077	-2.06E-21	0.00010773	0.00088013
1.5	0.001184831	0.00046516	0.0001395	0.00020784	0.00067019
2.5	0.001150731	0.00043194	0.00010716	0.0001764	0.00063966
4	0.001102663	0.00038517	6.1717E-05	0.00013231	0.00059695
6	0.001044324	0.00032853	6.84E-06	7.92E-05	0.00054576
10	0.000947365	0.00023487	-8.334E-05	-7.27E-06	0.00046309
15	0.00086314	0.00015458	-0.0001593	-7.86E-05	0.00039672
20	0.000819997	0.00011517	-0.0001945	-0.00010912	0.00037144
24	0.000815062	0.00011306	-0.0001933	-0.00010408	0.00038079

Table A.25 $C_{n,\delta a}$ for $\alpha = 4$

δ_e	-20	-10	0	10	20
M	$C_{n,\delta a}$	$C_{n,\delta a}$	$C_{n,\delta a}$	$C_{n,\delta a}$	$C_{n,\delta a}$
0.3	-0.00098888	-0.0001622	-4.39E-19	0.00016218	0.00098888
0.7	-0.00091825	-0.0001274	-4.39E-19	0.00012737	0.00091825
0.9	-0.0008821	-0.0001098	-4.39E-19	0.00010984	0.0008821
1.5	0.001280331	0.00055382	0.00022141	0.00028311	0.0007389
2.5	0.0012555	0.00052515	0.00018908	0.00024729	0.00069978
4	0.001221652	0.00048528	0.00014363	0.00019671	0.0006445
6	0.001182865	0.000438	8.8752E-05	0.00013513	0.00057714
10	0.00112704	0.00036355	-1.42E-06	3.21E-05	0.00046416
15	0.00109804	0.00030823	-7.742E-05	-5.89E-05	0.00036372
20	0.001114352	0.00029484	-0.0001126	-0.00010804	0.00030859
24	0.001160026	0.00031432	-0.0001114	-0.00011714	0.00029711

Table A.26 $C_{n,\delta a}$ for $\alpha = 10$

δ_e	-20	-10	0	10	20
M	$C_{n,\delta a}$	$C_{n,\delta a}$	$C_{n,\delta a}$	$C_{n,\delta a}$	$C_{n,\delta a}$
0.3	-0.00096759	-0.0001522	-1.30E-17	0.00015216	0.00096759
0.7	-0.00090367	-0.0001235	-1.30E-17	0.00012352	0.00090367
0.9	-0.00087883	-0.0001078	-1.30E-17	0.00010783	0.00087883
1.5	0.001353595	0.00061825	0.00027754	0.00033146	0.00078002
2.5	0.001341375	0.00059541	0.0002452	0.00029076	0.00073208
4	0.00132822	0.00056473	0.00019976	0.00023329	0.00066534
6	0.00132034	0.00053053	0.00014488	0.00016337	0.00058602
10	0.0013377	0.0004851	0.0000547	4.65E-05	0.0004605
15	0.0014215	0.00047138	-0.0000213	-5.65E-05	0.0003657
20	0.0015743	0.0005055	-5.65E-05	-0.0001117	0.0003399
24	0.00174622	0.00056725	-5.53E-05	-0.00012139	0.00036894

Table A.27 $C_{Y,\delta r}$ for $\alpha = -1$

δ_e	-20	-10	0	10	20
M	$C_{Y,\delta r}$	$C_{Y,\delta r}$	$C_{Y,\delta r}$	$C_{Y,\delta r}$	$C_{Y,\delta r}$
0.3	-0.00016824	-8.41E-05	0	8.41E-05	0.00016824
0.7	-8.06E-05	-4.03E-05	0	4.03E-05	8.06E-05
0.9	-3.67E-05	-1.84E-05	0	1.84E-05	3.67E-05
1.5	-0.03440634	-0.0176367	1.21E-18	0.01763668	0.03440634
2.5	-0.02327535	-0.0120712	2.65E-18	0.01207124	0.02327535
4	-0.00657853	-0.003723	2.30E-17	0.00372303	0.00657853
6	-0.0065988	-0.0032994	-3.63E-19	0.0032994	0.0065988
10	-0.005722	-0.002861	3.81E-19	0.002861	0.005722
15	-0.004626	-0.002313	1.31E-18	0.002313	0.004626
20	-0.00353	-0.001765	2.24E-18	0.001765	0.00353
24	-0.0026532	-0.0013266	2.99E-18	0.0013266	0.0026532

Table A.28 $C_{l,\delta r}$ for $\alpha = -1$

δ_e	-20	-10	0	10	20
M	$C_{l,\delta r}$	$C_{l,\delta r}$	$C_{l,\delta r}$	$C_{l,\delta r}$	$C_{l,\delta r}$
0.3					
0.7					
0.9					
1.5	-0.00223369	-0.0011168	-5.23E-19	0.00111685	0.00223369
2.5	-0.00216159	-0.0010808	-4.97E-19	0.0010808	0.00216159
4	-0.00205344	-0.0010267	-4.56E-19	0.00102672	0.00205344
6	-0.00190923	-0.0009546	-4.03E-19	0.00095462	0.00190923
10	-0.00162082	-0.0008104	-2.95E-19	0.00081041	0.00162082
15	-0.0012603	-0.0006302	-1.61E-19	0.00063015	0.0012603
20	-0.00089979	-0.0004499	-2.70E-20	0.0004499	0.00089979
24	-0.00061138	-0.0003057	8.04E-20	0.00030569	0.00061138

Table A.29 $C_{l,\delta r}$ for $\alpha = 4$

δ_e	-20	-10	0	10	20
M	$C_{l,\delta r}$	$C_{l,\delta r}$	$C_{l,\delta r}$	$C_{l,\delta r}$	$C_{l,\delta r}$
0.3					
0.7					
0.9					
1.5	-0.00197379	-0.0009869	-2.36E-19	0.00098689	0.00197379
2.5	-0.00190724	-0.0009536	-2.26E-19	0.00095362	0.00190724
4	-0.00180742	-0.0009037	-2.11E-19	0.00090371	0.00180742
6	-0.00167432	-0.0008372	-1.92E-19	0.00083716	0.00167432

10	-0.00140813	-0.0007041	-1.53E-19	0.00070406	0.00140813
15	-0.00107538	-0.0005377	-1.04E-19	0.00053769	0.00107538
20	-0.00074264	-0.0003713	-5.54E-20	0.00037132	0.00074264
24	-0.00047645	-0.0002382	-1.64E-20	0.00023823	0.00047645

Table A.30 $C_{l,\delta r}$ for $\alpha = 10$

δ_e	-20	-10	0	10	20
M	$C_{l,\delta r}$	$C_{l,\delta r}$	$C_{l,\delta r}$	$C_{l,\delta r}$	$C_{l,\delta r}$
0.3					
0.7					
0.9					
1.5	-0.0016619	-0.0008309	1.10E-19	0.00083095	0.0016619
2.5	-0.00160201	-0.000801	9.92E-20	0.00080101	0.00160201
4	-0.00151219	-0.0007561	8.31E-20	0.0007561	0.00151219
6	-0.00139242	-0.0006962	6.15E-20	0.00069621	0.00139242
10	-0.00115289	-0.0005764	1.84E-20	0.00057645	0.00115289
15	-0.00085348	-0.0004267	-3.55E-20	0.00042674	0.00085348
20	-0.00055407	-0.000277	-8.95E-20	0.00027703	0.00055407
24	-0.00031454	-0.0001573	-1.33E-19	0.00015727	0.00031454

Table A.31 $C_{n,\delta r}$ for $\alpha = -1$

δ_e	-20	-10	0	10	20
M	$C_{n,\delta r}$	$C_{n,\delta r}$	$C_{n,\delta r}$	$C_{n,\delta r}$	$C_{n,\delta r}$
0.3					
0.7					
0.9					
1.5	0.01033361	0.00516681	3.00E-18	-0.00516681	-0.0103336
2.5	0.00999735	0.00499868	2.85E-18	-0.00499868	-0.0099974
4	0.00949296	0.00474648	2.64E-18	-0.00474648	-0.009493
6	0.00882044	0.00441022	2.36E-18	-0.00441022	-0.0088204
10	0.0074754	0.0037377	1.79E-18	-0.0037377	-0.0074754
15	0.0057941	0.00289705	1.08E-18	-0.00289705	-0.0057941
20	0.0041128	0.0020564	3.75E-19	-0.0020564	-0.0041128
24	0.00276776	0.00138388	-1.92E-19	-0.00138388	-0.0027678

Table A.31 $C_{n,\delta r}$ for $\alpha = 4$

δ_e	-20	-10	0	10	20
M	$C_{n,\delta r}$	$C_{n,\delta r}$	$C_{n,\delta r}$	$C_{n,\delta r}$	$C_{n,\delta r}$
0.3					

0.7					
0.9					
1.5	0.00899056	0.00449528	1.32E-18	-0.00449528	-0.0089906
2.5	0.0086856	0.0043428	1.26E-18	-0.0043428	-0.0086856
4	0.00822816	0.00411408	1.16E-18	-0.00411408	-0.0082282
6	0.00761824	0.00380912	1.03E-18	-0.00380912	-0.0076182
10	0.0063984	0.0031992	7.82E-19	-0.0031992	-0.0063984
15	0.0048736	0.0024368	4.66E-19	-0.0024368	-0.0048736
20	0.0033488	0.0016744	1.50E-19	-0.0016744	-0.0033488
24	0.00212896	0.00106448	-1.03E-19	-0.00106448	-0.002129

Table A.31 $C_{n,\delta r}$ for $\alpha = 10$

δ_e	-20	-10	0	10	20
M	$C_{n,\delta r}$	$C_{n,\delta r}$	$C_{n,\delta r}$	$C_{n,\delta r}$	$C_{n,\delta r}$
0.3					
0.7					
0.9					
1.5	0.0073789	0.00368945	-6.94E-19	-0.00368945	-0.0073789
2.5	0.0071115	0.00355575	-6.63E-19	-0.00355575	-0.0071115
4	0.0067104	0.0033552	-6.16E-19	-0.0033552	-0.0067104
6	0.0061756	0.0030878	-5.54E-19	-0.0030878	-0.0061756
10	0.005106	0.002553	-4.30E-19	-0.002553	-0.005106
15	0.003769	0.0018845	-2.75E-19	-0.0018845	-0.003769
20	0.002432	0.001216	-1.20E-19	-0.001216	-0.002432
24	0.0013624	0.0006812	4.00E-21	-0.0006812	-0.0013624

*For $C_{Y,\delta r}$ values for $\alpha = 4$ and $\alpha = 10$ is zero.

APPENDIX B

AHV Model Simulation Code

The program code for the AHV model simulation is given below.

```
/ ------------------ AHV 3 DOF --------------------------
//============================
ccMem1=[0    -0.032973194
0.7   -0.038553848
0.9   -0.041309714
1.5   -0.005497759
2.5   -0.005375465
4   -0.005192024
6   -0.004947436
10   -0.00445826
15   -0.00384679
20   -0.00323532
24   -0.002746144]
ccMe4=[0    -0.03812239
0.7   -0.042548469
0.9   -0.044990884
1.5   -0.006323289
2.5   -0.006233015
4   -0.006097604
6   -0.005917056
10   -0.00555596
15   -0.00510459
20   -0.00465322
24   -0.004292124]
ccMe10=[0    -0.042484051
0.7   -0.048334559
0.9   -0.049702354
1.5   -0.007313925
2.5   -0.007262075
4   -0.0071843
6   -0.0070806
10   -0.0068732
15   -0.00661395
20   -0.0063547
24   -0.0061473]
ccLm1=[0.0    -0.018297169
0.7   -0.020004771
0.9   -0.020009696
1.5   -0.038046197
2.5   -0.043225858
4   -0.04412589
6   -0.014222008
10   -0.022666584
15   -0.014376709
20   -0.004556884
24   0.004940828]
ccL4=[0.0   0.06762333
0.7   0.078826588
0.9   0.08553757
1.5   0.080517511
2.5   0.059178313
4   0.039302282
6   0.062810272
10   0.045480736
15   0.043068736
20   0.042635936
24   0.044255008]
```

ccL10=[0.0   0.207304831
0.7   0.237821465
0.9   0.255647812
1.5   0.20236353
2.5   0.149064336
4   0.1041236
6   0.147721312
10   0.12226
15   0.1119475
20   0.10613
24   0.105252688]
ccLem1 = [0   0.059074397
    0.7   0.065822819
    0.9   0.069099065
    1.5   0.039986708
    2.5   0.019732487
    4   0.008563902
    6   0.0070419
    10   0.0063403
    15   0.0054633
    20   0.0045863
    24   0.0038847];
ccLe4 = [0   0.074206008
    0.7   0.081501733
    0.9   0.085621739
    1.5   0.047460743
    2.5   0.023969521
    4   0.005751972
    6   0.0081409
    10   0.0076013
    15   0.0069268
    20   0.0062523
    24   0.0057127];
ccLe10 = [0   0.089411461
    0.7   0.100607611
    0.9   0.095579868
    1.5   0.063431225
    2.5   0.027466063
    4   -0.001415542
    6   0.0094597
    10   0.0091145
    15   0.008683
    20   0.0082515
    24   0.0079063];
ccDm1=[0.0   0.010948266
0.7   0.020227468
0.9   0.043923569
1.5   0.048491413
2.5   0.041371981
4   0.026863349
6   0.002346163
10   0.001256723
15   0.002413348
20   0.004498873
24   0.005059249]
ccD4=[0.0   0.012444198
0.7   0.02581343
0.9   0.04991365
1.5   0.050920647
2.5   0.042159237
4   0.026393963
6   0.012093798
10   0.008639238
15   0.006934301

```
20   0.006263638
24   0.004694934]
ccD10=[0.0   0.044157929
0.7   0.059233737
0.9   0.092844534
1.5   0.085548073
2.5   0.066008756
4   0.042758767
6   0.037674232
10   0.031975
15   0.027995313
20   0.02564
24   0.023148448]
cc=[0.0 -0.06813941
0.7 -0.026598627
0.9 -0.031130145
1.5 -0.020888463
2.5 -0.00606527
15.6 0.000279095]
ccL=[0.0   0.207304831
0.7   0.237821465
0.9   0.255647812
1.5   0.20236353
2.5   0.149064336
4   0.1041236
6   0.147721312
10   0.12226
15   0.1119475
20   0.10613
24   0.105252688]
ccD=[0.0   0.044157929
0.7   0.059233737
0.9   0.092844534
1.5   0.085548073
2.5   0.066008756
4   0.042758767
6   0.037674232
10   0.031975
15   0.027995313
20   0.02564
24   0.023148448]
ccCmq1=[//0           -1.12505
    0.3   -1.12505
    0.7   -1.25005
    0.9   -1.31255
    1.5   -0.793902325
    2.5   -0.600395587
    4   -0.480870631
    6   -0.32726331
    10   -0.24736507
    15   -0.22202757
    20   -0.24835007
    24   -0.30004623];
ccCmq4=[//0           -1.12505
    0.3   -1.12505
    0.7   -1.25005
    0.9   -1.31255
    1.5   -0.79852436
    2.5   -0.593415603
    4   -0.487345476
    6   -0.34397456
    10   -0.26314832
    15   -0.23796707
    20   -0.26590832
```

```
   24   -0.31995248];
ccCmq10=[//0          -1.12505
    0.3   -1.12505
    0.7   -1.25005
    0.9   -1.31255
    1.5   -0.798259773
    2.5   -0.601149375
    4   -0.61499736
    6   -0.46735304
    10   -0.39365
    15   -0.38474375
    20   -0.43715
    24   -0.51666296];
ccMm1=[0.0   0.000303381
0.7   0.00052382
0.9   9.86E-05
1.5   0.005692055
2.5   0.005857435
4   -0.002869432
6   0.002746997
10   0.003574237
15   0.001070549
20   -0.001118163
24   -0.002592747]
ccM4=[0.0   -0.016813941
0.7   -0.026598627
0.9   -0.031130145
1.5   -0.020888463
2.5   -0.00606527
4   0.000279095
6   -0.002659505
10   0.001507254
15   0.002983567
20   0.004558854
24   0.00593995]
ccM10=[0.0   -0.057671239
0.7   -0.053565003
0.9   -0.057619331
1.5   -0.045453914
2.5   -0.013739854
4   0.004721997
6   -0.009275672
10   -0.002318
15   0.001558313
20   0.004324
24   0.005786504]
//   M    = [0 0.3 0.7 0.9 1.5 2.5 4 6 10 15 20 24];
//   PLA  = 0:0.1:1.1;        //% pilot lever angle (0% to 100%)
//   cch1  = []0:20000:200000;
ccPLA1 = [0   0
    0.3  0.1
    0.7  0.2
    0.9  0.3
    1.5  0.4
    2.5  0.5
    4.   0.6
    6.   0.7
    10.  0.8
    15.  0.9
    20.  1.
    24.  1.1];
//===================================
  time=0;
  timec=5;
```

```
  pi=22/7;
  rho=1.225;
  Vel=1;
  theta=0/57.3;
  q=0;
  R=0;
  H=0;
  pitch=2/57.3;
  mass=5080;//136080;
  g   = 9.81;
  Inertia = 50*10^5;//5*174/13;
  Cd_b = 0.85;
  dia= 25;//.122;
  A_ref=350;//0.0116839;//3.14*dia*dia/4;

function ydot=f(t, y)
 Vel  = y(1);
 theta = y(2);
 q  = y(3);
 pitch  = y(4);
 time  = y(5);
  Pow3=0;
  Pow2=0;
  Pow1=0;
  timec = time;
  del_e = 0;
//   Tmax   = 1467900 ;   //% maximum thrust, N
//   g      = 9.81 ;      //% m/s_sq.
//   Isp    = 1000*g  ;   //% specific impulse, g sec
//   PLA = 0.1
//   Pow   = PLA*(Tmax) ;
 alpha=pitch-theta;
 rho=1.225;
 q_bar=0.5*rho*(Vel^2);

 alp=alpha*57.3;
 dash=dia/(2*Vel);
//Cd_p= 0.51*alp + 0.1383;
//Cl=2*3.14*alpha;
//Cm=-011.6*alp ;
//=======================================
Dm1=interp1(ccDm1(:,1),ccDm1(:,2),Vel/340,'linear')
D4=interp1(ccD4(:,1),ccD4(:,2),Vel/340,'linear')
D10=interp1(ccD10(:,1),ccD10(:,2),Vel/340,'linear')
ccD=[-1  Dm1; 4 D4;10 D10 ]
yyD=interp1(ccD(:,1),ccD(:,2),alp,'linear')
Cd_p= yyD;
//=======================================
Lm1=interp1(ccLm1(:,1),ccLm1(:,2),Vel/340,'linear')
L4=interp1(ccL4(:,1),ccL4(:,2),Vel/340,'linear')
L10=interp1(ccL10(:,1),ccL10(:,2),Vel/340,'linear')
ccL=[-1  Lm1; 4 L4;10 L10 ]
yyL=interp1(ccL(:,1),ccL(:,2),alp,'linear')
Cl=yyL;
//=========================================
//Lem1=interp1(ccLem1(:,1),ccLem1(:,2),Vel/340,'linear')
//Le4=interp1(ccLe4(:,1),ccLe4(:,2),Vel/340,'linear')
//Le10=interp1(ccLe10(:,1),ccLe10(:,2),Vel/340,'linear')
//ccLe=[-1  Lem1; 4 Le4; 10 Le10 ]
//Cl_m10e=interp1(ccLe(:,1),ccLe(:,2),alp,'linear') // for -20 deflection
//ccLee=[10 -Cl_m10e; 0  Cl_0e; -10 Cl_m10e ]
//Cl=interp1(ccLee(:,1),ccLee(:,2),del_e,'linear')
//=========================================
Mm1=interp1(ccMm1(:,1),ccMm1(:,2),Vel/340,'linear')
```

```
M4=interp1(ccM4(:,1),ccM4(:,2),Vel/340,'linear')
M10=interp1(ccM10(:,1),ccM10(:,2),Vel/340,'linear')
ccM=[-1 Mm1; 4 M4;10 M10 ]
Cm_alpha=interp1(ccM(:,1),ccM(:,2),alp,'linear')
Cma_0e=Cm_alpha ; // a=alpha
//Cm_q=-0.6;
//=========================================
Mem1=interp1(ccMem1(:,1),ccMem1(:,2),Vel/340,'linear')
Me4=interp1(ccMe4(:,1),ccMe4(:,2),Vel/340,'linear')
Me10=interp1(ccMe10(:,1),ccMe10(:,2),Vel/340,'linear')
ccMe=[-1 Mem1; 4 Me4; 10 Me10 ]
Cma_m10e=interp1(ccMe(:,1),ccMe(:,2),alp,'linear') // for -20 deflection
ccMee=[10 -Cma_m10e; 0 Cma_0e; -10 Cma_m10e ]
Cm=interp1(ccMee(:,1),ccMee(:,2),del_e,'linear')
//Cm=interp1(Cma_0e,Cma_m10e,1,'linear') //del_e=1
//===============================================================
cmq1=interp1(ccCmq1(:,1),ccCmq1(:,2),Vel/340,'spline')
cmq4=interp1(ccCmq4(:,1),ccCmq4(:,2),Vel/340,'spline')
cmq10=interp1(ccCmq10(:,1),ccCmq10(:,2),Vel/340,'spline')
ccCmq=[-1 cmq1; 4 cmq4;10 cmq10 ]
yyCmq=interp1(ccCmq(:,1),ccCmq(:,2),alp,'spline')
Cm_q=yyCmq ;
//===============================================================
//PLA=interp1(ccPLA1(:,1),ccPLA1(:,2),Vel/340,'linear') // not working
//===============================================================
//   PLA = 1;
   h   = 140 ;
   M   = Vel/340;
//   Pow = PLA.*(7.53e02.*(M.^7) - 1.50e04.*(M.^6) + 1.16e05.*(M.^5)...
//      - 4.36e05.*(M.^4) + 8.07e05.*(M.^3) - 6.97e05.*(M.^2)...
//       + 3.94e05.*(M) + 3.93e-08);
   Pow=0.6*120000*4.44822;
   CX=-Cd_p;
   CY=Cl;
   Cmm_p=Cm+Cm_q*q*dash;
 FA_X=q_bar*350*CX;
 FA_Y=q_bar*350*CY;
 M_z=q_bar*350*dia*Cmm_p;
   ydot(1)=(1/mass)*(Pow*cos(alpha)-FA_X-mass*g*sin(theta));
   ydot(2)=(1/(mass*Vel))*(Pow*sin(alpha)+FA_Y-mass*g*cos(theta));
   ydot(3)=M_z/Inertia;
   ydot(4)=q;
   ydot(5)=1;
//   ydot(1)=(1/mass)*(FA_X+Pow-mass*g*sin(theta)-mass*q*Vel*tan(alpha)-mass*Vel);
//
ydot(2)=(FA_Y*(cos(alpha))^2)/Vel+(mass*g*cos(theta)*(cos(alpha))^2)/Vel+mass*q*(cos(alpha))^
2-(mass*sin(alpha)*cos(alpha)*ydot(1))/Vel;
//   ydot(3)=q;
//   ydot(4)=(M_z/Inertia)-q;
//   ydot(5)=1;
endfunction

t0=0;
y0=[Vel;theta;q;pitch;time];
//  1  2  3  4  5
t=0:.01:6.7;
y = ode(y0,t0,t,f);
subplot(231);plot(t,y(1,:)./340,'r');xlabel("t", "fontsize", 2);ylabel("M", "fontsize", 2);
subplot(232);plot(t,y(2,:).*57.3,'r');xlabel("t", "fontsize", 2);ylabel("gama", "fontsize", 2);
subplot(233);plot(t,y(4,:).*57.3,'r');xlabel("t", "fontsize", 2);ylabel("theta", "fontsize", 2);
subplot(234);plot(y(1,:)./340,(y(4,:)-y(2,:)).*57.3,'r');xlabel("M", "fontsize", 3);ylabel("alpha",
"fontsize", 3);
subplot(235);plot(t,y(4,:),'r');xlabel("t", "fontsize", 2);ylabel("q", "fontsize", 2);
subplot(236);plot(y(1,:)./340,y(5,:),'b');xlabel("M", "fontsize", 2);ylabel("del_e", "fontsize", 2);
```

```
//-------------------Trim Model of AHV----------M = 0.9
   time=0;
   pi=22/7
   mass=136080
   g = 9.81
   Inertia_yy = 5000000
   dia= 25
   Aref=350
   mass=136080
   h_ft=10000
   h=h_ft*0.3048;        //in ft*meter
   rho_o =  2.377e-3 ;    //% slug/ft3
//   if h < 36089
     rho1  =  rho_o*((1 - 6.875*(1e-6)*h_ft).^4.2561) ; //% air density
//   else
//     rho1  = 0.2971*rho_o*exp(-(h_ft - 36089)/20806.7) ;
//   end
   rho = rho1*515.379;  //  kg/m^3
   sspeed = sqrt(1.4*287*(288.15-6.5*(h/1000)));
   hft  = h_ft;
   Vel  = 0.9*sspeed;
   alpha= 0/57.3;
   theta= 0/57.3; //89/57.3; //-1.5708/57.3; //-1.3961606
   gama = 0/57.3; //-89/57.3;
   q=0;
//   h=10000;
//   pitch=10/57.3;

function ydot=f(t, y)
 Vel  =  y(1);
 gama  =  y(2);
 alpha =  y(3);
 theta =  y(4);
   q  =  y(5);
  hft  =  y(6);
   dele = 0;
   PLA = 0.3;
   M   = Vel/sspeed;
   hft = h/0.3048
// Subsonic Engine
   Pow1= PLA*(2.99*(10^5)-10*hft+1.33*(10^(-4))*hft*hft-6.48*(10^(-
10))*(hft.^3)+3.75*(10^3)*M.^3);
   Pow = 4.44822*Pow1;
   CD=0.5*rho*(Vel*Vel)*Aref*(0.00005*alpha*57.3+0.00006*dele)
   CL=0.5*rho*(Vel*Vel)*Aref*(0.0252*alpha*57.3-0.0032*dele)
   Cm=0.5*rho*(Vel*Vel)*Aref*dia*(-0.0052*alpha*57.3+0.0024*dele-1.31255*q*dia/(2*Vel))
   ydot(1)=(1/mass)*(Pow*cos(alpha)-CD-mass*g*sin(theta));
   ydot(2)=(1/(mass*Vel))*Pow*sin(alpha)-CL*(1/(mass*Vel))+g*cos(theta)*(1/Vel);
   ydot(3)=q-(1/(mass*Vel))*Pow*sin(alpha)-CL*(1/(mass*Vel))+g*cos(theta)*(1/Vel);
   ydot(4)=q;
   ydot(5)=Cm/(2*Inertia_yy);
   ydot(6)=Vel*sin(gama);
endfunction
t0=0;
y0=[Vel;gama;alpha;theta;q;h];
//  1  2  3  4  5
t=0:.01:10;
y = ode(y0,t0,t,f);
subplot(331);plot(t,y(1,:)./sspeed,'b');xlabel("t", "fontsize", 2);ylabel("M", "fontsize", 2);
subplot(332);plot(t,y(2,:).*57.3,'b');xlabel("t", "fontsize", 2);ylabel("gama", "fontsize", 2);
subplot(333);plot(t,y(3,:).*57.3,'b');xlabel("t", "fontsize", 2);ylabel("alpha", "fontsize", 2);
```

```
subplot(334);plot(t,y(4,:).*57.3,'b');xlabel("t", "fontsize", 2);ylabel("theta", "fontsize", 2);
subplot(335);plot(t,y(5,:),'b');xlabel("t", "fontsize", 2);ylabel("q", "fontsize", 2);
subplot(336);plot(t,y(6,:)./0.3048,'b');xlabel("t", "fontsize", 2);ylabel("h", "fontsize", 2);

//-------------------Trim Model of AHV----------M = 4
  time=0;
  pi=22/7
  mass=136080
  g = 9.81
  Inertia_yy = 5000000
  dia= 25
  Aref=350
  mass=136080
  h_ft=50000
  h=h_ft*0.3048;        //in ft*meter
  rho_o = 2.377e-3 ;    //% slug/ft3
//   if h < 36089
//     rho1  = rho_o*((1 - 6.875*(1e-6)*h_ft).^4.2561) ;  //% air density
//   else
      rho1 = 0.2971*rho_o*exp(-(h_ft - 36089)/20806.7) ;
//   end
  rho = rho1*515.379;  //  kg/m^3
  sspeed = sqrt(1.4*287*(288.15-6.5*(h/1000)));
  Vel  =4*sspeed;
  alpha=0/57.3;
  theta=0/57.3;//-1.5708/57.3; //-1.3961606
  gama =0/57.3;
  q=0;
//   h=10000;
//   pitch=10/57.3;

function ydot=f(t, y)
  Vel  = y(1);
  gama  = y(2);
  alpha = y(3);
  theta = y(4);
   q = y(5);
  hft = y(6);
  dele = 0;
  PLA = 0.6;
  M  = Vel/sspeed;
  hft=h/0.3048
 // Ramjet/Scramjet Engine
  Pow2 = PLA*(-1.8585*10^3+2.6294*10^3*M-9.5423*10^2*M*M+1.0834*10^2*(M^3));
  Pow  = 4.44822*Pow2;
  CD=0.5*rho*(Vel*Vel)*Aref*(-0.0009*alpha*57.3-0.0039*dele);
//0.0257+0.0003*(alpha*57.3)^2+0.0001*(dele^2)
  CL=0.5*rho*(Vel*Vel)*Aref*(0.0134*alpha*57.3+0.005*dele); // -0.0249-0.0002*(dele^2)
  Cm=0.5*rho*(Vel*Vel)*Aref*dia*(0.0007*alpha*57.3+0.0006*dele-0.480870631*q*dia/(2*Vel));
   ydot(1)=(1/mass)*(Pow*cos(alpha)-CD-mass*g*sin(theta));
   ydot(2)=(1/(mass*Vel))*Pow*sin(alpha)-CL*(1/(mass*Vel))+g*cos(theta)*(1/Vel);
   ydot(3)=q-(1/(mass*Vel))*Pow*sin(alpha)-CL*(1/(mass*Vel))+g*cos(theta)*(1/Vel);
   ydot(4)=q;
   ydot(5)=Cm/(2*Inertia_yy);
   ydot(6)=Vel*sin(theta);
endfunction

//-------------------Trim Model of AHV----------M = 6
Vel=6*sspeed;
M = Vel/sspeed;
alpha=0/57.3;
theta=0/57.3;//-1.5708/57.3; //-1.3961606
gama =0/57.3;
q=0;
```

```scilab
function ydot=f(t, y)
Vel  =  y(1);
gama  =  y(2);
alpha =  y(3);
theta =  y(4);
 q  =  y(5);
hft  =  y(6);
dele = 0;
PLA = 0.7;
M   = Vel/sspeed;
hft=h/0.3048
//  Ramjet/Scramjet Engine
Pow2 = PLA*(-1.8585*10^3+2.6294*10^3*M-9.5423*10^2*M*M+1.0834*10^2*(M^3));
Pow  = 4.44822*Pow2;
CD=0.5*rho*(Vel*Vel)*Aref*(0.0013*alpha*57.3-0.0006*dele);
//0.0002*(alpha*57.3)^2+0.00003*(dele^2)+0.0035
CL=0.5*rho*(Vel*Vel)*Aref*(0.0147*alpha*57.3-0.0006*dele); //+0.000008*(dele^2)+0.0017
Cm=0.5*rho*(Vel*Vel)*Aref*dia*(-0.0011*alpha*57.3-0.000005*dele-0.32726331*q*dia/(2*Vel));
ydot(1)=(1/mass)*(Pow*cos(alpha)-CD-mass*g*sin(theta));
ydot(2)=(1/(mass*Vel))*Pow*sin(alpha)-CL*(1/(mass*Vel))+g*cos(theta)*(1/Vel);
ydot(3)=q-(1/(mass*Vel))*Pow*sin(alpha)-CL*(1/(mass*Vel))+g*cos(theta)*(1/Vel);
ydot(4)=q;
ydot(5)=Cm/(2*Inertia_yy);
ydot(6)=Vel*sin(gama);
endfunction


//-------------------Trim Model of AHV----------M = 10
Vel=10*sspeed;
alpha=0/57.3;
theta=0/57.3;  //-1.5708/57.3; //-1.3961606
gama =0/57.3;
q=0;


function ydot=f(t, y)
Vel  =  y(1);
gama  =  y(2);
alpha =  y(3);
theta =  y(4);
 q  =  y(5);
hft  =  y(6);
dele = 0;
PLA = 0.8;
M   = Vel/sspeed;
hft = h/0.3048;
//  Rocket Engine
Pow3 = -5.43*10^4+0.664*hft+3.24*10^5*PLA+0.374*hft*PLA;
Pow=4.44822*Pow3;
CD=0.5*rho*(Vel*Vel)*Aref*(0.0008*alpha-0.0004*dele);
//0.0019+0.0002*(alpha^2)+0.00002*(dele^2)
CL=0.5*rho*(Vel*Vel)*Aref*(0.0132*alpha+0.001*dele);  //-0.0087-0.00004*(dele^2)
Cm=0.5*rho*(Vel*Vel)*Aref*dia*(-0.0004*alpha-0.0003*dele-0.24736507*q*dia/(2*Vel));
ydot(1)=(1/mass)*(Pow*cos(alpha)-CD-mass*g*sin(theta));
ydot(2)=(1/(mass*Vel))*Pow*sin(alpha)-CL*(1/(mass*Vel))+g*cos(theta)*(1/Vel);
ydot(3)=q-(1/(mass*Vel))*Pow*sin(alpha)-CL*(1/(mass*Vel))+g*cos(theta)*(1/Vel);
ydot(4)=q;
ydot(5)=Cm/(2*Inertia_yy);
ydot(6)=Vel*sin(gama)./100;
endfunction


//-------------------Trim Model of AHV----------M = 15
Vel=15*sspeed;
alpha=0/57.3;
theta=0/57.3;  //-1.5708/57.3; //-1.3961606
```

```
gama =0/57.3;
q=0;

function ydot=f(t, y)
Vel  =  y(1);
gama  =  y(2);
alpha =  y(3);
theta =  y(4);
 q  =  y(5);
hft  =  y(6);
dele = 0;
PLA = 0.9;
M   = Vel/sspeed;
hft = h/0.3048;
// Rocket Engine
Pow3 = -5.43*10^4+0.664*hft+3.24*10^5*PLA+0.374*hft*PLA;
Pow=4.44822*Pow3;
CD=0.5*rho*(Vel*Vel)*Aref*(0.0002*alpha-0.0005*dele);
CL=0.5*rho*(Vel*Vel)*Aref*(0.0115*alpha+0.0002*dele); //-0.0029-0.00002*(dele^2)-
0.00002*(dele^2)
Cm=0.5*rho*(Vel*Vel)*Aref*dia*(0.0006*alpha-0.00007*dele-0.22202757*q*dia/(2*Vel));
ydot(1)=(1/mass)*(Pow*cos(alpha)-CD-mass*g*sin(theta));
ydot(2)=(1/(mass*Vel))*Pow*sin(alpha)-CL*(1/(mass*Vel))+g*cos(theta)*(1/Vel);
ydot(3)=q-(1/(mass*Vel))*Pow*sin(alpha)-CL*(1/(mass*Vel))+g*cos(theta)*(1/Vel);
ydot(4)=q;
ydot(5)=Cm/(2*Inertia_yy);
ydot(6)=Vel*sin(theta);
endfunction

//-------------------Trim Model of AHV----------M = 24
Vel=24*sspeed;
alpha=0/57.3;
theta=0/57.3;  //-1.5708/57.3; //-1.3961606
gama =0/57.3;
q=0;

function ydot=f(t, y)
Vel  =  y(1);
gama  =  y(2);
alpha =  y(3);
theta =  y(4);
 q  =  y(5);
hft  =  y(6);
dele = 0;
PLA = 1.1;
M   = Vel/sspeed;
hft = h/0.3048
// Rocket Engine
Pow3 = -5.43*10^4+0.664*hft+3.24*10^5*PLA+0.374*hft*PLA;
Pow  = 4.44822*Pow3;
CD=0.5*rho*(Vel*Vel)*Aref*(-0.0009*alpha*57.3-0.0007*dele);
CL=0.5*rho*(Vel*Vel)*Aref*(0.0072*alpha*57.3-0.002*dele);
Cm=0.5*rho*(Vel*Vel)*Aref*dia*(0.0022*alpha*57.3+0.0002*dele-0.30004623*q*dia/(2*Vel));

ydot(1)=(1/mass)*(Pow*cos(alpha)-CD-mass*g*sin(theta));
ydot(2)=(1/(mass*Vel))*Pow*sin(alpha)-CL*(1/(mass*Vel))+g*cos(theta)*(1/Vel);
ydot(3)=q-(1/(mass*Vel))*Pow*sin(alpha)-CL*(1/(mass*Vel))+g*cos(theta)*(1/Vel);
ydot(4)=q;
ydot(5)=Cm/(2*Inertia_yy);
ydot(6)=Vel*sin(theta);
endfunction
```

APPENDIX C

Simulation of Trim Analysis of AHV with Control Surface Deflection

The 3DOF longitudinal AHV model is obtained considering the Eqn. (4.7-4.13) and the states represented as $x=[M,\gamma,\alpha,\theta,q,h]'$ and input as $u=[\delta_e, \delta_r]$. The dynamic 3DOF longitudinal model simulation is carried out for the different Cases of Case 1, Case 3 and Case 4 as outlined in the Table 4.2 for different Mach number, $M = 0.9$, 6 and 10 for corresponding altitude. The dynamic simulation is carried out for trim condition and variable control surface deflection considering the elevator deflection and rudder deflection, δ_e and δ_r, for the Cases 1, 3 and 4 shown in the Table 4.2 and magnitude of PLA is considered as incremental value between 0.1 to 1 for all cases. The aerodynamic coefficients with their derivatives from Table C.1 are used in the simulation for the different Cases 1, 3 and 4, and their dynamic simulation is given in Fig. C.1-C.4, Fig C.5- C.8 and Fig C.9- C.12 respectively.

Table C.1 – Mach Number with aerodynamic derivatives

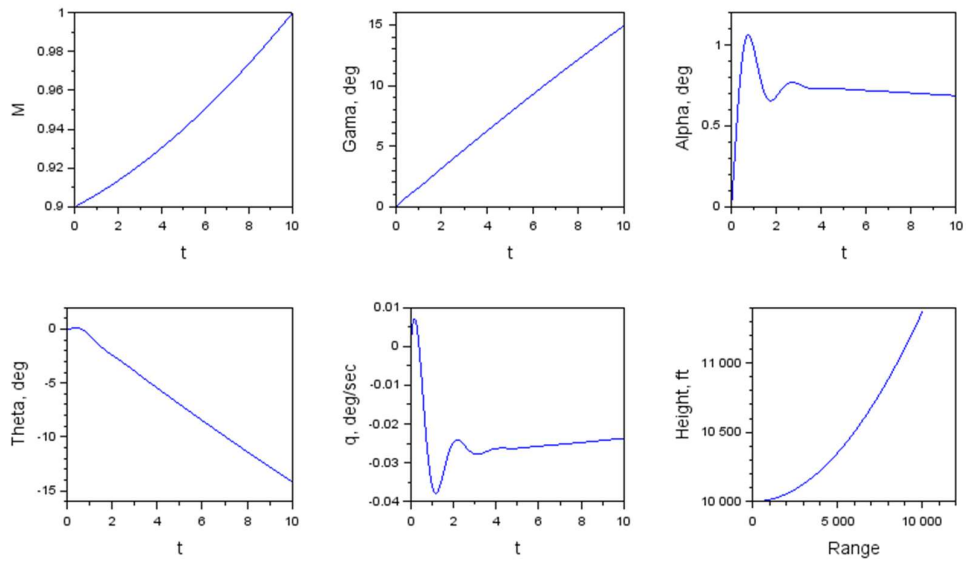| Mach No.	0.9	6	10
C_{L_α}	0.0252	0.0147	0.0132
$C_{L_{\delta e}}$	-0.0032	-0.0006	0.001
C_{D_α}	0.00005	0.0013	0.0008
$C_{D_{\delta e}}$	0.00006	-0.0006	-0.0004
C_{m_α}	-0.0052	-0.0011	-0.0004
$C_{m_{\delta e}}$	0.0024	-0.000005	-0.0003
$C_{D_{\delta r}}$	0.000094533	0.00001787	0.00001787
$C_{m_{\delta r}}$	0.0000579	0.0001092	0.0001092

Fig. C.1 - Dynamic Simulation Case 1 for M = 0.9, δ_e= 1º and δ_r=0º

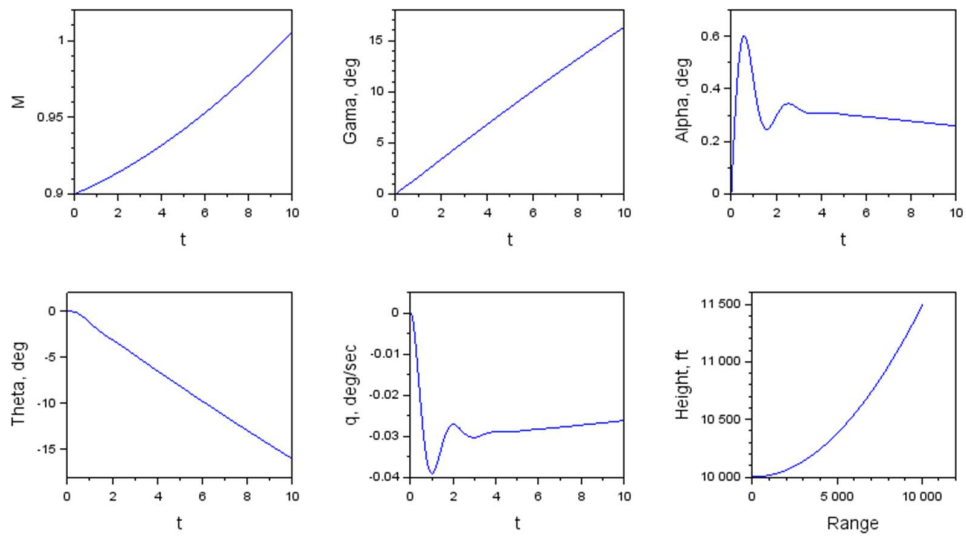
Fig. C.2 - Dynamic Simulation Case 1 for M = 0.9, δ_e= 0º and δ_r=1º
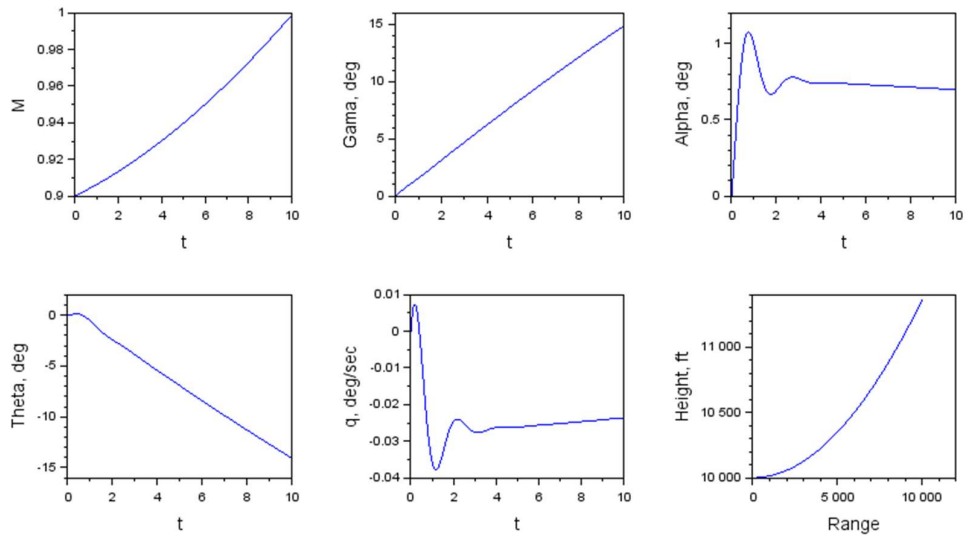
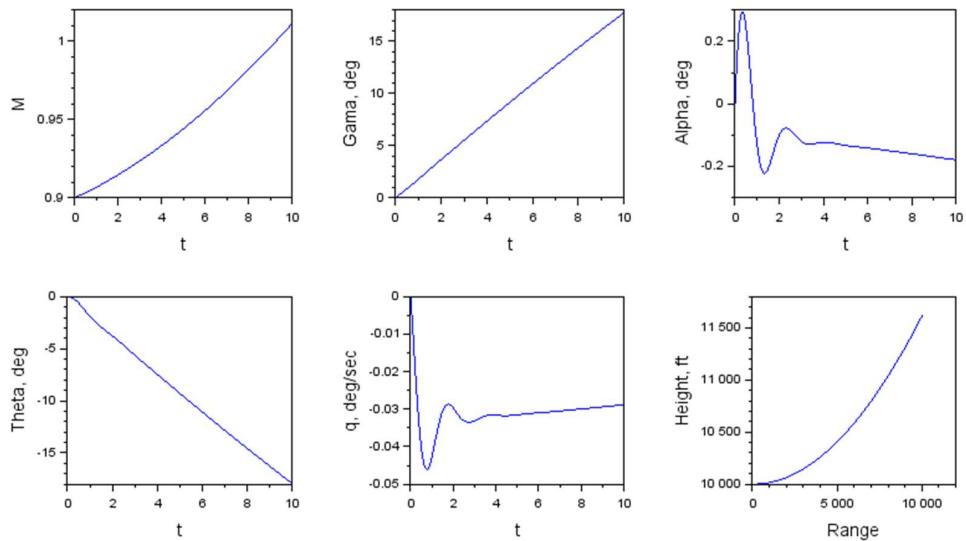Fig. C.3 - Dynamic Simulation Case 1 for M = 0.9, δ_e= 1º and δ_r=1º

Fig. C.4 - Dynamic Simulation Case 1 for M = 0.9, δ_e= -1º and δ_r=1º
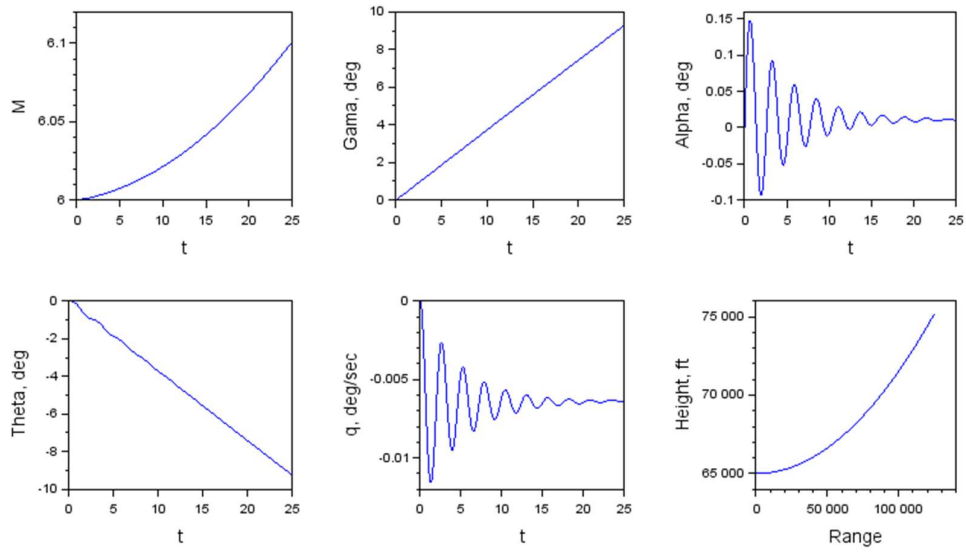
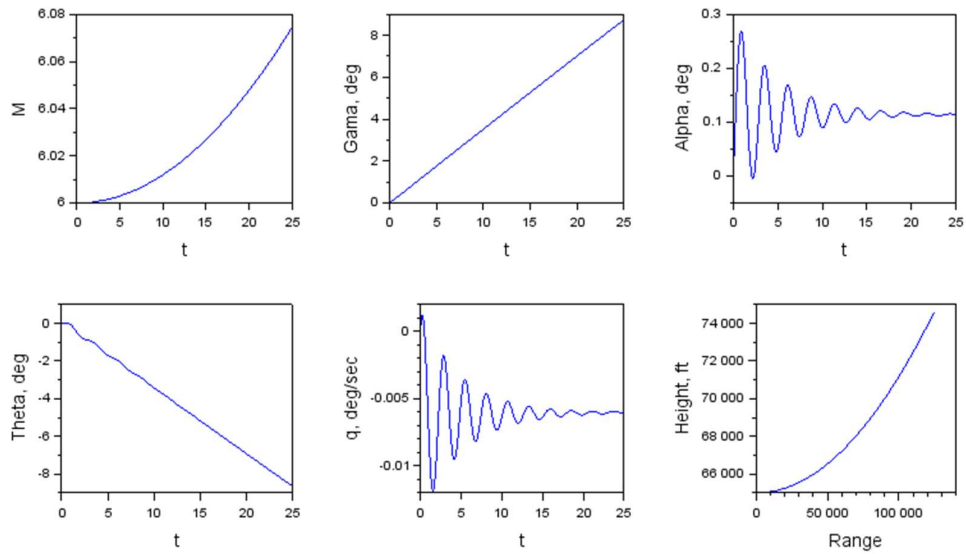Fig. C.5 - Dynamic Simulation Case 3 for M = 6, δ_e= 1º and δ_r=0º

Fig. C.6 - Dynamic Simulation Case 3 for M = 6, δ_e= 0º and δ_r=1º
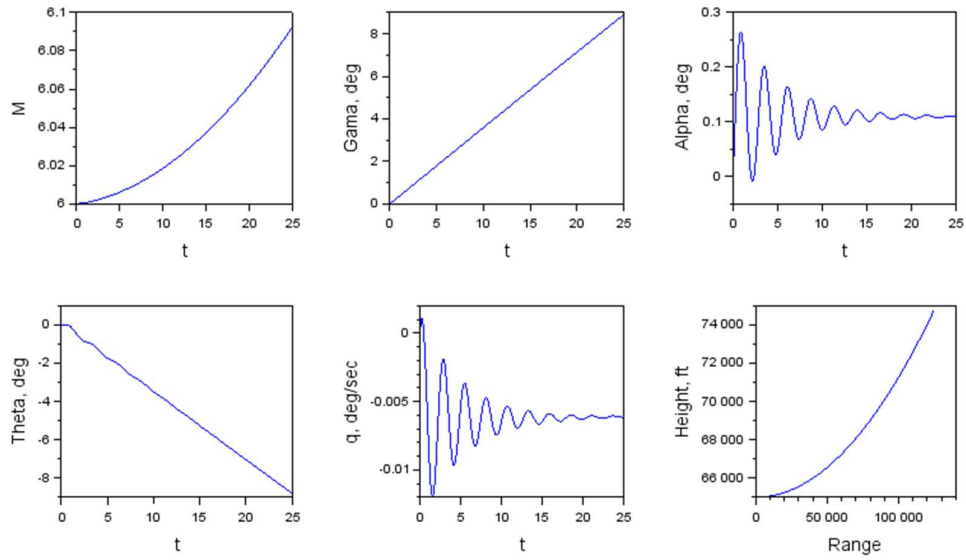
Fig. C.7 - Dynamic Simulation Case 3 for M = 6, δ_e= 1º and δ_r=1º
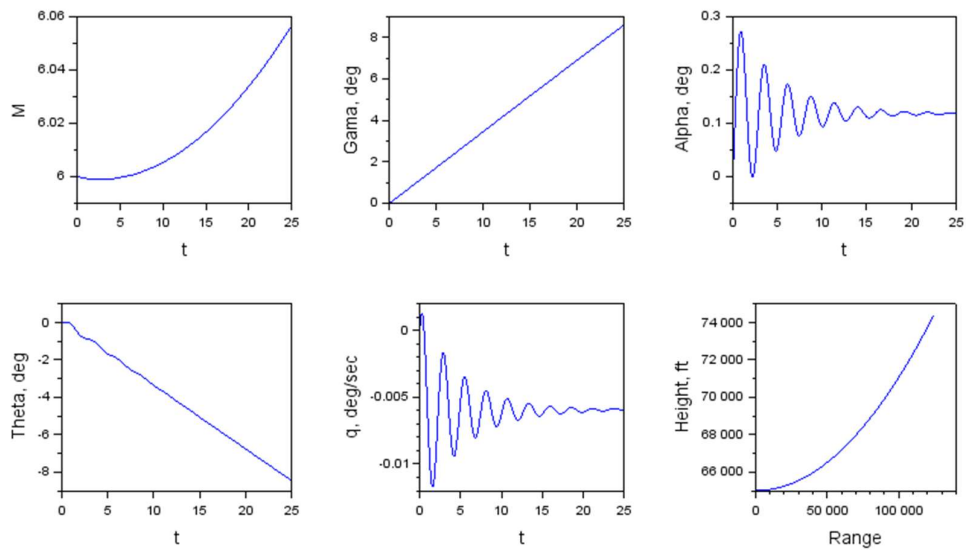

Fig. C.8 - Dynamic Simulation Case 3 for M = 6, δ_e= -1º and δ_r=1º
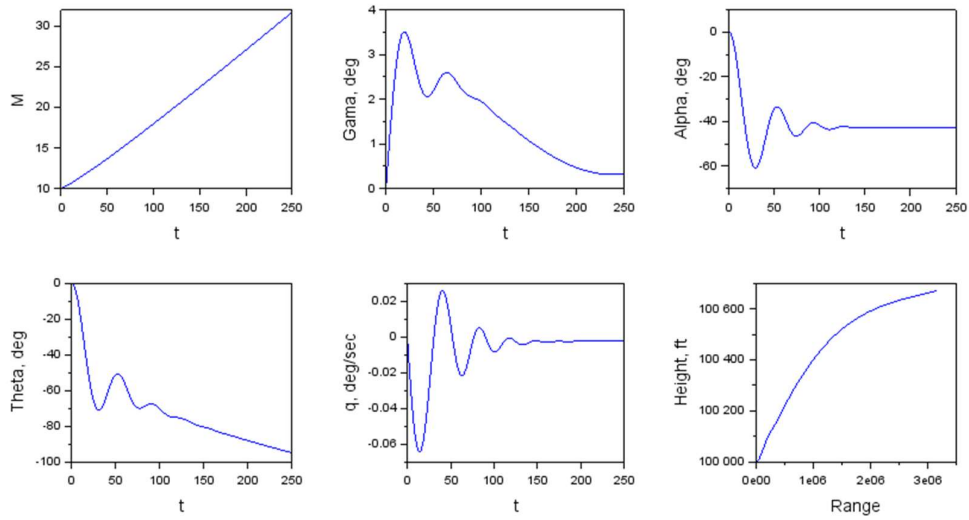
Fig. C.9 - Dynamic Simulation Case 4 for M = 10, δ_e= 1º and δ_r=0º
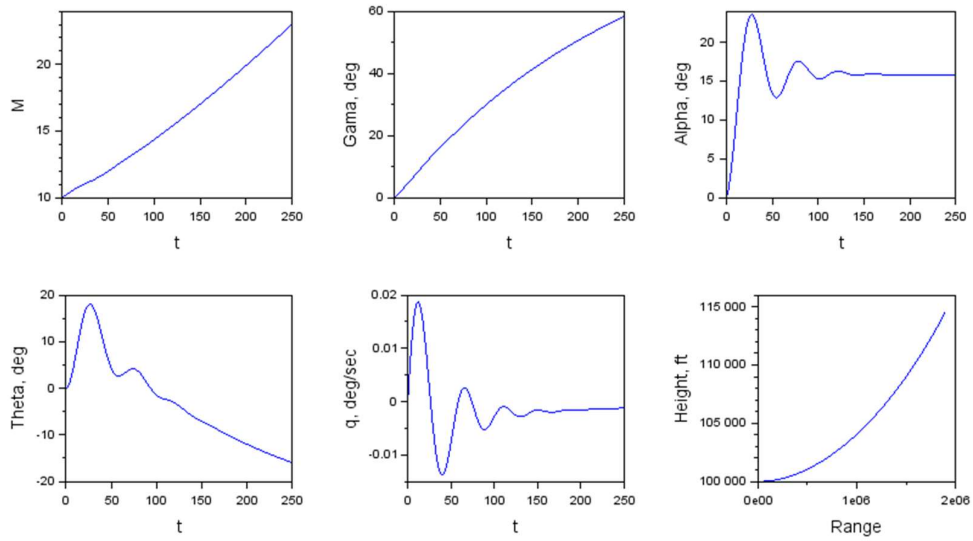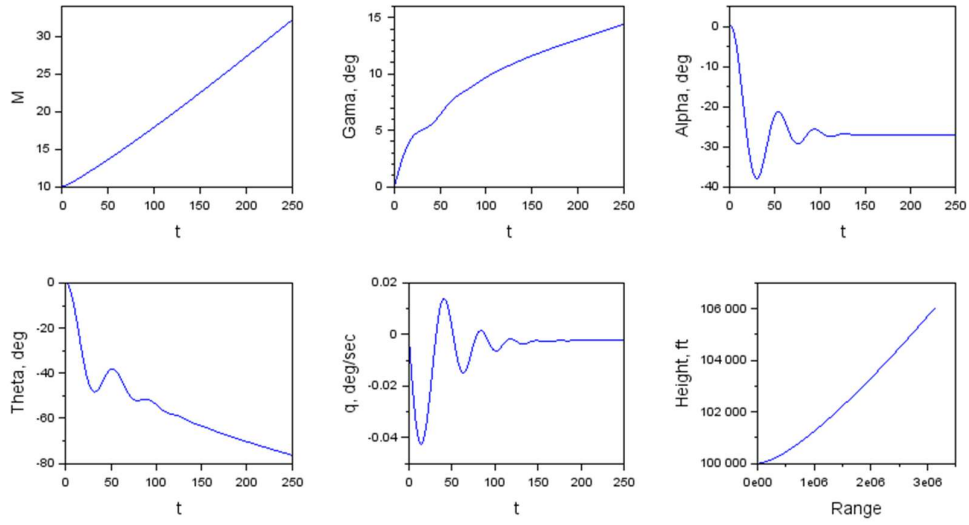

Fig. C.9 - Dynamic Simulation Case 4 for M = 10, δ_e= 0º and δ_r=1º

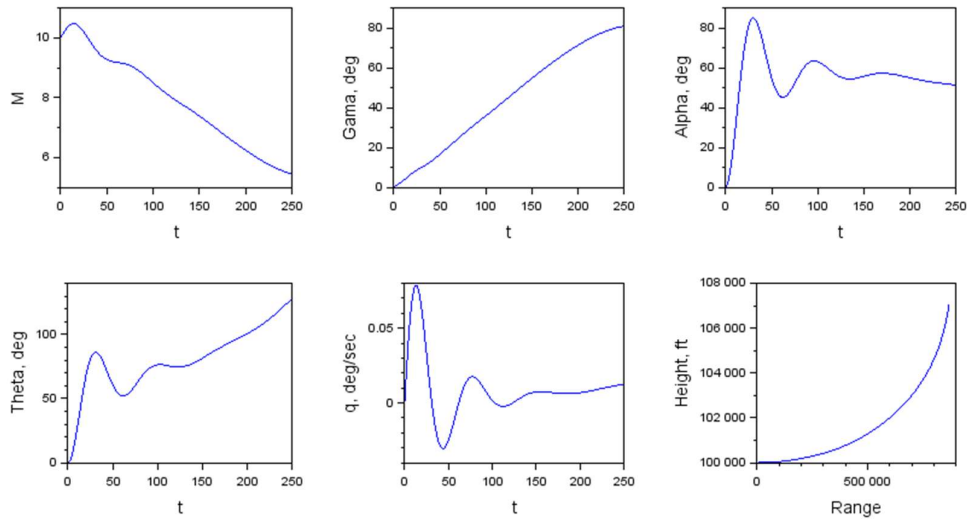Fig. C.9 - Dynamic Simulation Case 4 for M = 10, δ_e= 1º and δ_r=1º

Fig. C.9 - Dynamic Simulation Case 4 for M = 10, δ_e= -1º and δ_r=1º

APPENDIX D

AUTO-07p Program for 3DOF AHV ODE

The program to evaluate the ODE of AHV model is given below for the different

Cases from Table 3.3 and Table 4.1.

```
!------------------------M=0.9------------------------
SUBROUTINE FUNC(NDIM,U,ICP,PAR,IJAC,F,DFDU,DFDP)
DOUBLE PRECISION Vel, gama, alpha, theta, q, dele, mass,
g, Iyy, dia, Aref, hft, h
DOUBLE PRECISION rho0, rho1, rho, sspeed, Powlbf, Pow,
CD, CL, Cm
!  Vel   = U(1)
!  alpha = U(2)
!  theta = U(3)
!  q     = U(4)
   alpha = U(1)
   theta = U(2)
   q     = U(3)
!  gama  = U(4)

   dele  = PAR(1)
   mass=136080
   g=9.81
   Iyy=5000000
   dia=25
   Aref=350
   hft=10000
   h=hft*0.3048
   rho0=0.002377
   rho1=rho0*((1-6.875*(0.000001)*hft)**4.2561)
   rho=rho1*515.379;
   sspeed=sqrt(1.4*287*(288.15-6.5*(h/1000)))
   Vel=0.9*sspeed
!  Powlbf=0.3*(299000-10*hft+0.000133*(hft*hft)-
0.000000000648*(hft**3)+3750*((Vel/sspeed)**3))
!  Pow=4.44822*Powlbf
CD=0.5*rho*(Vel*Vel)*Aref*(0.00005*alpha*57.3+0.00006*del
e)
   CL=0.5*rho*(Vel*Vel)*Aref*(0.0252*alpha*57.3-
0.0032*dele)
   Cm=0.5*rho*(Vel*Vel)*Aref*dia*(-
0.0052*alpha*57.3+0.0024*dele-1.31255*q*dia/(2*Vel))
   Pow=CD
!  F(1)=(1/mass)*(Pow*cos(alpha*57.3)-CD-
mass*g*sin(theta*57.3))
!  F(2)=q-(1/(mass*Vel))*Pow*sin(alpha*57.3)-
CL*(1/(mass*Vel))+g*cos(theta*57.3)*(1/Vel)
!  F(3)=q
!  F(4)=Cm/(2*Iyy)
!  F(1)=q-(1/(mass*Vel))*Pow*sin(alpha)-
CL*(1/(mass*Vel))+g*cos(theta)*(1/Vel)
```

```
   F(1)=(1/(mass*Vel))*Pow*sin(alpha)-
CL*(1/(mass*Vel))+g*cos(theta)*(1/Vel)
   F(2)=q
   F(3)=Cm/(2*Iyy)
!  F(4)=(1/(mass*Vel))*Pow*sin(alpha)-
CL*(1/(mass*Vel))+g*cos(theta)*(1/Vel)


END SUBROUTINE FUNC

SUBROUTINE STPNT(NDIM,U,PAR,T)
   PAR(1) = 0.0d0
! Initialize the solution
!  U(1) = 295.521150d0
!  U(2) = 0.0d0/57.3
!  U(3) = -1.57080d0
!  U(4) = 0.0d0
   U(1) = 1.569d0
   U(2) = -1.569d0
   U(3) = 0.0d0
!  U(4) = 1.569d0
END SUBROUTINE STPNT
!--------------------------------------------------------
"
parnames = {1:'dele'}
unames = {1:'alpha', 2:'theta', 3:'q'}
NDIM=   3, IPS =   1, IRS =   0, ILP =   1
ICP =  ['dele']
NTST=   5, NCOL=   4, IAD =   3, ISP =   2, ISW = 1,
IPLT= 0, NBC= 0, NINT= 0
NMX=  200, NPR=   20, MXBF=   0, IID =   2, ITMX= 8,
ITNW= 5, NWTN= 3, JAC= 0
EPSL= 1e-07, EPSU = 1e-07, EPSS =0.0001
DS  =  0.01, DSMIN= 0.005, DSMAX=   0.1, IADS=   1
NPAR = 1, THL =  {}, THU =  {}
UZSTOP = {'dele': [-20.0, 20.0]} "

!------------------------M=4--------------------------

SUBROUTINE FUNC(NDIM,U,ICP,PAR,IJAC,F,DFDU,DFDP)

DOUBLE PRECISION Vel, alpha, theta, q, dele, mass, g,
Iyy, dia, Aref, hft, h, rho0, rho1, rho, sspeed, Powlbf,
Pow, CD, CL, Cm
!  Vel   = U(1)
!  alpha = U(2)
!  theta = U(3)
!  q     = U(4)
   alpha = U(1)
   theta = U(2)
   q     = U(3)

   dele  = PAR(1)
   mass=136080
   g=9.81
```

```
   Iyy=5000000
   dia=25
   Aref=350
   hft=50000
   h=hft*0.3048
   rho0=0.002377
   rho1=rho0*((1-6.875*(0.000001)*hft)**4.2561)
   rho=rho1*515.379;
   sspeed=sqrt(1.4*287*(288.15-6.5*(h/1000)))
   Vel=4*sspeed
!   Powlbf=0.3*(299000-10*hft+0.000133*(hft*hft)-
0.000000000648*(hft**3)+3750*((Vel/sspeed)**3))
!   Pow=4.44822*Powlbf
   CD=0.5*rho*(Vel*Vel)*Aref*(-0.0009*alpha*57.3-
0.0039*dele)

CL=0.5*rho*(Vel*Vel)*Aref*(0.0134*alpha*57.3+0.005*dele)
Cm=0.5*rho*(Vel*Vel)*Aref*dia*(0.0007*alpha*57.3+0.0006*d
ele-0.480870631*q*dia/(2*Vel))
   Pow=CD
!   F(1)=(1/mass)*(Pow*cos(alpha*57.3)-CD-
mass*g*sin(theta*57.3))
!   F(2)=q-(1/(mass*Vel))*Pow*sin(alpha*57.3)-
CL*(1/(mass*Vel))+g*cos(theta*57.3)*(1/Vel)
!   F(3)=q
!   F(4)=Cm/(2*Iyy)
   F(1)=q-(1/(mass*Vel))*Pow*sin(alpha)-
CL*(1/(mass*Vel))+g*cos(theta)*(1/Vel)
   F(2)=q
   F(3)=Cm/(2*Iyy)
END SUBROUTINE FUNC

SUBROUTINE STPNT(NDIM,U,PAR,T)
! Initialize the equation parameters
   PAR(1) = 0.0d0
! Initialize the solution
!  U(1) = 295.521150d0
!  U(2) = 0.0d0/57.3
!  U(3) = -1.50d0/57.3
!  U(4) = 0.0d0
   U(1) = 0.0d0
   U(2) = -1.57080d0
   U(3) = 0.0d0
END SUBROUTINE STPNT
!-------------------------M=6-------------------------
SUBROUTINE FUNC(NDIM,U,ICP,PAR,IJAC,F,DFDU,DFDP)
DOUBLE PRECISION Vel, alpha, theta, q, dele, mass, g,
Iyy, dia, Aref, hft, h, rho0, rho1, rho, sspeed, Powlbf,
Pow, CD, CL, Cm
!  Vel   = U(1)
!  alpha = U(2)
!  theta = U(3)
!  q     = U(4)
   alpha = U(1)
```

```
  theta = U(2)
   q    = U(3)

  dele  = PAR(1)
  mass=136080
  g=9.81
  Iyy=5000000
  dia=25
  Aref=350
  hft=65000
  h=hft*0.3048
  rho0=0.002377
  rho1=rho0*((1-6.875*(0.000001)*hft)**4.2561)
  rho=rho1*515.379;
  sspeed=sqrt(1.4*287*(288.15-6.5*(h/1000)))
  Vel=6*sspeed
!   Powlbf=0.3*(299000-10*hft+0.000133*(hft*hft)-
0.000000000648*(hft**3)+3750*((Vel/sspeed)**3))
!   Pow=4.44822*Powlbf
  CD=0.5*rho*(Vel*Vel)*Aref*(0.0013*alpha*57.3-
0.0006*dele)
  CL=0.5*rho*(Vel*Vel)*Aref*(0.0147*alpha*57.3-
0.0006*dele)
  Cm=0.5*rho*(Vel*Vel)*Aref*dia*(-0.0011*alpha*57.3-
0.000005*dele-0.32726331*q*dia/(2*Vel))
  Pow=CD
!   F(1)=(1/mass)*(Pow*cos(alpha)-CD-mass*g*sin(theta))
!   F(2)=q-(1/(mass*Vel))*Pow*sin(alpha)-
CL*(1/(mass*Vel))+g*cos(theta)*(1/Vel)
!   F(3)=q
!   F(4)=Cm/(2*Iyy)
  F(1)=q-(1/(mass*Vel))*Pow*sin(alpha)-
CL*(1/(mass*Vel))+g*cos(theta)*(1/Vel)
  F(2)=q
  F(3)=Cm/(2*Iyy)
END SUBROUTINE FUNC
!-------------------------------------------------------
SUBROUTINE STPNT(NDIM,U,PAR,T)
! Initialize the equation parameters
  PAR(1) = 0.0d0
! Initialize the solution
!   U(1) = 295.521150d0
!   U(2) = 0.0d0/57.3
!   U(3) = -1.50d0/57.3
!   U(4) = 0.0d0
  U(1) = 0.0d0
  U(2) = -1.57080d0
  U(3) = 0.0d0
END SUBROUTINE STPNT
!----------------------M=10-------------------------
SUBROUTINE FUNC(NDIM,U,ICP,PAR,IJAC,F,DFDU,DFDP)
DOUBLE PRECISION Vel, alpha, theta, q, dele, mass, g,
Iyy, dia, Aref, hft, h, rho0, rho1, rho, sspeed, Powlbf,
Pow, CD, CL, Cm
```

```fortran
!  Vel   = U(1)
!  alpha = U(2)
!  theta = U(3)
!  q     = U(4)
   alpha = U(1)
   theta = U(2)
   q     = U(3)

  dele  = PAR(1)
  mass=136080
  g=9.81
  Iyy=5000000
  dia=25
  Aref=350
  hft=100000
  h=hft*0.3048
  rho0=0.002377
  rho1=rho0*((1-6.875*(0.000001)*hft)**4.2561)
  rho=rho1*515.379;
  sspeed=sqrt(1.4*287*(288.15-6.5*(h/1000)))
  Vel=10*sspeed
!  Powlbf=0.3*(299000-10*hft+0.000133*(hft*hft)-
0.000000000648*(hft**3)+3750*((Vel/sspeed)**3))
!  Pow=4.44822*Powlbf
  CD=0.5*rho*(Vel*Vel)*Aref*(0.0008*alpha-0.0004*dele)
  CL=0.5*rho*(Vel*Vel)*Aref*(0.0132*alpha+0.001*dele)
  Cm=0.5*rho*(Vel*Vel)*Aref*dia*(-0.0004*alpha-
0.0003*dele-0.24736507*q*dia/(2*Vel))
  Pow=CD
!  F(1)=(1/mass)*(Pow*cos(alpha*57.3)-CD-
mass*g*sin(theta*57.3))
!  F(2)=q-(1/(mass*Vel))*Pow*sin(alpha*57.3)-
CL*(1/(mass*Vel))+g*cos(theta*57.3)*(1/Vel)
!  F(3)=q
!  F(4)=Cm/(2*Iyy)
  F(1)=q-(1/(mass*Vel))*Pow*sin(alpha)-
CL*(1/(mass*Vel))+g*cos(theta)*(1/Vel)
  F(2)=q
  F(3)=Cm/(2*Iyy)
END SUBROUTINE FUNC

SUBROUTINE STPNT(NDIM,U,PAR,T)
! Initialize the equation parameters
   PAR(1) = 0.0d0
! Initialize the solution
!  U(1) = 295.521150d0
!  U(2) = 0.0d0/57.3
!  U(3) = -1.50d0/57.3
!  U(4) = 0.0d0
   U(1) = 0.0d0
   U(2) = -1.57080d0
   U(3) = 0.0d0
END SUBROUTINE STPNT
```

```
!-----------------------M=15-------------------------
SUBROUTINE FUNC(NDIM,U,ICP,PAR,IJAC,F,DFDU,DFDP)
DOUBLE PRECISION Vel, alpha, theta, q, dele, mass, g,
Iyy, dia, Aref, hft, h, rho0, rho1, rho, sspeed, Powlbf,
Pow, CD, CL, Cm
!  Vel   = U(1)
!  alpha = U(2)
!  theta = U(3)
!  q     = U(4)
   alpha = U(1)
   theta = U(2)
    q    = U(3)

  dele  = PAR(1)
  mass=136080
  g=9.81
  Iyy=5000000
  dia=25
  Aref=350
  hft=100000
  h=hft*0.3048
  rho0=0.002377
  rho1=rho0*((1-6.875*(0.000001)*hft)**4.2561)
  rho=rho1*515.379;
  sspeed=sqrt(1.4*287*(288.15-6.5*(h/1000)))
  Vel=15*sspeed
!  Powlbf=0.3*(299000-10*hft+0.000133*(hft*hft)-
0.000000000648*(hft**3)+3750*((Vel/sspeed)**3))
!  Pow=4.44822*Powlbf
  CD=0.5*rho*(Vel*Vel)*Aref*(0.0002*alpha-0.0005*dele)
  CL=0.5*rho*(Vel*Vel)*Aref*(0.0115*alpha+0.0002*dele)
  Cm=0.5*rho*(Vel*Vel)*Aref*dia*(0.0006*alpha-
0.00007*dele-0.22202757*q*dia/(2*Vel))
  Pow=CD
!  F(1)=(1/mass)*(Pow*cos(alpha*57.3)-CD-
mass*g*sin(theta*57.3))
!  F(2)=q-(1/(mass*Vel))*Pow*sin(alpha*57.3)-
CL*(1/(mass*Vel))+g*cos(theta*57.3)*(1/Vel)
!  F(3)=q
!  F(4)=Cm/(2*Iyy)
  F(1)=q-(1/(mass*Vel))*Pow*sin(alpha)-
CL*(1/(mass*Vel))+g*cos(theta)*(1/Vel)
  F(2)=q
  F(3)=Cm/(2*Iyy)
END SUBROUTINE FUNC

SUBROUTINE STPNT(NDIM,U,PAR,T)
! Initialize the equation parameters
   PAR(1) = 0.0d0
! Initialize the solution
!  U(1) = 295.521150d0
!  U(2) = 0.0d0/57.3
!  U(3) = -1.50d0/57.3
!  U(4) = 0.0d0
```

```fortran
    U(1) = 0.0d0
    U(2) = -1.57080d0
    U(3) = 0.0d0
END SUBROUTINE STPNT
!------------------------M=24------------------------
SUBROUTINE FUNC(NDIM,U,ICP,PAR,IJAC,F,DFDU,DFDP)
" IMPLICIT NONE
  INTEGER, INTENT(IN) :: NDIM, IJAC, ICP(*)
  DOUBLE PRECISION, INTENT(IN) :: U(NDIM), PAR(*)
  DOUBLE PRECISION, INTENT(OUT) :: F(NDIM)
  DOUBLE PRECISION, INTENT(INOUT) ::
DFDU(NDIM,NDIM),DFDP(NDIM,*)"
  DOUBLE PRECISION Vel, alpha, theta, q, dele, mass, g,
Iyy, dia, Aref, hft, h, rho0, rho1, rho, sspeed, Powlbf,
Pow, CD, CL, Cm
!  Vel   = U(1)
!  alpha = U(2)
!  theta = U(3)
!  q     = U(4)
   alpha = U(1)
   theta = U(2)
   q     = U(3)

  dele  = PAR(1)
  mass=136080
  g=9.81
  Iyy=5000000
  dia=25
  Aref=350
  hft=100000
  h=hft*0.3048
  rho0=0.002377
  rho1=rho0*((1-6.875*(0.000001)*hft)**4.2561)
  rho=rho1*515.379;
  sspeed=sqrt(1.4*287*(288.15-6.5*(h/1000)))
  Vel=24*sspeed
!  Powlbf=0.3*(299000-10*hft+0.000133*(hft*hft)-
0.000000000648*(hft**3)+3750*((Vel/sspeed)**3))
!  Pow=4.44822*Powlbf
  CD=0.5*rho*(Vel*Vel)*Aref*(-0.0009*alpha*57.3-
0.0007*dele)
  CL=0.5*rho*(Vel*Vel)*Aref*(0.0072*alpha*57.3-
0.002*dele)
Cm=0.5*rho*(Vel*Vel)*Aref*dia*(0.0022*alpha*57.3+0.0002*d
ele-0.30004623*q*dia/(2*Vel))
  Pow=CD
!  F(1)=(1/mass)*(Pow*cos(alpha*57.3)-CD-
mass*g*sin(theta*57.3))
!  F(2)=q-(1/(mass*Vel))*Pow*sin(alpha*57.3)-
CL*(1/(mass*Vel))+g*cos(theta*57.3)*(1/Vel)
!  F(3)=q
!  F(4)=Cm/(2*Iyy)
  F(1)=q-(1/(mass*Vel))*Pow*sin(alpha)-
CL*(1/(mass*Vel))+g*cos(theta)*(1/Vel)
```

```
  F(2)=q
  F(3)=Cm/(2*Iyy)
END SUBROUTINE FUNC

SUBROUTINE STPNT(NDIM,U,PAR,T)
! Initialize the equation parameters
   PAR(1) = 0.0d0
! Initialize the solution
!  U(1) = 295.521150d0
!  U(2) = 0.0d0/57.3
!  U(3) = -1.50d0/57.3
!  U(4) = 0.0d0
   U(1) = 0.0d0
   U(2) = -1.57080d0
   U(3) = 0.0d0
END SUBROUTINE STPNT
!--------------------------------------------------------
```

LIST OF PUBLICATIONS

1. Singh, R., Prakash, O., & Joshi, S. (2024), Longitudinal Air-Breathing Hypersonic Vehicle Nonlinear Dynamic Simulation with Different Control Inputs. *SAE International Journal of Aerospace* 17 (2), 1-19. https://doi.org/10.4271/01-17-02-0015 (**Web of Science, Scopus**)

2. Singh, R., Prakash, O., & Joshi, S. (2023), Control Design using PID with State Feedback for Air-Breathing Hypersonic Vehicle. *FME Transactions*, 51 (2), 221-230. https://doi.org/10.5937/fme2302221S (**Web of Science, Scopus**).

3. Singh, R., Prakash, O., Joshi, S., & Jeppu, Y. (2022), Longitudinal Trim and Stability Analysis of Generic Air-Breathing Hypersonic Vehicle using Bifurcation Method. *National Institute for Aerospace Research*, *INCAS Bulletin*, 14 (3), 111-123. https://doi.org/10.13111/2066-8201.2022.14.3.10 (**Scopus**).

4. Singh, R., Prakash, O., Joshi, S., & Jeppu, Y. (2021), Flight Dynamics Analysis using High Altitude & Mach Number for Generic Air-Breathing Hypersonic Vehicle. *AIAA Propulsion and Energy 2021 Forum*, AIAA, Virtual Event, USA. https://doi.org/10.2514/6.2021-3271 (**Scopus**).

5. Singh, R., Prakash, O., Joshi, S., & Jeppu, Y. (2022), Bifurcation Analysis of Longitudinal Dynamics of Generic Air-Breathing Hypersonic Vehicle for different Operating Flight Conditions. *Springer Proceedings in Complexity, Nonlinear Dynamics and Applications: Proceedings of the ICNDA*. https://doi.org/10.1007/978-3-030-99792-2_97 (**Scopus**).

6. Singh, R., Prakash, O., Joshi, S., & Jeppu, Y. (2022), Development of 3DOF Longitudinal Dynamic Model of Generic Air-breathing Hypersonic Vehicle. *IEEE International Conference for Advancement in Technology*, Goa. https://doi.org/10.1109/ICONAT53423.2022.9725896 (**Scopus**).

7. Singh, R., Prakash, O., Joshi, S., & Jeppu, Y. (2022), Linear Controller Design for Generic Air-Breathing Hypersonic Vehicle for different Control Inputs. *IEEE International Conference for Advancement in Technology*, Goa. https://doi.org/10.1109/ICONAT53423.2022.9725951 (**Scopus**).

UPES

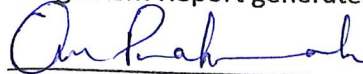## PLAGIARISM CERTIFICATE

1. We   Dr. Om Prakash (Internal Guide),   and   Dr. Sudhir Joshi (External Guide)

    certify that the Thesis titled Flight Dynamics Analysis of Generic Air-Breathing Hypersonic Vehicle

    using Bifurcation Method submitted by Scholar Mr. **RITESH SINGH** having SAP ID **500048549** has

    been run through a Plagiarism Check Software and the Plagiarism Percentage is reported to
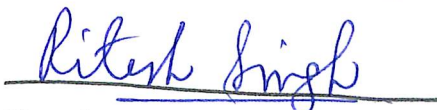
    be **8** %.

    The published papers from the research/Thesis work given below are excluded during the

    Plagiarism Check.

    1. Singh, R., Prakash, O., & Joshi, S. (2024), Longitudinal Air-Breathing Hypersonic Vehicle Nonlinear Dynamic Simulation with Different Control Inputs. *SAE International Journal of Aerospace* 17 (2), 1-19. https://doi.org/10.4271/01-17-02-0015
    2. Singh, R., Prakash, O., & Joshi, S. (2023), Control Design using PID with State Feedback for Air-Breathing Hypersonic Vehicle. *FME Transactions*, 51 (2), 221-230. https://doi.org/10.5937/fme2302221S
    3. Singh, R., Prakash, O., Joshi, S., & Jeppu, Y. (2022), Longitudinal Trim and Stability Analysis of Generic Air-Breathing Hypersonic Vehicle using Bifurcation Method. *National Institute for Aerospace Research*, INCAS Bulletin, 14 (3), 111-123. https://doi.org/10.13111/2066-8201.2022.14.3.10
    4. Singh, R., Prakash, O., Joshi, S., & Jeppu, Y. (2021), Flight Dynamics Analysis using High Altitude & Mach Number for Generic Air-Breathing Hypersonic Vehicle. *AIAA Propulsion and Energy 2021 Forum*, AIAA, Virtual Event, 3271-3284. https://doi.org/10.2514/6.2021-3271
    5. Singh, R., Prakash, O., Joshi, S., & Jeppu, Y. (2022), Bifurcation Analysis of Longitudinal Dynamics of Generic Air-Breathing Hypersonic Vehicle for different Operating Flight Conditions. *Springer Proceedings in Complexity, Nonlinear Dynamics and Applications: Proceedings of the ICNDA 2022*, Springer, Sikkim, 1149-1158. https://doi.org/10.1007/978-3-030-99792-2_97
    6. Singh, R., Prakash, O., Joshi, S., & Jeppu, Y. (2022), Development of 3DOF Longitudinal Dynamic Model of Generic Air-breathing Hypersonic Vehicle. *IEEE International Conference for Advancement in Technology*, IEEE, Goa, India. https://doi.org/10.1109/ICONAT53423.2022.9725896
    7. Singh, R., Prakash, O., Joshi, S., & Jeppu, Y. (2022), Linear Controller Design for Generic Air-Breathing Hypersonic Vehicle for different Control Inputs. *IEEE International Conference for Advancement in Technology*, IEEE, Goa, India. https://doi.org/10.1109/ICONAT53423.2022.9725951

2. Plagiarism Report generated by the Plagiarism Software is attached.

_____
Signature of the Internal Guide

_____
Signature of External Guide

_____
Signature of the Scholar

UPES_500048549_PhD Thesis (Engineering)_Ritesh Singh_11Mar 2024

8%	**6**%	**6**%	**2**%
SIMILARITY INDEX	INTERNET SOURCES	PUBLICATIONS	STUDENT PAPERS

PRIMARY SOURCES

1   **www.iieta.org**
Internet Source   **1**%

2   Abhishek Kumar, Om Prakash. "Longitudinal Trim and Stability Analysis of Hybrid Airship with Suspended Payload for Single Body and Two Body Dynamics Using Bifurcation Method", Mathematical Modelling of Engineering Problems, 2023
Publication   <**1**%

3   Submitted to Institute and Faculty of Actuaries
Student Paper   <**1**%

4   Submitted to Cranfield University
Student Paper   <**1**%

5   arc.aiaa.org
Internet Source   <**1**%

6   web.wpi.edu
Internet Source   <**1**%

7   dokumen.pub